

<https://helda.helsinki.fi>

Anatomy and Physiology of Macaque Visual Cortical Areas V1, V2, and V5/MT : Bases for Biologically Realistic Models

Vanni, Simo

2020-06

Vanni , S , Hokkanen , H , Werner , F & Angelucci , A 2020 , ' Anatomy and Physiology of Macaque Visual Cortical Areas V1, V2, and V5/MT : Bases for Biologically Realistic Models ' , Cerebral Cortex , vol. 30 , no. 6 , pp. 3483-3517 . <https://doi.org/10.1093/cercor/bhz322>

<http://hdl.handle.net/10138/323969>

<https://doi.org/10.1093/cercor/bhz322>

unspecified

acceptedVersion

Downloaded from Helda, University of Helsinki institutional repository.

This is an electronic reprint of the original article.

This reprint may differ from the original in pagination and typographic detail.

Please cite the original version.

Anatomy and physiology of macaque visual cortical areas V1, V2 and V5/MT: bases for biologically realistic models

Running title: Neuroinformatics of macaque vision

Simo Vanni* simo.vanni@helsinki.fi

HUS Neurocenter, Neurology, Helsinki University Hospital, Finland.

Department of Neurosciences, University of Helsinki, Finland.

Henri Hokkanen henri.hokkanen@helsinki.fi

HUS Neurocenter, Neurology, Helsinki University Hospital, Finland.

Department of Neurosciences, University of Helsinki, Finland.

Francesca Werner francesca.werner@studio.unibo.it

HUS Neurocenter, Neurology, Helsinki University Hospital, Finland.

Department of Neurosciences, University of Helsinki, Finland.

Department of Biomedical and Neuromotor Sciences, University of Bologna, Italy.

Alessandra Angelucci alessandra.angelucci@hsc.utah.edu

Department of Ophthalmology and Visual Sciences,

Moran Eye Institute, University of Utah,

Salt Lake City, Utah, USA.

Keywords: microcircuit, neural network, neuroinformatics, biomimetic

*** Corresponding author:**

Email: simo.vanni@helsinki.fi Address: Biomedicum Helsinki, Neurology Research Unit, PO Box 700, 00290 Helsinki, Finland. Tel. +358 50 586 5530.

30 **Abstract**

31 The cerebral cortex of primates encompasses multiple anatomically and
32 physiologically distinct areas processing visual information. Areas V1, V2 and V5/MT are
33 conserved across mammals and are central for visual behavior. To facilitate the generation
34 of biologically accurate computational models of primate early visual processing, here we
35 provide an overview of over 350 published studies of these three areas in the genus
36 *Macaca*, whose visual system provides the closest model for human vision.

37 The literature reports 14 anatomical connection types from the lateral geniculate
38 nucleus of the thalamus to V1 having distinct layers of origin or termination, and 194
39 connection types between V1, V2 and V5, forming multiple parallel and interacting visual
40 processing streams. Moreover, within V1, there are reports of 286 and 120 types of
41 intrinsic excitatory and inhibitory connections, respectively.

42 Physiologically, tuning of neuronal responses to 11 types of visual stimulus parameters
43 have been consistently reported. Overall, the optimal spatial frequency of constituent
44 neurons decreases with cortical hierarchy. Moreover, V5 neurons are distinct from
45 neurons in other areas for their higher direction selectivity, higher contrast sensitivity,
46 higher temporal frequency tuning and wider spatial frequency bandwidth.

47 We also discuss currently unavailable data that could be useful for biologically
48 accurate models.

49

50

51

52

53 One of the fundamental aims of visual neuroscience is to understand the computational
54 principles underlying biological vision. How do the biophysics of single neurons and
55 network interactions generate neuronal receptive fields (RFs), process sensory inputs and
56 cause visual behavior? Decades of studies have provided a wealth of data and multiple
57 descriptive and quantitative models of vision. Nevertheless, we still lack the ability to
58 construct accurate computational models that can reproduce a biologically meaningful
59 visual system. Such models and related computer simulations could help bridge the gap
60 between the physiological responses of single neurons and existing abstract models of
61 vision, as well as provide a better understanding of cortical processing.

62 The continuous increase of computational power has recently enabled the first
63 comprehensive microcircuit simulations of the rat somatosensory cortex (Markram et al.
64 2015). Recent simulations of macaque monkey visual cortex have explored large-scale
65 interactions between visual cortical areas (Mejias et al. 2016), replicated natural firing
66 rate statistics in a laminar network model of the primary visual cortex (V1; Rasch et al.,
67 2011), or described the generation of orientation tuning and the dynamics of V1 sublayer
68 4C alpha (Chariker et al. 2016). However, we are still far from being able to replicate the
69 multiplicity of cortical functions, let alone visual behavior, with biologically realistic
70 model simulations.

71 Accurate numerical model simulations require quantitative data on the anatomy and
72 physiology of the system, as well as on the structure and biophysical parameters of
73 distinct cell types. With unavoidable gaps in available data, unknown parameters need to
74 be explored against known neural RF properties, and eventually compared with visual
75 behavior.

76 To facilitate the generation of realistic computational models of visual cortex, here we
77 have collated data from more than 350 publications on connectivity, physiological RF

78 properties and single neuron biophysical properties in three visual cortical areas (V1, V2
79 and V5 or Middle Temporal –MT–) of the macaque monkey, one of the best studied
80 animal genus in vision research, and the available animal model closest to humans (Kaas
81 1992; Preuss 2004).

82 In macaques, visual information drives a network of about 30 interconnected cortical
83 areas organized into a hierarchical network according to laminar connectivity patterns
84 (Maunsell and Van Essen 1983b; Ungerleider and Desimone 1986; Zeki and Shipp 1988;
85 Felleman and Van Essen 1991; Merigan and Maunsell 1993; Barone et al. 2000; Van
86 Essen 2003; Shipp 2007; Kravitz et al. 2011, 2013; Markov, Vezoli, et al. 2014). V1, at
87 the bottom of this hierarchy, sends prominent connections to areas V2, V3, V4, V5/MT
88 and V6; in turn these V1-recipient cortical areas are interconnected with each other.

89 Here we focus on areas V1, V2 and V5/MT, as there is general agreement on the
90 location and macroscopic boundaries of these areas in primates and humans, and their
91 anatomy and electrophysiological properties have been extensively characterized. In
92 contrast, there is ongoing debate regarding the exact parcellation and function of the areas
93 that occupy the cortical territory between V2 and V5 (Kaas 1992, 2003; Van Essen 2003;
94 Wandell et al. 2007; Angelucci and Rosa 2015; Angelucci et al. 2015; Zhu and Vanduffel
95 2019). V1, V2 and V5 participate in early visual processing and are mutually connected.
96 These areas represent multiple low- and middle-tier visual stimulus features at various
97 scales, necessary for visually guided behavior (Hegd  and Van Essen 2003; Born and
98 Bradley 2005; Sincich and Horton 2005; Vidyasagar and Eysel 2015; Zeki 2015).
99 Phylogenetically, V1 and V2 are conserved in mammals, and V5 is found in all primate
100 species studied (Kaas 1995, 2003; Large et al. 2016) suggesting that these three areas play
101 a fundamental role in cortical processing of visual signals.

102 Despite challenges, such as the occurrence of multidimensional RFs, the complexity of

103 the cortical microcircuit, different definitions of the various parameters in different
104 studies, and missing data, this review attempts to report the available data in a consistent
105 way. We also attempt to provide a balanced overview of controversial issues, and to
106 emphasize quantitative data. The latter are reported as numerical quantities, or best
107 estimates of proportions or relative strengths, when these are available in the literature.
108 When quantitative data are not available, we cover qualitatively topics, which we
109 consider important for building computational models.

110

111 **Anatomical and physiological database and conventions**

112 All data reported here are limited to the Old World monkey genus *Macaca*, including
113 mainly the species *M. fascicularis*, *M. nemestrina*, *M. mulatta*, and *M. fuscata*. In
114 addition, we report data from functional anatomy studies performed in *M. arctoides*, *M.*
115 *assamensis*, *M. irus* or *M. radiata*. When different developmental stages were compared
116 in a study, we extracted only data from young adult individuals.

117 For consistency and brevity, we have excluded data from New World monkeys which
118 are phylogenetically more distant from humans than macaques [for phylogenetic
119 comparison of primate visual cortices, see (Kaas 2003, 2005; Rosa and Tweeddale 2005)].
120 However, for some experimental questions and methodological approaches, the New
121 World primates are better suited animal models. For example, the smooth cortical
122 structure of the marmoset cortex allows easier and simultaneous access to multiple visual
123 cortical areas.

124 We have combined data from several species of the genus *Macaca*. Brain volume
125 across the included species varies by a factor of about 1.7 (Marino 1998), which may
126 introduce variability in quantifications between different datasets. Given the similar
127 pattern of V1 layers across primate species (Balaram and Kaas 2014), we expect little

128 structural variation across macaque subspecies. Saleem et al (2007) studied the
129 anatomical differences of medial temporal lobe areas between *M. fuscata*, *M. fascicularis*
130 and *M. mulatta*. They found a similar anatomical organization of cortical layers, but one
131 of the four areas studied showed a shift in areal boundary across sub-species. Similarly,
132 the primary auditory cortex and its surrounding fields are smaller in *M. fascicularis* than
133 in *M. fuscata*, whereas the laminar distributions of various histochemical stains were
134 similar (Jones et al. 1995). These studies suggest that subtle differences in the
135 macroscopic anatomy of visual cortical areas are likely to exist among macaque
136 subspecies, but the general functional architecture is likely conserved.

137 Moreover, animal gender can introduce additional variability, as for example, in *M.*
138 *mulatta*, the volume of the male brain is on average 1.26 times larger than that of the
139 female (Franklin et al. 2000). However, the primary driver of variability is likely the body
140 weight, as this is closely correlated with brain weight (Jerison 1955), therefore requiring
141 knowledge of the body weight of the individual animals, more than their species or
142 gender, in order to calibrate the data; unfortunately we lacked this information, therefore,
143 our reports are not corrected for any of these factors.

144 Tuning properties of neuronal responses to eleven visual stimulus parameters were
145 reported consistently across the literature and are summarized in the figures. For other
146 parameter values in the text and tables, we report the mean and range of the mean values
147 reported across studies (but no range if there was only one study). For a model system
148 this can serve as the range of possible mean parameter values. The distribution of values
149 behind the means were inconsistently reported across studies and, of course, it was
150 impossible for us to control for outliers. These original distributions are omitted in this
151 review, unless descriptive statistics, such as standard deviation, were available for the
152 whole data in the original studies. The supplementary material comprises both anatomical

153 and physiological data in machine readable csv format.

154

155 Anatomical conventions

156 There are two different nomenclatures for V1 layers in the literature. We follow the
157 more widely used Brodmann's nomenclature, according to which layer (L) 4 has four
158 subdivisions (4A, 4B, 4C α , 4C β ; Brodmann 1909, translated by Garey, 2006). Hassler's
159 nomenclature is based on the same histological subdivisions, but layers 4A and 4B of
160 Brodmann are considered part of L3 (Hassler 1966).

161 Area V5 is also known as MT, for middle temporal, following its original naming in
162 the New World monkeys. In V1, we group L2 with L3A, as typical in many interlaminar
163 connectivity studies.

164 Here connection strength is defined mainly as the number of labeled neurons in
165 retrograde tracer studies, or density of axonal projections of singly labeled neurons. Such
166 anatomical definition of strength does not obviously reflect the actual physiological
167 strength of a connection, which depends on several other factors such as neuron identity,
168 and the number, strength and locations of pre-synaptic boutons on the postsynaptic
169 neuron. Note, also, that connection strength can only be compared within single tracer
170 injections, because the number of labeled cells varies across injections of different size.
171 When quantitative data were unavailable, connection strength was estimated from figures
172 or from the text and reported in Figure 2 and Supplementary Table 1 as sparse, medium or
173 dominant connection strength to indicate the approximate number of presynaptic somata
174 or axonal terminations. For interareal connections, the term "dominant" indicates the
175 combined dominant origin and termination of a given connection. In the absence of any
176 description of connection strength in the original publications, we set the strength to
177 medium. For contradicting results in different studies, we gave more weight to the data

178 that were more rigorously quantified. When quantitative data were available, sparse,
 179 medium and dominant connections (in Figure 2 and Supplementary Table 1) indicate
 180 <10%, 10-50% and >50%, respectively, of cells (for a given tracer injection), or of
 181 synapses/boutons/axonal length (for intracellular microinjections).

182 When axons of traced neurons were reported to terminate at a border between two
 183 cortical layers, the connection was marked as terminating in both layers. We included
 184 studies using glutamate uncaging (Sawatari and Callaway 2000; Briggs and Callaway
 185 2001, 2005; Yabuta et al. 2001). This method reveals connections to neurons with somata
 186 and dendrites located within the postsynaptic layer, as well as to neurons with somata
 187 residing in other layers but with dendrites extending into the postsynaptic layer.
 188 Connectivity studies based on degeneration were not included.

189 For interareal connectivity studies, single tracer injections are typically not confined to
 190 a layer and therefore the layers of origin and termination within the injection site could
 191 not be identified. Therefore, in Supplementary Table 1, we report separately the literature
 192 references for the connections' origin and termination; moreover, for each laminar origin
 193 and termination the same reference is repeated for each laminar termination and origin,
 194 respectively. These data are visualized in Figure 2 reporting the existence and density of
 195 inter-areal connections between different layers of the connected areas. For example,
 196 Lund et al. (1981), following retrograde tracer injections across all V2 layers found
 197 labeled cells in V1 L2/3A, 4A and 4B, while following anterograde tracer injections into
 198 all V1 layers they found labeled terminations in V2 L4 and L3B with sparser spread into
 199 L3A, and at the L5 and 6 border. For the retrograde tracer injection of this study, in
 200 Supplementary Table 1 and Figure 2, we report 3 types of connections from V1 to V2,
 201 one arising from V1 L2/3A, the second from V1 L4A, and the third from V1 L4B, each
 202 terminating in V2 L3A , 3B, 4, 5B and 6, and cite this study five times for each of the

203 three V1 layers of origin.

204

205 Description of physiological parameters.

206 Physiological RF data were reported as the total number or percent of cells in a given
207 area as a function of a given RF parameter. This allowed us to combine different datasets
208 if the reported values were comparable. To this goal, we extracted and digitized data from
209 the figures in the original publications and reported in our figures the proportion of cells
210 across studies as a function of a given physiological parameter value. Because we are not
211 analyzing the original raw data, but summary histograms, the descriptive statistics we
212 report here inevitably include some inaccuracies, for example errors in the centering of
213 the bins on the X-axis of the original data, residual rotation, and calibration and
214 digitization errors. As a quality control, we visualized all data-reporting figures,
215 calibration and digitized points, and then re-digitized all data exceeding 10% mismatch
216 between the total number of cells reported in the original study and that reported in our
217 data.

218 Different studies used different metrics for data analysis. We included only data from
219 one of these metrics, or data that could be converted into a standard metrics using a
220 simple transformation. For example, different datasets report either circular variance (CV)
221 or orientation selectivity index ($OSI=1 - CV$), as measures of orientation selectivity. In
222 this case, we converted OSIs to CV.

223

224 **Anatomy**

225 Anatomical data show significant individual variability, and many studies are based on
226 only few monkeys. Thus, some of the mean values reported below may not reflect real
227 population means.

228 Recently, mouse neocortical cells have been classified into 133 transcriptomic clusters
 229 based on single-cell RNA sequencing. These clusters included 61 GABAergic, 56
 230 glutamatergic, and 16 non-neuronal types (Tasic et al. 2018). However, the number of
 231 such clusters depends on the cut point of the clustering method. Based on axonal
 232 projection patterns mainly in rodents, cortical excitatory cells have been classified into
 233 three major groups, intratelencephalic (projection to cortex and striatum), pyramidal tract
 234 (projections mainly to the brainstem, spinal cord and midbrain) and corticothalamic
 235 (projections mainly to the ipsilateral thalamus), with ongoing subgrouping efforts based
 236 on morphology, gene expression and physiology (reviewed in Shepherd 2013; Harris and
 237 Shepherd 2015). Following existing literature on the neuroanatomy of macaque visual
 238 cortex, largely from the 80's until the last decade (Gilbert 1983; Nieuwenhuys 1994;
 239 Douglas and Martin 2004), below we divide excitatory cells into two major
 240 morphological groups, spiny stellate and pyramidal cells. Further subgrouping pyramidal
 241 cell is challenging, due to the wide diversity of pyramidal cell dendritic and axonal
 242 morphologies, which could result in an intricate classification according to soma position,
 243 branching patterns or axonal targets (examples in Larkman 1991; Markram, Muller,
 244 Ramaswamy, Reimann, Schurmann, et al. 2015); moreover, such a subgrouping across
 245 layers has not been systematically applied to macaque visual cortex. The pyramidal and
 246 spiny stellate cells receive excitatory input predominantly onto their spines, and inhibitory
 247 input onto their somas, dendritic shafts and axon initial segments.

248 Likewise, a general system for GABAergic interneuron classification is missing [for
 249 reviews, see (Markram et al. 2004; Ascoli et al. 2008; DeFelipe et al. 2013)]. Cells
 250 immunoreactive for the calcium-binding proteins calbindin, calretinin, and parvalbumin
 251 are distributed non-uniformly across laminae in macaque V1 and V2 (DeFelipe et al.
 252 1999), but these markers are not uniquely mapped to morphological cell types (Ascoli et

al. 2008; Markram et al. 2015). In rodent cortex, interneurons have been classified into three major types based on expression of parvalbumin, somatostatin and 5HT_{3A}-receptor, each type having a different embryonal origin (Lee et al. 2010; Rudy et al. 2011). However, a similar classification has not been systematically applied to macaque visual cortex.

GABA-releasing inhibitory interneurons can be further classified based on the morphological, physiological or molecular phenotype (Ascoli et al. 2008; DeFelipe et al. 2013). At least eight morphological subtypes exist (Jones 1993; DeFelipe et al. 2013), with the double bouquet cell following a unique developmental path in primates (reviewed in DeFelipe, 2011; Betizeau et al., 2013). In the 80's and 90's, Jennifer Lund and colleagues published a series of Golgi-staining studies describing the various morphological inhibitory cell types in macaque V1 and their distinct laminar distributions of dendritic and axonal projections (Lund 1987; Lund et al. 1988; Lund and Yoshioka 1991; Lund and Wu 1997). These studies, however, did not quantify these cells' morphological features. Recently introduced automatic classifier methods might help generating a more unified classification of cell type morphologies (DeFelipe et al. 2013), but presently there exist no quantitative analyses of inhibitory cells in distinct areas and layers of macaque visual cortex.

271

272

273 Area size and cell numbers, types and locations

274 **Lateral Geniculate Nucleus (LGN).** In each LGN of *M. Mulatta*, the two
 275 magnocellular (Magno) layers, one for each eye, comprise on average 148×10^3 neurons
 276 (range across monkeys $91\text{--}235 \times 10^3$), and the four parvocellular (Parvo) layers, two for
 277 each eye, 1270×10^3 neurons (range $900\text{--}1700 \times 10^3$, Ahmad and Spear, 1993). Earlier

estimates of Magno- and Parvo LGN cell numbers, including data from undefined macaque species, give values between the ranges above (le Gros Clark, 1941; Connolly and Van Essen, 1984; reviewed in Peters et al., 1994). Of the numbers above, 35% of cells in the Magno layers, and 25% of cells in the Parvo layers are immunoreactive for the inhibitory neurotransmitter gamma-aminobutyric acid (GABA), therefore are local inhibitory interneurons, the remaining being thalamocortical projection neurons (Montero and Zempel 1986).

A neurochemically distinct population of koniocellular (Konio) cells was recognized later (Hendry and Yoshioka 1994). It occupies primarily the spaces between and below the Magno- and Parvo layers in LGN, forming six distinct layers, termed the intercalated or K layers (reviewed in Hendry and Reid, 2000; Casagrande et al., 2007). These layers comprise about 100×10^3 projection neurons, and apparently no inhibitory interneurons. In addition, small neurons with the chemical signature of K cells are also scattered within the M and P layers and form bridges between the K layers (Hendry and Yoshioka 1994).

V1, V2, V5: Area size. The sizes and neuron numbers of cortical areas vary across individual monkeys, being related to body weight, which has an allometric relation to cortical surface (Maunsell and Van Essen 1987; Hofman 1989).

In the adult macaque monkey, the whole cortical surface of one hemisphere may comprise up to 130-140 functionally distinct areas (Van Essen et al. 2012) and covers, on average, an area of 10430 mm^2 ($N = 10$ hemispheres from 3 *M. mulatta* and 7 *M. fascicularis*, range across monkeys $8286\text{--}14113 \text{ mm}^2$; Sincich et al., 2003). V1 represents about 13% and V2 about 10% of this total area. Table 1 reports the surface areas for V1, V2 and V5. The corresponding surface area ratios between these three areas are 1:0.80:0.042, respectively.

Table 1. Cortical surface areas (mm²) from anatomical studies. N = total number of hemispheres. The mean values across studies were weighted by the N hemispheres in each study. Parenthesis enclose the range across the means of individual studies. Min and max values indicate the lowest and highest values in individual monkeys across all studies. References: 1. Gattass et al. 1981; Van Essen et al. 2. 1981, 3. 1986, 4. 2002; 5. O’Kusky and Colonnier 1982a; 6. Ungerleider and Desimone 1986a; 7. Maunsell and van Essen 1987; 8. Olavarria and Van Essen 1997; 9. Sincich et al. 2003.)

	V1	V2	V5
Mean	1181 (797-1343)	944 (730-1012)	50 (33-73)
Min	690	660	24
Max	1817	1412	99
N	58	17	37
Refs	1-5,9	1,3,8-9	2,6-7,9

303

304

305 **V1: neuron numbers and types.** Pyramidal cell bodies occur in all V1 layers, except
 306 4C and 1 (Lund 1973). Moreover, the apical dendrites of pyramidal cells residing in L5
 307 and L6 have few spines in L4C. Spiny stellate cells occur in all V1 L4 subdivisions, and
 308 in L4C they constitute 85-95% of all neurons (Mates and Lund 1983; Fitzpatrick et al.
 309 1987). Moreover, Briggs et al. (2016) have recently reported some spiny stellate cells in
 310 V1 L6A. Inhibitory stellate cells occur in all V1 layers.

311 Figure 1 depicts the modular organization of V1, which includes the ocular dominance
 312 columns (ODC) and cytochrome oxidase (CO) blobs, as well as the six layers of V1.
 313 Monocular RFs predominate in L4C, and the blob structure is most evident in L3. Above
 314 and below these layers, RFs are biased to represent the same ODC, blob/interblob
 315 compartment, and other RF properties such as preference for the orientation of edges,

usually referred to as columnar organization.

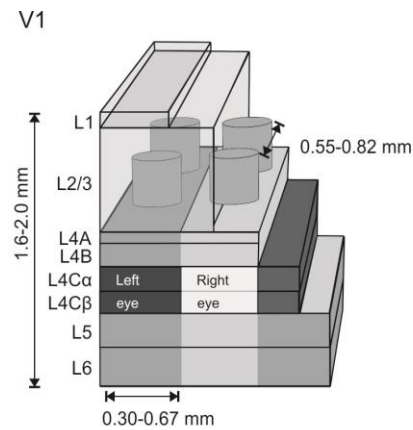


Figure 1. Schematics of cytochrome oxidase (CO) and ocular dominance modules in V1. The cylinders in L3 depict CO blobs, and the lighter and darker columnar gray bands the ocular dominance columns (ODC), most emphasized in L4C (Hubel and Wiesel 1968). References for cortical thickness (range of means; Chow et al. 1950; Lund 1973; O’Kusky and Colonnier 1982b); layer thickness is drawn approximately to scale (Lund 1973); reported distance between CO blobs is the range across monkeys (Horton 1984; Landisman and Ts’o 2002); reported width of ODC is the range across monkeys (LeVay et al. 1975; Horton and Hocking 1996).

Table 2 reports the total number of neurons and the relative number of inhibitory neurons in each layer of area V1. The total number of neurons in one hemisphere of adult macaque V1 ($N=2$ *M. fascicularis* and 4 *M. mulatta*) is 161×10^6 ($SD=18$), and the total number of synapses is 381×10^9 ($SD=53$). V1 covers on average 841 mm^2 ($SD=88$) surface area ($N=7$ hemispheres; O’Kusky and Colonnier, 1982). A recent study based on rigorous stereological methods estimated V1 neuron numbers more than double the original estimates. (Table 2; Giannaris and Rosene, 2012).

Table 2. Total number of neurons, synapses/neuron, and the proportion of inhibitory interneurons in each cortical layer of area V1. * Layers 2 and 3 together; ** Layers 4Ca and 4C β together. References: 1. O’Kusky and Colonnier 1982b; 2. Fitzpatrick et al. 1987; 3. Hendry et al. 1987; 4. Beaulieu et al. 1992; 5. Giannaris and Rosene 2012.)

Layer	N neurons x 10 ⁶	Synapses / neuron x 10 ³	% inhibitory	N neurons x 10 ⁶
1	0.47	61.8	84	<u>Supragr.</u> 215
2	44*	2.6*	20	
3			20	
4A	17	1.6	22	Granular 121
4B	17	2.7	19	
4Ca	14	1.9	16**	
4C β	24	1.4		
5	20	1.7	20	<u>Infragr.</u> 80
6	24	2.1	15	
Total	161	2.3		416
Refs	1	1	2-4	5

328

329

330 In V1, 19% (range 18.5-19.6%) of neurons are GABA immunoreactive, while in
 331 extrastriate cortex surrounding V1, including area V2, the proportion of inhibitory
 332 neurons is 25% (range 24.2-25.3%, N=5 hemispheres, Hendry et al., 1987). No apparent
 333 difference in the density of GABAergic cells exists between the CO blobs and interblobs
 334 of V1 (Beaulieu et al. 1992).

335 In primate evolution, L4 of area V1 has become specialized into three sublayers
 336 (reviewed in Casagrande and Kaas, 1994), and correspondingly the number of neurons in
 337 V1 per unit surface area doubled compared with other cortical areas (Hendry et al. 1987).
 338 In addition, of all cortical areas, the density of neurons per unit volume is highest in V1.

339 The mean density of neurons across all layers in V1 is $230 \times 10^3/\text{mm}^3$ (range 190–280 x
 340 $10^3/\text{mm}^3$; average of three *M. fascicularis* monkeys), and drops in V2 to $130 \times 10^3/\text{mm}^3$
 341 (range 110–140 $\times 10^3/\text{mm}^3$; average of two *M. fascicularis*, and one *M. mulatta*, Kelly
 342 and Hawken, 2017). The neuronal densities per unit mass show similar trends, being
 343 highest in V1 ($130\text{--}177 \times 10^6/\text{g}$) and somewhat lower in V2 ($89\text{--}114 \times 10^6/\text{g}$) and V5 (85
 344 $\times 10^6/\text{g}$; *M. mulatta*, Collins, 2011).

345 Layer 4A has a unique honeycomb-like appearance consisting of parvocellular
 346 geniculate afferent axons, local groups of pyramidal neurons in cone-like arrangement
 347 ($30\text{--}80 \mu\text{m}$ wide, mean $60 \mu\text{m}$), separated by neuropil, and vertical apical dendritic
 348 clusters ($1270 \text{ clusters}/\text{mm}^2$) arising from L5 pyramidal cells (Peters and Sethares 1991a,
 349 1991b).

350 **V2: neuron numbers and types.** Only sparse quantitative data exist for V2. Rockland
 351 (1997) estimated that beneath 1mm^2 area of V2 lay about 92600 neurons (of which 31200
 352 in L3, 37200 in L4, 10600 in L6). In contrast to V1, there are no spiny stellate neurons in
 353 V2 L4 or elsewhere in cortex, and infragranular pyramidal cells in V2 have spines in L4,
 354 which further emphasizes the functional uniqueness of V1 among visual areas (Lund et al.
 355 1981). In L4 of V2, over 90% of cells are pyramidal, with short apical dendrites, rising up
 356 to L3.

357 Data on neuron numbers and types for the individual layers of area V5 have not been
 358 reported.

359 Layer-specific quantifications of distinct neuron types would be of paramount
 360 importance for modeling.

361

362 Connections between subcortical nuclei and V1, V2 and V5

363 Geniculocortical and corticogeniculate connections

364 Three main pathways, Magno- Parvo- and Koniocellular streams, convey visual
 365 signals from the retina through the LGN to V1 (Figs. 2 *top*, 3 *top*, Supplementary Table
 366 1A). These pathways are functionally distinct and computationally assumed to convey
 367 independent dimensions of visual information from the retina to the visual cortex
 368 (Derrington et al. 1984; Gegenfurtner 2003; Lennie and Movshon 2005). The Magno
 369 layers of the LGN, whose cells mediate achromatic vision, have high temporal but low
 370 spatial frequency tuning, and respond non-linearly to changes in luminance and contrast,
 371 send denser projections to V1 L4C α , and sparser and fine axon collaterals to the lower
 372 part of L6. The Parvo layers, whose cells mediate red-green contrast, have high spatial but
 373 low temporal frequency tuning, and respond linearly to dynamic stimuli and contrast
 374 changes, send their most dominant projection to L4C β , and sparser projections from a
 375 separate population of cells to layers 4A and the upper part of L6 (Figs. 2 *top* and 3
 376 *top*; Hubel and Wiesel 1972; Hendrickson et al. 1978; Blasdel and Lund 1983). In L4C,
 377 the thalamic afferents form arborizations covering one monocular column, with a
 378 complementary pattern of projection representing the other eye. The width of this periodic
 379 arborization shows individual variability from 0.5 to 1.2 mm (Hubel and Wiesel 1972).

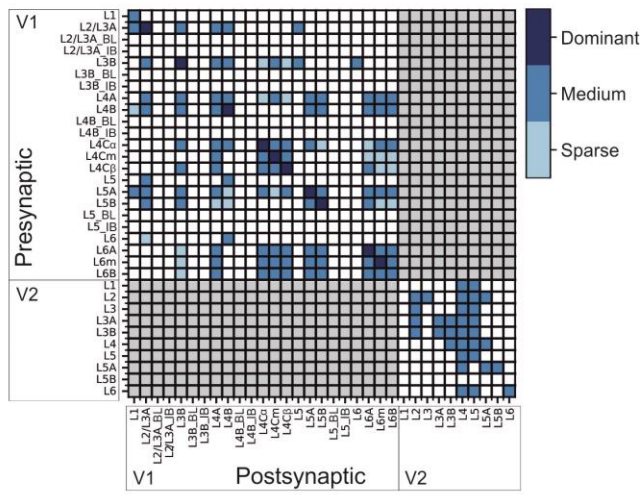
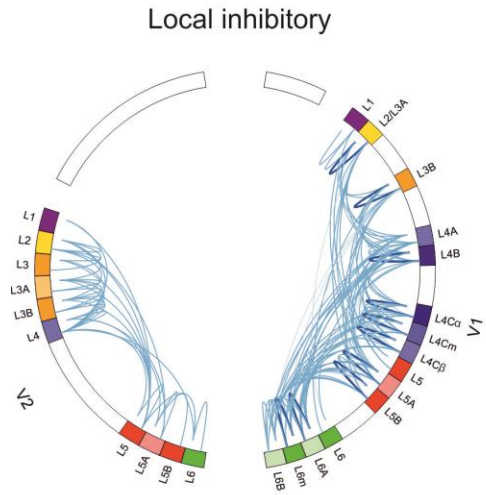
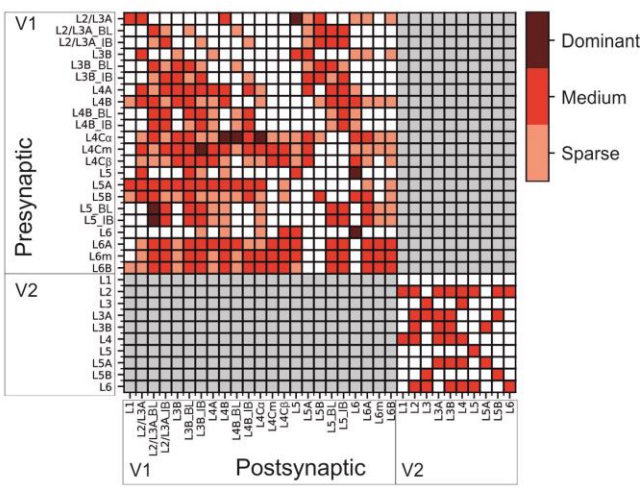
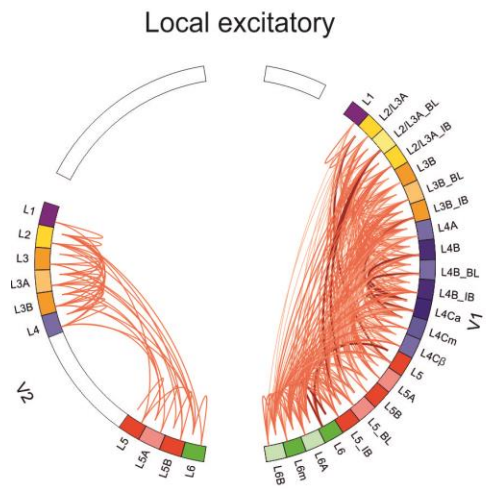
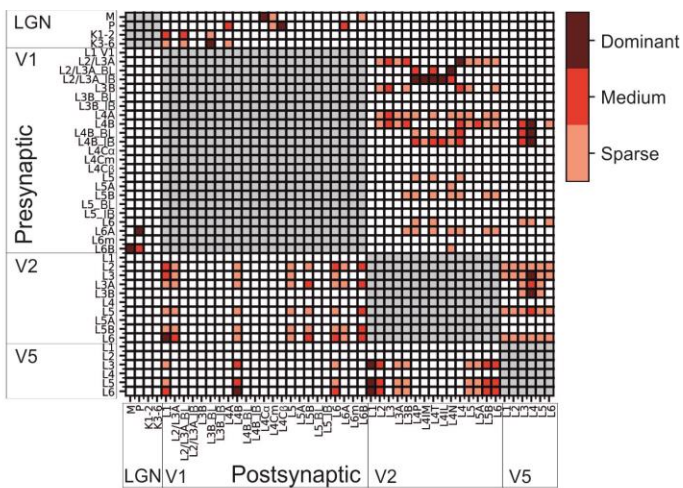
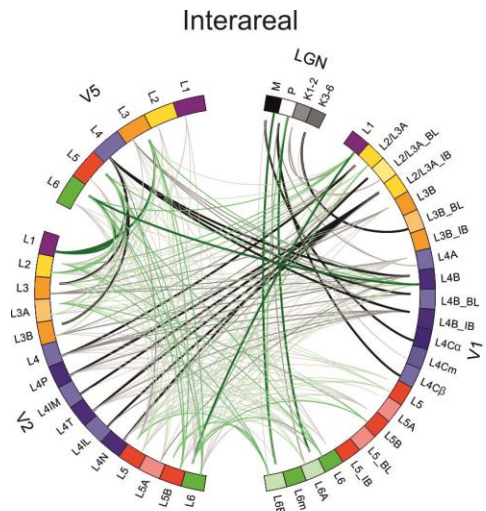
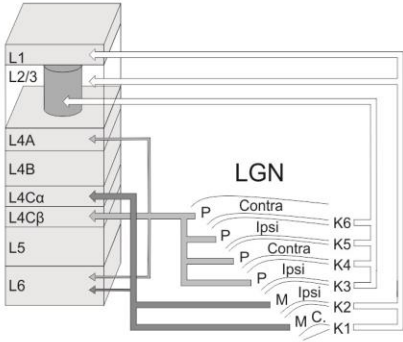


Figure 2. Connections between LGN, V1, V2, and V5 and within V1 and V2. For references, see Supplementary Table 1D. Top, middle and bottom rows indicate inter-areal, intra-areal excitatory and intra-areal inhibitory connections, respectively.

LEFT COLUMN: Connectograms (Krzywinski et al. 2009) showing connections between distinct layers. Each colored segment in the circular perimeter indicates a cortical layer, sublayer or CO compartment. Line width and color intensity indicate the robustness of the connection. Unknown strengths are marked as medium; for V2 interlaminar connections (middle and bottom connectograms), the paucity and qualitative character of the available studies did not allow us to estimate connection strength. The origin (soma) of a projection neuron is marked as a line slightly displaced from the outer edge of the circle, while its termination (axon terminals) is marked as a line reaching the outer edge of the circle. Top Left: Interareal connections and connections between LGN and areas V1, V2, V5. Black lines indicate FF connections, and green lines FB connections. V2 L4P = L4 pale stripe (no distinction between lateral/medial stripes), L4IM = L4 interstripe (or pale stripe) medial, L4T = L4 thick stripe, L4IL = L4 interstripe (or pale) lateral, L4N = L4 thin stripe. All interareal connections are excitatory. Middle left: Local excitatory connections. Bottom Left: Local inhibitory connections; none of the studies reviewed here identified the CO compartments.

RIGHT COLUMN: Matrix of the connections. No connection (*white squares*) indicates that the connection either does not exist or was not studied. *Red squares* indicate excitatory connections, and *blue squares* inhibitory connections. Color intensity indicates the strength of the connection. |

V1



V1 Blobs:
Color/Hue: 1-4
Lack of orientation specificity: 4
Low spatial frequency: 5-7
High contrast sensitivity: 5

Interblobs:
Orientation: 4
Mid and high SF: 5-7
Low contrast sensitivity: 5

Layer 4B:
High direction selectivity: 8

V2 Pale medial (type II): contours
Orientation: 9, 10

Thick stripes: disparity, motion
Orientation: 4, 11-18
Low and High SF: 19
Illusory contours: 20
Retinal disparity: 12, 13, 17, 21
High contrast sensitivity: 19
Motion direction: 14, 18, 22

Pale lateral (type I): unknown
Orientation (weak): 9

Thin stripes: surface
Color, spectral sensitivity: 4, 11-15, 19, 23, 24
Luminance: 25
Low SF: 19
Brightness: 26, 27

Pale, undifferentiated (early data)
Illusory contours: 20, 28
Orientation: 4, 11, 13, 15, 16, 18
High SF: 19

V5/MT

Speed tuning: 29-31
Orientation: 32
Direction tuning: 30, 32, 33
Disparity: 34, 35

V5/MT

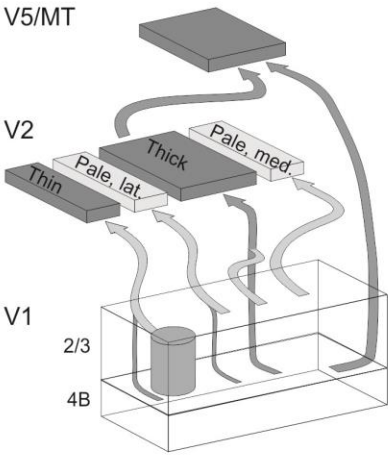


Figure 3. Feedforward pathways and specialization of functional compartments in LGN, V1, V2 and V5. TOP: Main LGN to V1 pathways (Hendrickson et al. 1978; Blasdel and Lund 1983; Kaplan 2003; Casagrande et al. 2007). Arrow thickness indicates the relative contribution of Parvo and Magno geniculocortical afferents to the different V1 layers. BOTTOM: Main FF pathways between V1, V2 and V5 (Sincich and Horton 2002; Sincich et al. 2007, 2010; Federer et al. 2013). In both top and bottom schematics, additional sparse connections were omitted for clarity.

The CO compartments of V1 and V2 contain multiple functional feature maps and their constituent neurons show specific receptive field tuning properties, as indicated on the right. Numbers refer to the following references:

1, Tootell, Silverman, Hamilton, De Valois, et al. 1988; 2, Landisman and Ts'o 2002; 3, Xiao et al. 2007; 4, Lu and Roe 2008; 5, Edwards et al. 1995; 6, Silverman et al. 1989; 7, Tootell, Silverman, Hamilton, Switkes, et al. 1988; 8, Gur and Snodderly 2007; 9, Felleman et al. 2015; 10, Shipp and Zeki 2002a; 11, Shipp and Zeki 2002b; 12, DeYoe and Van Essen 1985; 13, Roe and Ts'o 1995; 14, Munk et al. 1995; 15, Gegenfurtner et al. 1996; 16, Vanduffel et al. 2002; 17, Ts'O et al. 2001; 18, Levitt, Kiper, et al. 1994; 19, Tootell and Hamilton 1989; 20, Peterhans and von der Heydt 1993; 21, Chen et al. 2008; 22, Lu et al. 2010; 23, Tootell et al. 2004; 24, Xiao et al. 2003b; 25, Wang et al. 2007; 26, Lu and Roe 2007; 27, Roe et al. 2005; 28, Heider et al. 2000; 29, Lagae et al. 1993; 30, Maunsell and Van Essen 1983c; 31, Perrone and Thiele 2001; 32, Albright 1984; 33, Dubner and Zeki 1971; 34, Maunsell and Van Essen 1983a; 35, DeAngelis and Newsome, 1999. |

383

384 Data on single thalamocortical axon arborization patterns are very sparse. An
385 individual Magno axon terminating in L4C α may divide into two or perhaps more arbors.
386 These arbors form a cluster, each covering 0.3-0.4 mm² surface area. Each cluster
387 contains 6490 synapses (mean from Blasdel and Lund, 1983 and Freund et al., 1989; both
388 studies reported data from one filled axon).

389 The corresponding coverage for the Parvo pathway axon terminal in L4C β is much
390 smaller, 0.067 mm² (Blasdel and Lund 1983). Freund et al. (1989) filled two Parvo axons,
391 and counted on average 3154 synapses/axon cluster. A single Parvo axon in L4A formed a
392 single terminal field with a honeycomb-like pattern, including 764 boutons covering
393 0.058 mm² surface area (Blasdel and Lund 1983). Assuming an average of 2.2

394 synapses/bouton [mean of Parvo synapses per bouton, from (Freund et al. 1989)], this
 395 would result in 1681 synapses/axon cluster.

396 The Konio stream of the macaque LGN, a fraction of which mediates blue-yellow-
 397 contrast, is organized in 6 cellular layers (K1-K6), located between and below the four
 398 Parvo and two Magno layers (Figs. 2 *top* and 3 *top*; Casagrande et al. 2007). Layers K1-
 399 K2 project mainly to V1 L1 (47% of K1-K2 projecting boutons) and the upper part of L3
 400 (38% of boutons; named 3A in Casagrande et al., 2007), with minor projections to L2
 401 (3%) and the lower part of L3 (12%); each axon has on average 134 boutons (range 55-
 402 255, N=9 axons). Cells in the LGN layers K3-K6 project mainly to the lower part of V1
 403 L3 (93% of boutons; named 3B α in Casagrande et al., 2007), targeting mainly the CO-
 404 rich blobs (Hendry and Yoshioka 1994; Casagrande et al. 2007), with minor projections to
 405 L1 (2%), upper L3 (3%), and L4A (2%); each axon has on average 217 boutons (range
 406 90-430, N=9 axons). The number of thalamocortical synapses per bouton in the Konio
 407 stream is unknown.

408 A subset of L6 neurons in V1 projects back to LGN (Wiser and Callaway 1996; Briggs
 409 et al. 2016) in a stream-specific manner (Lund et al. 1975), i.e. separate cells in L6A and
 410 6B project to the Parvo and Magno layers, respectively, each with functional properties
 411 resembling their LGN targets (Briggs and Usrey 2009). In addition to V1, also some V2
 412 L6 neurons project back to LGN (Briggs et al. 2016). Because the target layers in LGN
 413 are unknown for this V2 projections, these connections are omitted in Figure 2 and
 414 Supplementary Table 1A.

415 The LGN also projects directly to V2 (Bullier and Kennedy 1983; Markov et al. 2011),
 416 and about 1% of, or 8000, LGN neurons project directly to V5 (Sincich et al. 2004).
 417 Interestingly, these geniculate connections to V2 and to V5 both originate primarily from
 418 the intercalated Konio layers (Bullier and Kennedy 1983; Sincich et al. 2004), which

419 represent the phylogenetically older blue-yellow color system (Carlos and Silveira 2003).
 420 Unfortunately, we do not know the target layers in V2 and V5 for this LGN projection,
 421 and thus we have omitted these connections from Figure 2 and Supplementary Table 1A.

422

423 Other subcortical afferents to V1, V2 and V5

424 Of all subcortical inputs to V1, one of the largest arises from the claustrum (0.3% of
 425 all retrogradely labeled neurons after injections in V1), whereas for LGN inputs this
 426 fraction does not exceed 0.2% (Markov et al. 2011). V1 receives also afferents from the
 427 pulvinar (to layers 1 and 2, Lund et al., 1981), and the amygdala (Markov et al. 2011).
 428 The largest fraction of subcortical projecting neurons to V2 arises from both inferior and
 429 lateral pulvinar (Benevento and Rezak 1976; Trojanowski and Jacobson 1976) [0.3%
 430 (Markov et al. 2011), terminating primarily in L3B (Lund et al. 1981)], and from the
 431 claustrum (0.5%; Markov et al. 2011). In addition, V1 and V2 receive sparse projections
 432 from thalamic intralaminar nuclei and the nucleus basalis of Meynert (Kennedy and
 433 Bullier 1985). Area V5 also receives projections from the pulvinar (Adams et al. 2000)
 434 and claustrum (Gattass et al. 2014). Unlike the very localized inputs from LGN and
 435 pulvinar, inputs from the claustrum and thalamic intralaminar nuclei show much larger
 436 spread (Perkel et al. 1986).

437

438 Interareal Connections

439 Overview of cortico-cortical connections

440 Interareal connections between V1, V2 and V5 have been reviewed previously (Zeki
 441 and Shipp 1988; Felleman and Van Essen 1991; Merigan and Maunsell 1993; Gattass et
 442 al. 2005; Sincich and Horton 2005; Angelucci and Bressloff 2006; Nassi and Callaway
 443 2009). Later, quantitative studies have provided significant new information on the

relative connection strengths between cortical areas (Markov et al. 2011; Markov, Ercsey-Ravasz, et al. 2014), and on-line databases have also enabled targeted searches of existing literature (Kötter 2004; Bakker et al. 2012). In addition to visual inputs, V1 and V2 receive feedback from auditory and parietal cortices suggesting that multimodal signals are available to all visual areas, not just to association areas positioned at higher levels of the anatomical hierarchy (Falchier et al. 2002; Rockland and Ojima 2003).

The macaque cortex consists of a moderately dense network of functional areas, where one estimate suggests that 66% of possible direct connections between two areas exist, with the number of projecting neurons between any two areas spanning a scale of 10^5 (Markov, Ercsey-Ravasz, et al. 2014). With the caution that these numbers are based mainly on one species, *M fascicularis*, and thus cannot be applied to other macaque species, these data suggest that the number of projecting neurons $p(d)$ follows an exponential cortical distance rule (Markov et al. 2013):

457

$$p(d) = c e^{-\lambda d}; \text{ SD of } p(d) = \sqrt{\mu + \frac{\mu^2}{\theta}}$$

459

where, c is a scaling constant, λ is the spatial decay constant, and d is distance across white matter. Markov et al. (2013) reported $\lambda = 0.19 \text{ mm}^{-1}$ for macaques, interpreting it to reflect the cost of wiring. Variability of λ between monkeys was not reported, but individual injections show SD which follows the mean, fitting best to negative binomial model with dispersion parameter $\theta = 7.6$. (Markov et al. 2011).

Between areas, the fraction of supragranular presynaptic projection neurons is correlated with hierarchical distance from the target area, so that in lower-order areas supragranular projection neurons predominate, whereas in higher order areas projection

468 neurons lay primarily in infragranular layers (Barone et al. 2000; Markov et al. 2013).

469 A large fraction of V1 excitatory cells sends their axons into the white matter. In a
 470 study based on 9 monkeys (*Macaca radiata*; (Callaway and Wiser 1996), white matter-
 471 projecting axons were found for 50% (3/6 cells) of excitatory cells in layers 2/3A, 60%
 472 (3/5 cells) in L3B, 83% (5/6 cells) in L4B, and 19% in L5 (3/16 cells). In L6, 28% of
 473 cells (16/56 cells; 8 monkeys; *Macaca radiata*) projected to white matter (Wiser and
 474 Callaway 1996). Many projection neurons have also extensive intra- and interlaminar
 475 local collaterals in V1 (Lund and Boothe 1975; Callaway and Wiser 1996; Yarch et al.
 476 2017).

477 Markov et al. (2014a) have provided important quantitative data on corticocortical
 478 connections (Table 3). They injected retrograde tracers in multiple areas, including V1,
 479 V2 and V5, counted the number of cells projecting to these areas, and calculated each
 480 area's relative input from different areas. V1 receives about three fourths of its interareal
 481 input from V2, and vice versa V2 receives three fourths of its input from V1, representing
 482 the densest mutual connectivity in the macaque brain. Rockland (1997) estimated that
 483 under each mm² of cortex, 14600 V1 neurons send feedforward (FF) projections to V2
 484 (range 8800-21600), whereas 11300 (range 8000-12800) V2 neurons send feedback (FB)
 485 projections to V1. Moreover, 41-68% of V2 L6 neurons provide FB connections to V1
 486 (Rockland 1994).

487

Table 3. Relative strength of mutual connections between V1, V2 and V5. Numbers indicate the percent of total presynaptic neurons, labeled in the source area after a retrograde tracer injection in the target area (e.g. after a tracer injection in V2, $76.4 \pm 2.7\%$ of all labeled presynaptic cells reside in V1; (Markov, Ercsey-Ravasz, et al. 2014). Data from: <http://core-nets.org/index.php?action=download>. Data are from adult monkeys, five hemispheres were injected in V1 (four monkeys, all females), three in V2 (two monkeys, all males) and one in V5 (female).

V1 to V2		V2 to V1	
Mean	76.4%	Mean	73.2%
Std	2.7%	Std	3.5%
Min	73.3%	Min	68.3%
Max	78.3%	Max	76.6%
V1 to V5		V5 to V1	
Mean	1.9%	Mean	5.9%
		Std	1.1%
		Min	5.2%
		Max	7.8%
V2 to V5		V5 to V2	
Mean	11.9%	Mean	3.6%
		Std	0.6%
		Min	3.0%
		Max	4.1%

488

489

490 Given this robust mutual connectivity between V1 and V2, it is interesting that these
 491 two areas exert rather different impacts on each other's neuronal responses; whereas
 492 inactivating V1 silences V2 (reviewed in Bullier et al. 1994), inactivating V2 has much
 493 subtler effects on V1 responses (Hupé et al. 1998, 2001; Nassi et al. 2013; Nurminen et
 494 al. 2018) indicating that the anatomical strength of a connection does not dictate its
 495 physiological strength. Other factors, such as the strength of synaptic connections and
 496 their location on the postsynaptic cell are likely important determinants of physiological
 497 strength of a connection.

498 The proportion of afferent connections to V5 arising from V1 and V2, as well as the
 499 FB connections from V5 to V1 and V2 are clearly sparser, but still significant (Table 3).

500 Many studies suggest that connections between V1 and V2, V2 and V5 and V1 and V5
 501 are retinotopically organized in such a way that neighboring patches of cortex represent
 502 neighboring regions in the visual field (Ungerleider and Mishkin 1979; Weller and Kaas
 503 1983; Ungerleider and Desimone 1986; Shipp et al. 1989). However, the cell populations
 504 projecting from V1 to V2 and V5 are largely distinct (Sincich and Horton 2003; Nassi and
 505 Callaway 2007).

506 Figure 2 *top*, 3 *bottom* and Supplementary Table 1A summarize the interareal
 507 connectivity between V1, V2 and V5. CO staining in V2 reveals a periodic stripe pattern
 508 consisting of dark thick and thin stripes with interleaving pale stripes (Fig. 3 *bottom*). A
 509 robust connection from V1 to V2 arises from L2/3A interblobs, followed by the
 510 projection from L2/3A blobs. A second robust, but generally sparser (except for the
 511 projection to thick CO stripes) pathway arises from L4B interblob and blob columns, and
 512 sparse inputs arise from layers 3B, 4A, 5B and 6A. In V2, the majority of V1 afferents
 513 terminate in L4 of the different CO stripes (thick, thin and pale), with minor terminations
 514 in layers 3A, 3B, 5A, 5B and 6. The FB projections from V2 to V1 arise predominantly

515 from L6, followed by layers 2-3A, with minor efferent connections from layers 3B and
 516 5B. Earlier studies, using less sensitive anterograde tracers or bidirectional tracers
 517 suggested that V2 FB projections terminate predominantly in L1 of V1, with only minor
 518 projections or collaterals to other layers (2/3 and 5) (Rockland and Pandya 1979; Lund et
 519 al. 1981; Rockland and Virga 1989; Rockland 1994; Gattas et al. 1997). Recent studies,
 520 using more sensitive and exclusively anterograde viral vectors of fluorescent proteins,
 521 however, have shown strong V2 FB projections not only to L1, but also to L5B and 6B of
 522 V1, with sparser terminations in layers 2/3, 4B, 5A and 6A (Ta'afua et al. 2018). This
 523 arrangement suggests that the layer-wise connectivity between V1 and V2 is largely
 524 reciprocal, i.e. the same V1 layers sending FF projections to V2 receive direct FB
 525 connections from V2. Such symmetry suggests the existence of FF-FB loops, for fast
 526 modulation of incoming V1 FF signals by V2 FB connections. However, the lack of FB
 527 connections arising from L4, the dominant FB arising from L6, and the dominant FB
 528 terminations in L1 are exception to an exact FF-FB reciprocity, showing anatomical
 529 asymmetry. How this asymmetry affects the cells' integrative function is unclear.
 530 Connections to dendrites distant from the soma, such as the FB to L1, may contact the
 531 apical dendrites of pyramidal cells with somata in deeper layers. However, studies in
 532 rodents and modeling work have shown that the postsynaptic signals relayed at these
 533 distal sites are attenuated (Rall 1962; Williams and Stuart 2002), and their effect may
 534 depend on coincident inputs onto the proximal dendrite (Larkum et al. 2004; Larkum
 535 2013). These dendritic intracellular interactions may affect the layer-specific timing of
 536 visual responses carried by feedforward, horizontal and feedback connections (Self et al.
 537 2013; Bijanzadeh et al. 2018).

538 FF connections from V1 to V5 arise from layers 4B (both blobs and interblobs) and 6
 539 and target primarily L4 and less so L3 of V5. Similar to V2-to-V1 FB, FB connections

540 from V5 originate predominantly in L6, with smaller contributions from layers 5 and 3,
 541 while L4 sends no FB to V1. FB projections from V5 to V1 terminate predominantly in
 542 layers 4B and 6 (Maunsell and Van Essen 1983b; Ungerleider and Desimone 1986; Shipp
 543 et al. 1989), i.e. the source layers of the V1-to-V5 FF projection. Only in the peripheral
 544 visual field ($>10^\circ$ eccentricity), does V5 FB target also V1 L1 (Ungerleider and Desimone
 545 1986; Shipp et al. 1989). FF connections from V2 to V5 arise predominantly from L3B,
 546 but also from layers 2, 3A and 5, with a minor contribution from L6. These connections
 547 terminate mainly in L4 of V5 with some spread into the neighboring layers 3 and 5. FB
 548 from V5 to V2 arises from V5 layers 3, 5 and 6, and terminates predominantly in V2
 549 layers 1 and 6, but also 2, 3A, 5B, with minor terminations also in layers 3B and 5A. In
 550 contrast to V2, where the supragranular origin of FB connections is mainly from L2-3A,
 551 the supragranular FB from V5 seems to originate only from L3; while Rockland and
 552 Pandaya (1979) reported it to originate in L3A, Weller and Kaas (1983) did not specify
 553 from which subdivision of L3 V5 FB originates.

554

555 Characteristics of connections between V1 and V2

556 The major target layer of V1-to-V2 projections is L4, where axon terminals form 0.2-
 557 0.5 mm wide clusters; 1-3 clusters are arranged in 0.2 (single cluster) to 1.2 mm (multiple
 558 clusters) long and 0.3 mm wide terminal fields (Rockland and Virga 1990; Anderson and
 559 Martin 2009). Sparse axonal terminations also occur contiguously in layers 3 and 5
 560 (Rockland and Pandya 1979). In V2, the most frequent targets of V1 FF projections are
 561 the dendritic spines of excitatory neurons, with sparse terminations onto shafts, the latter
 562 mainly (about 60%) onto inhibitory neurons (Anderson and Martin 2009). Of the spines
 563 receiving V1 FF projections, only 19% receive a second inhibitory synapse in addition to
 564 excitatory synapses.

565 As mentioned above, macaque V2 has four CO stripe compartments (thick, thin, and 2
 566 pale stripes), each with unique afferent and efferent connectivity (Fig. 2 *top*, 3 *bottom*,
 567 Supplementary Table 1A). Retrograde tracer injections confined to distinct V2 stripes
 568 result in spatially segregated clusters of labeled somata in V1, which align preferentially
 569 with distinct V1 CO compartments (blobs or interblobs), suggesting parallel FF pathways
 570 from V1 to V2 (Livingstone and Hubel 1984a, 1988a; Sincich and Horton 2002; Federer
 571 et al. 2013). Livingstone and Hubel (1984b, 1988) first proposed a tripartite model of V1-
 572 to-V2 projections. This model was later modified by Sincich and Horton (2002) and,
 573 subsequently, Federer et al. (2013) as illustrated in Figure 3 *bottom*. According to this
 574 model, thin stripes receive projections from CO blobs, and thick and pale stripes from
 575 interblobs. V1 projections to all stripes arise predominantly from L2-3 with sparse
 576 projections from layers 4A and 5-6; projections from L4B are densest to thick stripes,
 577 moderate to thin stripes and one set of pale stripes (type I, also termed pale-lateral as they
 578 are located laterally to thick stripes), and absent to the second set of pale stripes (type II,
 579 also termed pale-medial). Importantly, this segregation is not strict, as all stripe types
 580 receive sparser projections from both blobs and interblobs.

581 After paired injections of different retrograde tracers into thick and pale stripes, 16%
 582 of all V1 labeled neurons were double labeled in the interblobs (Sincich and Horton
 583 2002); even smaller percentages of double labeled neurons were found after paired
 584 retrograde tracer injections into thin and pale stripes (Sincich and Horton 2002), or pale-
 585 lateral and pale-medial stripes (1-3% of all labeled neurons, Federer et al. 2013),
 586 demonstrating that different stripe types receive inputs predominantly from different V1
 587 cells, but at least some common inputs from the same cells, and that the segregation of
 588 inputs is more marked for thin vs thick/pale stripes compared to thick vs. pale or pale-
 589 lateral vs. pale-medial stripes.

Using intra-V2 injections of a glycoprotein-deleted rabies virus carrying the gene for green fluorescent protein (GFP), Nassi and Callaway (2007) found that on average 17% of V1 L4B neurons projecting to V2 had spiny stellate morphology and 83% (N= 2 hemispheres, 82% and 85%, respectively) had pyramidal morphology. By confining injections of the same virus to thick or thin stripes, Yarch et al. (2019) reported that on average >60% of L4B inputs to thick stripes and about 40% to thin stripes arises from stellate cells, and the rest from pyramids. The difference between the results of Nassi and Callaway (2007) and those of Yarch and colleagues (2019) suggests that most V1 L4B stellate cells that project to V2 target the thick stripes, and that pale stripes receive dominant or exclusive V1 L4B inputs from pyramidal cells. Alternatively, viral injections in the two studies may have been confined to different subcompartments or layers within the stripes, or the virus differentially infected different populations of L4B cells in the two studies. Yarch et al. (2019) additionally fully reconstructed the intra-V1 axon arbors of single L4B neurons projecting to thick stripes; using unbiased cluster analysis of these neurons' intra-V1 laminar axon projection patterns, they identified at least two (possibly three) major classes within this L4B subpopulation. Most reconstructed neurons (65%, 15/23 neurons) belonged to Class 1, sending narrowly focused axonal projections to L2/3, and laterally extending projections to layers 4B and 5. Class 2 cells (26%), instead, sent collaterals mainly to L5, and the rare Class 3 cells (9%) predominantly to L6. The somata of all these cell classes lay preferentially outside CO blobs, and their axon projections in all layers also avoided CO blobs, indicating that the intra-V1 connections of L4B neurons projecting to thick stripes preserve segregation between blobs and interblobs.

Rockland and Virga (1989), reported that V2 to V1 FB axons form terminal clusters in V1 with extents of $4.0 \times 10^6 \mu\text{m}^3$ (range $0.2 \times 10^6 - 15.4 \times 10^6$), primarily in L1, with sparser terminations in layers 2 and 5. Most single FB axons travel 0.75-2 mm in L1,

615 sending clusters at 350-650 μm intervals (Rockland 1994). In L5, however, the terminals
 616 travel <0.75 mm. The density of boutons varies from 3 to 15 boutons/100 μm of axon.

617 Using more sensitive viral vectors of GFP (AAV9) confined to distinct V2 stripes,
 618 Angelucci and colleagues (Federer et al. 2015; Ta'afua et al. 2018) have recently reported
 619 dominant V2 FB projections to V1 layers 1, 2A, 5B and 6B, and sparser projections to
 620 2B, 3, 5A and 6A, from all stripe types. Sparse, but significant projections to L4B were
 621 observed after thick and pale-lateral stripe injections but were virtually absent after thin
 622 stripe injections. Moreover, V2 FB projections mimicked the parallel organization of the
 623 reciprocal FF V1-to-V2 pathways: in all V1 layers of termination, thin stripes projected
 624 predominantly to blobs and pale and thick stripes to interblobs.

625

626 Characteristics of V5 afferent pathways

627 The most direct LGN Magno inputs reach V5 tri-synaptically via V1 layers 4C α and
 628 4B. In contrast, most Parvo input travels a longer route, via V2, to reach V5 (see Fig. 3
 629 in Nassi and Callaway 2006). More specifically, the pyramidal neurons in V1 L4B
 630 receive Magno and Parvo inputs from both layers 4C α (via direct 4C α -to-4B projections)
 631 and 4C β (via 4C β -to-3 projections contacting the apical dendrites of L4B pyramids in
 632 L3), whereas the 4B spiny stellate neurons receive only Magno input from L4C α (Yabuta
 633 et al. 2001). L4B spiny stellates then carry Magno data directly to V5 (Nassi and
 634 Callaway 2007). After injections of retrograde tracers into V5, Nassi and Callaway (2007)
 635 found that on average 76% (N=3 hemispheres, range 67-93%) of the labeled cells in V1
 636 L4B had spiny stellate morphology and only 24% had pyramidal morphology. This
 637 contrasted with the much larger fraction of pyramids (~80%) projecting to V2. Moreover,
 638 the V5-projecting V1 L4B neurons were larger in size compared to the V2-projecting
 639 ones, and the V5-projecting pyramidal cells were more likely to reside under CO blobs

640 and have longer dendritic trees extending more often up to L1. Other studies found that
 641 L4B cells projecting to V5 are equally located under blobs and interblobs (Shipp et al.
 642 1989; Sincich and Horton 2003), and that V1 projections to V5 arise predominantly from
 643 L4B (97.8% of V1 inputs), and sparsely from L6 projection (2.2%; Nhan and Callaway
 644 2012).

645 Individual axons from V1 terminate into 1.0 – 1.8 mm wide patchy fields in L3, L4
 646 and L6 of area V5 (Rockland 1989; Anderson et al. 1998). Each axonal branch forms up
 647 to 4 terminal arbors up to 250 μm in diameter in the L4 and L3, and up to 50-100 μm in
 648 L6 (Rockland 1989). The axons form excitatory synapses with dendritic spines (54%;
 649 with the largest synapses, mean area 0.127 μm^2 , SEM 0.011), shafts (33%; 0.071 μm^2 ,
 650 SEM 0.07) and somata (13%; 0.031 μm^2 , SEM 0.008). All connections to the soma and
 651 26% of those on shafts were found to be on inhibitory postsynaptic cells, the reminder
 652 (78% of all connections) being on excitatory cells (Anderson et al. 1998). These authors
 653 estimated that of the $5\text{-}10 \times 10^3$ synapses present on single V5 neurons, only few
 654 hundreds are made by V1 afferents, which is analogous to LGN-to-V1 projections where
 655 a small number of synapses have a disproportionally strong impact on the target neurons.

656 Similar to V1 projections, V2 afferent axons to V5 form terminal patches in L3-4, each
 657 patch being up to 200-250 μm in width, with an interpatch distance of up to 600 μm
 658 (Rockland 1995). Moreover, as in V1, most V2 afferent synapses land onto spines (67%
 659 in L4, 82% in L2/3), and only 4-6% of synapses onto L4 neurons are made by V2 afferent
 660 axons (Anderson and Martin 2002). In contrast to V1 projections, some V2 axon arbors
 661 extend from L4 upward into L1; moreover, V2 afferent axons are thinner than V1
 662 afferents (diameter of about 3.0 μm in V1 vs. 1.0 μm in V2), and send no collaterals to L6
 663 (Rockland 1995; Anderson and Martin 2002).

664

Divergence and convergence in feedforward and feedback connections

Some of the earliest anatomical studies of interareal connections reported that the tangential extents of the FF and FB connectional fields were asymmetric (reviewed in Zeki and Shipp 1988). The forward connections converged to a local region in higher order areas, and it was hypothesized that they represent the anatomical substrate for the increasing RF size of neurons along the cortical hierarchy. In contrast, the backward projecting system was typically more divergent, thus possibly serving widespread modulation of low-order areas.

Angelucci et al. (2002) tested the hypothesis that widespread FB connections from extrastriate cortical areas provide an anatomical substrate for contextual modulation of V1 neuron responses arising from outside the neurons' classical RF (also termed the RF surround). By combining tracer injections with electrophysiological recordings at the injection site and in the cortical region of expected tracer transport, these authors were able to compare the spatial extent of extrastriate FB connections to V1 with the spatial extent of V1 neurons' classical and extra-classical RFs. Anterograde tracer injections confined to the V2 upper layers produced a pattern of labeled patchy FB terminations in V1 upper layers. Injections including also the deep V2 layers additionally produced less patchy, and more extensive terminal FB label in layers 5/6. The diameter of the V2 FB axon terminal field in V1 was 6.8 ± 0.4 mm (mean \pm SEM, range 6.4-7.6 mm), while FB terminations from V5 extended over 13.4 ± 0.5 mm (range 12.9-13.9) mm in V1. These authors also made injections of retrograde tracers into V1 and measured the extent of the retrogradely-labeled fields of neurons in V2, and V5 sending convergent FB projections to the injected V1 region. When converted to visuotopic coordinates, on average, the V2 and V5 L5/6 FB neurons labeled by small injections of retrograde tracers in V1 encompassed a visual field region of $3.8^\circ \pm 0.6$ and $26.6^\circ \pm 3.0$, respectively, in diameter.

690 In contrast, the field of long-range intra-V1 horizontal connections converging to the
 691 same V1 injection sited was only $2.9^\circ \pm 0.4$ in diameter. Expressed in units of V1
 692 classical RF size, the visuotopic extents of V2 FB fields correspond to 4.0 ± 0.4 times
 693 (range 2.7-5.3; for FB from V2 L2/3) and 4.6 ± 0.2 times (4.0-5.1; for FB from V2 L5/6)
 694 the size of the classical RF of V1 neurons. FB from V5 L2/3 and 5/6, instead, extends
 695 15.0, and 25.0 ± 4.0 (21-29) times, respectively, the V1 neurons' classical RF size.
 696 Importantly, the FB fields to V1 are much larger than the extent of visual field
 697 encompassed by the intra-V1 long-range horizontal connections, which, instead,
 698 encompass 2.7 (L2/3) to 3.7 (L4B) times the classical RF size of V1 cells. In conclusion,
 699 horizontal connections can mediate contextual integration of visual signals from just
 700 outside the V1 neurons' RF (the "near surround"), while FB connections provide V1 cells
 701 with a much larger area for integrating visual signals arising from the most distant regions
 702 of the RF surround (the "far surround").
 703

704 Intra-areal connections

705 Local cortical connectivity is complex. For example, a recently implemented model of
 706 the microcircuit of rat somatosensory cortex comprises almost 2000 connection types
 707 between 55 morphological cell types (Markram et al. 2015). For modeling purposes, the
 708 complex connectivity needs to be simplified to basic principles, including distance
 709 distributions, major local inter-laminar pathways, and main connection motifs for
 710 excitatory and inhibitory neurons. This information is only partially available for
 711 macaque cortex.

712 Overall, there seem to be two major categories of connections, long-range
 713 (millimeters-long) horizontal connections, which are most prominent within the lamina of
 714 origin (Fisken et al. 1975; Rockland and Lund 1983; Angelucci, Levitt, Walton, et al.

715 2002), and short local connections, which often cross layer boundaries.

716

717 Horizontal connectivity

718 Most inputs to cortical neurons arise from their local neighborhood. On average 79%
 719 of incoming axons to any cortical point originate within the same functional area (Markov
 720 et al. 2011). In addition, the intra-areal intrinsic connectivity is highly local (Barone et al.
 721 2000; Markov et al. 2011), i.e. following injection of a retrograde tracer in cortex, the
 722 number of resulting retrogradely labeled neurons drops as a function of distance (d) from
 723 the injected site:

724

725
$$\text{Number of neurons} \sim \frac{1}{e^{\lambda d}}$$

726

727 For example, in V1 lambda is 1/0.23 mm, resulting in 95% of labeled presynaptic
 728 neurons being located within 2.2 mm of the injection site; in V2 the corresponding value
 729 is 1.8 mm. On average, across the studied cortical areas, 95% of labeled intrinsic neurons
 730 are within 1.9 mm of the injected site (Markov et al. 2011). Moreover, on average 63% of
 731 these retrogradely labeled V1 neurons are supragranular, and the drop in number as a
 732 function of distance appears similar in the supra- and infragranular layers (Barone et al.
 733 2000).

734 The extent of local horizontal connections varies in different layers of V1. Using
 735 bidirectional tracers (which label both axon terminals anterogradely and cell bodies
 736 retrogradely), Angelucci et al. (2002) showed average horizontal extents of 3 mm (radius
 737 from the injection site) in L2/3, 3.4 mm in L4B/upper 4C α , and 4 mm in L5/6. The largest
 738 axonal extents in these layers were 4.5, 5.0 and 4.8 mm, respectively. In contrast,
 739 connections in the remainder of L4C seem to be highly local, extending laterally mainly

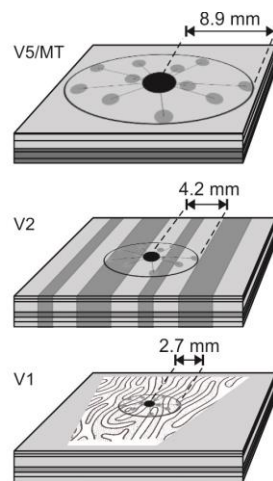
740 within one functional column (up to 0.2 mm radius, Fiskens et al., 1975; Katz et al., 1989).

741 The number of synapses between any two horizontally connected cells appears to be
 742 very low: only 2 out of 33 postsynaptic dendritic branches (sample of two neurons)
 743 received two inputs from the same presynaptic neuron (McGuire et al. 1991). This study,
 744 however, looked only at single branches and, thus, could not exclude targets on different
 745 dendritic branches of the same postsynaptic cell.

746

747 Functional organization of horizontal connections

748 Figure 4 depicts the relative extent of horizontal connections in V1, V2 and V5, and
 749 Table 4 summarizes key measurements. Horizontal connections extend over progressively
 750 larger distances in higher-order areas (Amir et al. 1993).



751

Figure 4. Extent of intra-areal horizontal connections in the tangential domain of areas V1, V2 and V5.

Horizontal connections in V1 are most prominent in L2/3 and 5 but exist also in L4B/upper 4C α and 6 (Amir et al. 1993; Angelucci, Levitt, Walton, et al. 2002). In V2, horizontally spreading connections emerge from L2, L3 and some from L5 and L6 (Levitt, Yoshioka, et al. 1994). In V5, locally projecting neurons are predominantly found in L2 and L3 and, following deep layer injections, also in L6 (Ahmed et al. 2012).

In the center of each cortical slab is a halo (*black dot*) of dense, unspecific local connectivity, surrounded by more specific patches of terminal clusters (*gray dots*). In V1, the ocular dominance pattern (modified from LeVay et al. 1975), and in V2 the schematics of the CO bands, are approximately at scale. In V5, the darker shading in layers 4-6 depicts heavier myelination. The horizontal connection extents are average maxima across studies from *M. Fascicularis* and *M. Mulatta*: V1, (Amir et al. 1993; Angelucci, Levitt, Walton, et al. 2002), V2 (Amir et al. 1993), V5 (Ahmed et al. 2012).

752

Table 4. Summary of horizontal connectivity. Mean (range) across studies. Distances are in mm. Data from 1. Amir et al. 1993; 2. Malach et al. 1993; 3. Levitt, Yoshioka, et al. 1994; 4. Yoshioka et al. 1996; 5. Angelucci, Levitt, Walton, et al. 2002; 6. Ahmed et al. 2012.)

	V1	V2	V5
Most distant terminal cluster	2.7 (2.1-2.9)	4.1 (4.0-4.2)	8.9
Anisotropy ratio	1.7 (1.6-1.8)	1.6	1.2
Cluster size	0.21 (0.18-0.23)	0.25 (0.25-0.25)	0.52
Inter-cluster separation	0.61	0.88 (0.60-1.15)	2.3
References	1-2,4-5	1,3	6

753

754 In layers 2/3 of V1, horizontal connections labeled by retrograde tracer injections into
755 V1 form patches of axon terminals and somata around the injection site (Rockland and
756 Lund 1983; Angelucci, Levitt, Walton, et al. 2002; Tanigawa et al. 2005). Single tracer
757 injections label on average 11 (range 3-21) patches (Yoshioka et al. 1996; Tanigawa et al.
758 2005), each about 0.1-0.2 mm wide, which repeat at 0.5-0.6 mm intervals (Rockland and

759 Lund 1983). The 0.2 mm patch diameter matches the width of the dendritic fields of
760 pyramidal cells in the supragranular layers, and, together with the characteristic interpatch
761 distance, reflects the preference of these connections to link V1 domains with similar
762 functional tuning (Malach et al. 1993; Yoshioka et al. 1996). Patchy horizontal
763 connections are also prominent in L5 (Lund et al. 1993).

764 Tracer injections targeted to specific orientation-preference domain in the V1
765 orientation map send horizontal connections preferentially (70%) to other V1 domains
766 with similar orientation preference ($\pm 45^\circ$) as that of the injected site. In the local
767 neighborhood of the injected site the connection targets show wider orientation diversity
768 (Malach et al. 1993).

769 Horizontal connections in V1 layer 2/3 also prefer domains of similar ocular
770 dominance (OD) and CO compartment (blob/interblob, Livingstone and Hubel 1984b;
771 Yoshioka et al. 1996). Tracer injections targeted to a specific OD column resulted in
772 labeled patches of horizontal connections, of which on average 54% resided in the
773 surrounding OD columns representing the same eye territory, 18% at the border between
774 the left and right eye representation, and 28% in the opposite eye territory. For tracer
775 injections targeted to blob/interblob domains, 71% of connection targets remained in the
776 same domain, the rest were located at blob/interblob borders or into the opposite CO
777 compartment (Yoshioka et al. 1996).

778 Taken together, in layers 2 and 3 of V1 the horizontal connectivity is locally (within
779 dendritic and axonal field) not specific to functional domains, but long-range connections
780 form terminal patches with a preference for similar-domain cells.

781 In thalamorecipient L4C β , the dendritic fields of both spiny and non-spiny stellate
782 cells seem to avoid crossing OD boundaries, whereas axons of both cell classes cross to
783 the opposite domain. Since these axons are only about 100 μ m long, they nevertheless

784 mainly remain in their home eye column (Katz et al. 1989). Functionally, this results in
785 strictly monocular cells in this layer (Hubel and Wiesel 1968).

786 Horizontal connections in layers 4B/upper4C α also show some domain-specific
787 clustering. When columnar tracer injections encompass L2 to upper L4C α , the clusters of
788 horizontal connections in L2/3 and those in L4B/upper4C α are vertically aligned, but
789 clusters in L4B/upper4C α are band-like rather than patch-like as in L2/3 (Angelucci,
790 Levitt, and Lund 2002; Lund et al. 2003).

791 In L6, a specialized class of large pyramidal Meynert cells shows little clustering of
792 their horizontal connections and appear to form diffuse terminations (Li et al. 2003). In
793 other layers, the horizontal connectivity in relation to functional domains has not been
794 systemically studied.

795 The distribution of horizontal connections is anisotropic. The ratio between the long
796 and short axes of the antero- and retrogradely-labeled connection fields ranges from 1.5 in
797 L4B/upper 4C α to 1.8 in L5/6 (Angelucci, Levitt, Walton, et al. 2002). Interestingly, the
798 visual field representation of these horizontal connection fields appears isotropic, i.e. their
799 spatial anisotropy in cortex translates to an isotropic distribution in visual field. This
800 results from the anisotropic columnar organization in V1, primarily due to the OD
801 columns, interrupting an otherwise smooth retinotopic representation (Blasdel and
802 Campbell 2001).

803 In V2, horizontal connections are also patchy (Rockland 1985; Amir et al. 1993;
804 Levitt, Yoshioka, et al. 1994). From each injection site, efferent axons travel in layers 1-3
805 to form 10-15 terminal patches, each 0.25-0.3 mm wide. The patches are found up to 4
806 mm away from the injection site, with a gamma-like, positively skewed, distribution,
807 peaking at 1 mm distance. The patches form an oval field, with median longer/shorter
808 axis ratio of 1.6 (range 1-3.8), and the longer axis of the field being oriented orthogonal to

the CO stripes. Given the anisotropy of visual field representation in V2, due to the presence of CO stripes, the connections seem to connect roughly a circular area of visual field. After tracer injections confined to the upper layers, some labeled horizontal connection are also observed in L5.

The stripe specificity of horizontal connections in V2 remains unclear. It appears that over short distances, they cross CO stripe boundaries (Levitt, Yoshioka, et al. 1994), but over longer projection distances they preferentially target the same stripe type as that of the injected site (Baldwin et al. 2012). Interestingly, GABAergic connections seem to create an oval-shaped connectivity along, rather than across, the CO stripes, in contrast to excitatory connections (Kritzer et al. 1992); their maximum lateral spread is also shorter, 1.4 mm in superficial layers and 1.1 mm in the infragranular layers. Functionally, this difference in excitatory vs. inhibitory topography would seem to indicate that V2 excitatory horizontal connections combine signals from different visual processing streams, while the more local inhibitory connections suppress nearby activation within one stream.

In V5, horizontal connections form the longest-range connections, with clusters up to 10 mm from the injection site (Ahmed et al. 2012). A tracer injection in the upper layers labels horizontal connections that are restricted to supragranular layers, whereas a tracer injection in the deep layers labels horizontal axons in both supragranular and L6 neurons with a similar distribution of clusters (mean space between clusters 2 mm).

Overview of interlaminar connections

Interlaminar connections in V1 and V2 (Figs. 2 *middle, bottom*, Supplementary Table 1B-D) have been previously reviewed (Gilbert 1983; Lund 1988; Lund et al. 1994; Levitt et al. 1996; Callaway 1998a; Douglas and Martin 2004). We found no intrinsic

834 interlaminar connectivity studies of macaque V5.

835 From a modeling perspective, it is interesting that lamination might reflect a
 836 developmental hierarchy. The major laminar borders and layer-specific connections
 837 develop first, guided by ontogenetic molecular markers, whereas sublamina-specific
 838 connectivity (e.g. axons targeting 3 vs. 4B, 4C α vs. 4C β) might emerge postnatally,
 839 guided by either molecular markers or visual input (Callaway 1998b). Eventually,
 840 interlaminar connectivity becomes highly complex with multiple unique combinations of
 841 layer inputs (Sawatari and Callaway 2000; Nassi and Callaway 2009).

842 The excitatory and inhibitory local circuit neurons have been clearly distinguished in
 843 the literature, as light and electron microscopic observations allow straightforward
 844 identification of excitatory cells, as having spinous dendrites and forming asymmetric
 845 synapses, in contrast to inhibitory cells which instead have smooth dendrites and form
 846 symmetric synapses. However, there are sparser data describing the extent of axonal
 847 spread in a target layer. Moreover, in these studies, cell samples were typically small,
 848 precluding statistical analyses, and the distance covered by the projecting axons is often
 849 reported only as largest extent within the small sample. An even greater challenge is the
 850 classification of inhibitory and excitatory cells into different morphological subtypes and
 851 describing the subtype-specific connectivity. While attempts to classify neurons into
 852 distinct subtypes have been made, the relative proportions of the different subtypes and
 853 the statistics of their inputs and outputs is sporadic and largely missing in macaques.
 854 However, a general rule that has emerged from these studies is that both excitatory and
 855 inhibitory neuron types typically project strongly within their home layer.

856

857 Excitatory interlaminar connections

858 In Figure 2 (*Middle*) and in Supplementary Table 1 B, we report, separately for V1 and

859 V2, the layer location of the somata giving rise to interlaminar projections and a semi-
860 quantitative description of their axonal target layers.

861 **V1 excitatory neuron connectivity.** Excitatory neurons in L4C α and L4C β project
862 strongly to their home layer, but they also target 4Cm, a sub-layer of cells which occupies
863 the middle of L4C between the α and β sub-layers, and which receives only sparse direct
864 LGN connections. L4C α sends robust projections to layers 3B and 4B, which align with
865 CO blobs, but sparser projections also to other layers, except L1 and 5B. L4C β sends a
866 robust projection to L3B, which instead aligns with both interblobs and blobs. L4C β also
867 sends more moderate projections to other layers, except 1 and 5B. The L3B blob and
868 interblob compartments seem to distribute efferent connections primarily to
869 corresponding blob or interblob compartments, respectively, in other layers (2/3A, 4B
870 (sparse) and 5), and L3B interblob neurons in addition project to 5A. L2/3A interlaminar
871 connections are partially selective for blob/interblob divisions, emphasizing connections
872 within their home compartment, but not totally avoiding crossing CO boundaries. L4A,
873 which receives direct LGN Parvo input, projects to L3B interblobs, but also to layers
874 2/3A, 4B and 5A. Cells in L4B blobs seem to be targeting mainly interblobs within 4B
875 itself and in L5; in contrast, cells in L4B interblobs target primarily interblobs in these
876 layers. L4B projections to layers 2/3A and 3B, instead, terminate in CO blobs, regardless
877 of whether their soma sits in a blob or interblob column. However, Yarch et al. (2017)
878 have recently shown that the L4B output cells that project to the thick CO stripes of V2
879 do not obey this local L4B to L3-blob connectivity rule; instead, these cells have somata
880 that typically lay at a blob border or an interblob, and in L3 they avoid blobs but project
881 to the same CO compartment where their soma resides, i.e. blob border or interblob.

882 L5A and 5B neurons seem to be widely projecting to supragranular and granular
883 layers, avoiding, however, L4Cm. L5A and 5B both send some axons to L6, too. L6 cells

884 are connected to almost all other layers, with some emphasis on L4C.

885 In V1, the mutual connectivity between the L5 and 6 sublayers has not been studied.
 886 Sub-layers 5A and 5B are most likely highly interconnected (Kisvarday et al. 1989;
 887 Briggs and Callaway 2005), but this has not been explicitly studied. The illustrations in
 888 Wiser and Callaway (1996), together with the quantification of pyramidal cell types in
 889 L6A, L6m and L6B seem to suggest that there is dense mutual sublayer connectivity
 890 between these L6 subdivisions.

891 L6 pyramidal cells have been classified into subgroups based on their specific laminar
 892 targets (Wiser and Callaway 1996). L6 neurons target either the L4C sublayers and L4A
 893 in different combinations avoiding all other layers (type I) or avoid L4C and show strong
 894 mutual connectivity within L6 (type II). The L6 projections to CO blobs vs. interblobs
 895 seem to be nonspecific (Wiser and Callaway 1996) and only a subset of type I pyramids
 896 project selectively to particular OD columns in L4C (Wiser and Callaway 1997).

897 **V2 excitatory neuron connectivity.** For V2 interlaminar connections, we found only
 898 three studies (Valverde 1978; Lund et al. 1981; Levitt, Yoshioka, et al. 1994), limiting the
 899 robustness of the connectivity graph and especially the classification of connection
 900 strength (Fig. 2 *Middle*, Supplementary Table 1B). First, local excitatory connections
 901 show the typical intralaminar self-connectivity. Input layer 4 sends projections to
 902 supragranular layers, whereas no direct infragranular projection has been reported from
 903 this layer. L3B connects to layers 3A, 5A and 2. L3A projects to L3B, 2 and 5B. L2 sends
 904 axonal projections to every layer except 5A. L5A connects back to L4 and sends
 905 projections to both 3A and 3B. L5B projects to layers 3A and 3B. Finally, L6 sends
 906 efferent axons to all other layers, except L1.

907

908 Inhibitory interlaminar connections

909 Jennifer Lund and colleagues studied the inhibitory neurons and their interlaminar
 910 connections of V1 in a series of four papers (Lund 1987; Lund et al. 1988; Lund and
 911 Yoshioka 1991; Lund and Wu 1997), based on Golgi impregnation of thick tissue sections
 912 and reconstructions of single neurons within single sections. The limitations of these
 913 studies are the incomplete impregnation and the fact that neurons cannot be reconstructed
 914 beyond individual impregnated sections, therefore leading to incomplete neuron
 915 reconstructions. The inhibitory local circuit neurons of V2, instead, have been studied
 916 mainly together with excitatory neurons (Valverde 1978; Lund et al. 1981; Levitt,
 917 Yoshioka, et al. 1994). Kritzer et al. (1992) used 3H-nipecotic acid to retrogradely label
 918 GABAergic cells. Their data suggest that inhibitory connections are made nearly across
 919 all layers in both V1 and V2, with the probability of connections decreasing with laminar
 920 distance. This is consistent with data in rodents (Markram et al. 2015). Due to poor
 921 confinement of tracer injections to single layers in Kritzer et al. (1992), in Figure 2 and
 922 Supplementary Table 1 we have omitted most data from this study.

923 **V1 inhibitory neuron connectivity.** The dendritic fields of inhibitory interneurons
 924 often spread vertically outside the layer where the parent soma is located (Lund 1987).
 925 Albeit spreading to other layers, the dendritic fields spread uniformly, sampling
 926 apparently unselectively across their depth. Horizontally, the dendritic fields of smooth
 927 inhibitory neurons in supragranular layers 1-4B are local, measuring 250-350 μm in
 928 diameter (Lund and Yoshioka 1991; Lund and Wu 1997).

929 It is safe to claim that more than half of the inhibitory synapses are formed within the
 930 layer of the parent soma. The exceptions in Figure 2 (*bottom*) and Supplementary Table 1
 931 are L1, for which sparse data do not allow quantitative estimates, and L4A, which is too
 932 narrow to include most of the local axonal tree. In contrast to dendrites, the axons may

933 also cross layers, but without sprouting, targeting specific upper or lower layers. A subset
 934 of inhibitory neurons with somata either in L4C α or L4C β sends axons to the opposite
 935 geniculo-cortical stream (i.e. L4C α \Rightarrow L4C β , L4A or L4C β \Rightarrow L4C α), potentially
 936 causing cross-inhibition between the Magno and Parvo streams (Lund 1987).
 937 Horizontally, the axons of inhibitory neurons may spread considerable distances, albeit
 938 much less than the horizontal spread of excitatory cells; the largest distances are reached
 939 by the L2/3 wide-arbor Basket cells, whose axon terminals may reach up to 1.5 mm from
 940 the soma (Lund and Wu 1997).

941 The layer-specific connectivity in relation to CO compartments has not been
 942 extensively studied for inhibitory interneurons, thus this is omitted in Fig. 2 (*bottom*).
 943 Overall, however, the few available studies seem to indicate that inhibitory connections
 944 preserve CO specificity (Kritzer et al. 1992), similar to excitatory neurons.

945 L4C α interneurons connect to all 4C sublayers, as well as to layers 4B, 4A, 3B, 5A,
 946 and the bottom of L6. Sparse axonal projections from L4C α target, in addition, layers 5B
 947 and 6A. L4C β interneurons show similar connectivity as those of 4C α , but with emphasis
 948 on L6A instead of 6B, and a missing projection to L4B.

949 L4B interneurons target layers 3B, 4A, both 5A and 5B and all L6 sublayers. Sparse
 950 projections reach L1 and L2/3A. L4A inhibitory neurons have similar targets as those of
 951 L4B. In contrast to L4B, L4A inhibitory neurons send weaker projections to L6, while
 952 targeting L4C (4Cm, as well as, weakly, 4C α and 4C β). L3B inhibitory neurons target
 953 predominantly L4A, and moderately layers 2/3A, 4B, 4Cm, 5A and 5B, and all three
 954 sublayers of L6. L2/3A interneurons send dominant projections to layers 1, 3B, 4A, 4B
 955 and 5B, and sparse connections to L6. L1 interneurons send axons to layers 2/3A, 3B and
 956 4B, but not to L4C or infragranular layers. L5A sends inhibitory axons to layers 1, 3B, as
 957 well as to all L4C and L6 sublayers. L5B is very different from 5A, as it sends inhibitory

axon projections to layers 2/3A, 5A and 6A, and sparse projections to 3B, 4A, 4B, and the bottom two L6 sublayers. L6 interneurons project to layers 4A, all 4C sublayers, 5, and heavily to all L6 sublayers.

The two most apparent distinctions between inhibitory and excitatory intrinsic connectivity within V1 are in L1, which has more extensive inhibitory than excitatory connectivity, and in L6, which inhibits only the thin L4A, but excites most supragranular layers. Horizontally, the inhibitory connections do not seem to form terminal axon clusters, as excitatory neurons do, but their axon density decreases continuously as a function of distance (Kritzer et al. 1992).

Lund et al. (1988) suggested that some L5B inhibitory neurons send axons to the white matter, which would be an important exception to the rule that all white matter tracts are excitatory. Later, long-range inhibitory projections have been found in many species and systems (Caputi et al. 2013) but they are sparse, originating from about 0.5% of neocortical GABA neurons in mice (Tamamaki and Tomioka 2010). In macaques, long-distance projecting inhibitory neurons are predominantly inside the white matter (81%) and in the gray matter they reside predominantly in L3 (12%; L1 0.5%, L2 3%, L5 2%, L6 1.5%, L4 none, Tomioka and Rockland 2007). The functional role of these neurons has remained unknown.

V2 inhibitory neuron connectivity. In V2, the inhibitory connectivity graph is sparse due to availability of only sparse data and will likely need to be modified when new data will become available. The extensive connectivity of L4 is mainly reported in Kritzer et al. (1992), but the ³H-nipecotic acid retrograde tracing data seem to show an overall more diffusely connected system across layers than, e.g. the Golgi stained single cell data of Lund et al. (1981).

983 Interlaminar feedback

984 Despite the paucity of data on V2 excitatory interlaminar connectivity compared to
985 V1, some similarities between the two areas are apparent.

986 The input layers 4C and 4 in V1 and V2, respectively, preferentially target the
987 supragranular layers, particularly 3B, but also 3A and 2. In contrast, L2 avoids projecting
988 back to these input layers. Given the lack of direct L2 FB to L4, it may be interesting to
989 investigate whether L2 provides FB-like inputs to other layers.

990 L6 projects to all layers containing excitatory neurons. Given the large RFs and their
991 broader tuning in L6 (Gur et al. 2005), L6 interlaminar projections could provide fast
992 intracolumnar FB inputs relaying local contextual information to more sharply tuned cells
993 in other layers. Moreover, as V1 L6 (together with L1) is a major recipient of inter-areal
994 FB projections arising from higher visual areas (as discussed above), L6 is also in a
995 position to relay global contextual information (arising from the “far surround” of V1
996 neurons) to all V1 layers to which it projects. This idea is consistent with the observation
997 that V1 L6 (but also L1) shows the shortest onset latency of local field potential (LFP)
998 responses (i.e. is activated earlier than other layers) following presentation of a visual
999 stimulus in the far RF surround of neurons in a recorded V1 column (Bijanzadeh et al.
1000 2018). These early far-surround responses in V1 L6 (and L1) are thought to be generated
1001 by inter-areal FB connections from extrastriate cortex (Angelucci, Levitt, Walton, et al.
1002 2002; Angelucci and Bressloff 2006; Angelucci et al. 2017).

1003 Anatomical reconstruction of microcircuits remains a challenge. Here, we have
1004 reviewed studies, most of which are based on injections of neuroanatomical tracers
1005 followed by microscopy analysis of labeled tracts or reconstructions of single labeled
1006 neurons across serial tissue sections. These approaches have well recognized limitations,
1007 for example difficulty and errors in serial section reconstruction of single neurons,

variability in tracer transport across injections and animals, etc. Serial block surface imaging with electron microscopy (EM) allows for accurate and high resolution 3D reconstruction of circuits, at the level of synapses (Denk and Horstmann 2004), and recently automated transmission EM has allowed synapse-level analysis of excitatory network in rodents (Lee et al. 2016). These methods are, however, difficult to apply to large tissue blocks, e.g. encompassing macaque V1, let alone the whole macaque visual cortex. Recently developed methods based on viral vector-mediated high-resolution fluorescent labeling of neuronal circuits (Luo et al. 2008), followed by tissue clearing, to render intact tissue blocks optically transparent (Chung et al. 2013), and deep-tissue imaging (Denk et al. 1990; Stelzer 2015), to image labeled neurons through intact tissue blocks, are making it possible to characterize primate and even human (Mortazavi et al. 2019) brain circuits at cellular resolution. However, lack of algorithmic and computational solutions to visualize, analyze and reconstruct the massive amount of neuronal data that are being collected remains a major challenge that requires development of cyberinfrastructure and computational approaches (Venkat et al. 2016; Petruzza et al. 2017, 2018).

Functional anatomy

Cell structure and synaptic coverage

The heterogeneity of cellular structures and their development across brain areas has been previously reviewed (Elston 2003; Elston and Fujita 2014). In V1, dendritic morphology does not seem to change as a function of RF eccentricity. V1 L3 pyramidal neurons show similar number of dendritic branches, total dendritic length, and basal dendritic fields across eccentricities (Oga et al. 2016).

In contrast, along the hierarchy of visual areas dendritic field size and complexity

increase. For L3 pyramidal cells, the area of basal dendrites, which form the largest extent of horizontal dendritic field coverage, increases from V1 ($36 \pm 5.5 \times 10^3 \mu\text{m}^2$; range 27-49 $\times 10^3 \mu\text{m}^2$) to V2 ($45 \pm 10 \times 10^3 \mu\text{m}^2$; range 18-66 $\times 10^3 \mu\text{m}^2$), to V5 ($84 \pm 11 \times 10^3 \mu\text{m}^2$; range 56-104 $\times 10^3 \mu\text{m}^2$; Elston and Rosa 1997). Moreover, there are more dendritic branches per unit area in V5 than in V1 or V2.

The L3 pyramidal neuron basal dendritic field area is somewhat larger in the CO blobs ($27 \pm 11 \times 10^3 \mu\text{m}^2$; range 5-49 $\times 10^3 \mu\text{m}^2$) of V1 compared with the interblobs ($20 \pm 10 \times 10^3 \mu\text{m}^2$; range 6-51 $\times 10^3 \mu\text{m}^2$; Elston and Rosa 1998). There was a similar trend for larger dendritic fields in the V2 thin stripes compared with pale stripes, but without statistical significance.

The V1 L5 pyramidal cell basal dendritic area ($40 \pm 19 \times 10^3 \mu\text{m}^2$; Oga et al. 2017) is comparable to that of L3 mentioned above.

The total length of the apical dendrite of V1 L3 pyramidal neurons averages (mean \pm SD) $1,530 \pm 114 \mu\text{m}$ (trunk 9% of total length, oblique branches 50% and tuft 41%) with 15.3 ± 1.2 branch points, and the total length of the basal dendrites averages $1,659 \pm 138 \mu\text{m}$ with 16.8 ± 1.8 branch points (Gilman et al. 2017). The apical dendrites have on average 855 ± 92 spines, and the basal dendrites $1,030 \pm 157$ spines.

The apical dendrite spine necks, retrieved from two pyramidal cells in V1 L3, range from 0.2 to 1.2 μm in width, most being 0.4-0.8 μm (McGuire et al. 1991).

The proportion of LGN afferent synapses relative to the total number of synapses (summarized in Peters et al., 1994) in Magno-recipient L4C α was originally reported to be between 1.3-1.9% (18-40/neuron), and in Parvo-recipient L4C β 3.7-8.7% (37-191/neuron; O’Kusky and Colonnier 1982b; Beaulieu et al. 1992). The corresponding number of synapses per number of neurons were (mean \pm SD) $1.9 \pm 0.2 \times 10^3$ in L4C α , and $1.4 \pm 0.2 \times 10^3$ in L4C β (O’Kusky and Colonnier 1982b). A recent quantitative 3D

microscopy study (Garcia-Marin et al. 2017) reported higher average thalamocortical synaptic densities: 0.46 (range 0.39 - 0.53) $\times 10^8/\text{mm}^3$ in $L4C\alpha$, and 0.82 (range 0.70 - 0.93) $\times 10^8/\text{mm}^3$ in $L4C\beta$. These densities correspond to 15% of all excitatory synapses in $L4C\alpha$ (197 /neuron), and 20% in $L4C\beta$ (200 /neuron) being thalamocortical synapses, suggesting a much stronger thalamocortical drive than previously assumed. In $L4A$ the thalamocortical synapses had an anisotropic honeycomb arrangement, with thalamocortical synaptic density of 0.35 (0.23 - 0.49) $\times 10^8/\text{mm}^3$. In $L6$ the corresponding density was 0.13 (0.08 - 0.16) $\times 10^8/\text{mm}^3$.

There might be a trend for higher inhibitory synaptic coverage of the spiny stellate cell somas compared with pyramidal cell somas. Otherwise different layers and animals showed variable (between 20-60% of circumference) inhibitory synapse coverage of their somata (Lund et al. 2001).

Although $V1$ $L2$ - 3 CO blobs and interblobs differ in several physiological properties, their pyramidal neurons show no significant difference in soma area, spine density, number of basal dendrites, dendritic radius, or dendritic branching pattern (Hubener and Bolz 1992). Moreover, the dendritic fields of the pyramidal cells cross blob boundaries suggesting continuous dendritic sampling.

Proportions and synaptic densities of excitatory and inhibitory connections in

$V1$

About 85-90% of $V1$ connections are excitatory, forming asymmetric synapses with postsynaptic cells, the rest being inhibitory, i.e. forming symmetric synapses (Fisken et al. 1975; Medalla and Luebke 2015). The horizontal and interlaminar connections seem target dendritic spines and shafts in similar proportions. Labeling single $V1$ $L3$ pyramidal cells by intracellular injections of HRP ($N=2$), McGuire et al. (1991) studied both local

and long-range excitatory connections of layer 2/3 PCs and found that 75% of synapses are made onto dendritic spines and 25% onto shafts. This is consistent with the overall population of V1 layer 2/3 excitatory neurons, which make 75% of their synaptic contacts onto dendritic spines, with a mean density of $365 \pm 54 \times 10^6$ synapses / mm³ (mean \pm SEM), and 25% with shafts, with a mean density of $119 \pm 10 \times 10^6$ / mm³ (Medalla and Luebke 2015). Inhibitory neurons, instead, target spines more seldom (34%; mean density of $33 \pm 7 \times 10^6$ / mm³) than dendritic shafts (66%; $62 \pm 24 \times 10^6$ / mm³, Medalla and Luebke, 2015). Although lower in volumetric density, the density of synapses along inhibitory cells' dendritic shafts (average of 1.9 synapses/ μ m, range 0.8-3.9 synapses/ μ m) is much higher than the density of synapses along excitatory cells' dendrites (average of 0.3 synapses/ μ m, range 0.1-0.5 synapses/ μ m, McGuire et al., 1991). A similar synaptic density was found on the cell bodies of the smooth inhibitory cells, with about 200-300 synapses over the whole soma surface.

Diversity of response properties in V1 and V2 layers

Layers 4C α and 4C β show response properties similar to those of their respective afferent Magno and Parvo LGN neurons (Blasdel and Fitzpatrick 1984). The minimum response field size of neurons (defined as the RF size measured using small bar or square stimuli) is about two times larger in L4C α than in L4C β . Correspondingly, the contrast threshold increases up to 3.5-fold from the top of L4C α to the bottom of L4C β . In supragranular layers, in both blob and interblob regions, cells receive input from both Magno- and Parvo streams (Nealey and Maunsell 1994).

Gur and colleagues (Gur et al. 2005; Gur and Snodderly 2007, 2008) measured RF properties of neurons in different V1 layers in alert monkeys and found significant variability. Orientation and direction tuning in V1 show high laminar variability, with the

1108 input layers, 4C α and 4C β , 4A and 6 housing less selective units (Gur et al. 2005). In
 1109 addition, the input layers show higher spontaneous firing rates [layer: mean (range across
 1110 cells) in light / mean (range) in darkness, Hz: L4A: 27 (1-74) / 24 (3-113); L4C α : 13 (<1-
 1111 52) / 10 (<1-28); L4C β : 30 (11-59) / 17 (5-28); L6: 13 (<1 – 27Hz) /10 (<1-25) Hz]
 1112 compared to the output layers whose mean firing rates are generally <1 Hz [L3: 3 (<1 –
 1113 14) / <1 (one cell); L4B: 1 (<1 – 3) / 1 (<1-3); L5: <1 (<1 – <1) / <1 (<1 – <1), from Fig
 1114 5 top in Snodderly and Gur 1995)]. The high spontaneous firing rate in the input layers
 1115 may be inherited from the LGN, where the mean spontaneous firing rate is about 13Hz
 1116 (Spear et al. 1994). Mapping RF size with bars of light increments or decrements, Gur et
 1117 al. (2005) found that V1 layers receiving direct input from LGN (L4A, L4C α , L4C β , L6)
 1118 have larger RFs than other layers (L2/3, L4B, L4Cm, L5). These findings challenged
 1119 earlier studies of layer 4C which reported much smaller RF sizes (Schiller et al. 1976;
 1120 Hubel and Wiesel 1977; Blasdel and Fitzpatrick 1984). This discrepancy can perhaps be
 1121 attributed to the effects of anesthesia in the earlier studies, which is known to alter LGN
 1122 activity and multiple RF properties downstream of LGN (Gur et al. 2005). As an
 1123 alternative explanation, the discrepancy may emerge from less accurate laminar
 1124 differentiation and RF mapping in awake animals. Moreover, the method and visual
 1125 stimuli used to map RF size affect the measurements (Angelucci and Bressloff 2006). For
 1126 example, estimates of RF sizes based on the cortical spread of deoxyglucose uptake
 1127 (Tootell, Switkes, et al. 1988) allows accurate laminar definition and indicate that layers 2
 1128 and 6 have the widest RFs (spread could not be quantified), followed by L5 (half the
 1129 spread from the edge of the stimulus, about 0.5 mm). L4C α and L4B show intermediate
 1130 spread (0.35 and 0.33 mm, respectively), followed by L3 (0.24 mm), and last L4C β (0.14
 1131 mm). Importantly, RF sizes vary by a factor of over 10 within layers (Dow et al. 1981;
 1132 Van Essen and Newsome 1984). Given the inverse relationship between spatial frequency

and the RF size (Teichert et al. 2007) spatial frequency data suggests that large RFs are horizontally clustered into CO blobs (Tootell, Silverman, et al. 1988).

Most V1 laminae have a median circular variance, a measure of orientation selectivity ($CV = 1 - \text{orientation selectivity index}$), close to 0.5, but in L3B CV reaches up to 0.75, i.e. L3B is less orientation selective (Ringach et al., 2002). L4 has an intricate parcellation, with layers 4A, 4C α and 4C β having higher CV values, and 4Cm much smaller values (Gur et al. 2005). Overall, L4Cm, the sublayer located between 4C α and 4C β , behaves like a non-input layer: it has small RFs, sharp orientation and direction tuning and low spontaneous activity.

Direction selectivity emerges first in layer 4C α , and thereafter highly direction selective cells are found in L4Cm, L3, L4B and L6 (Gur and Snodderly 2007). Downstream from L4C α , the L4Cm projects to L3, and it has been proposed to represent a third motion pathway from V1 to V2, in addition to the monosynaptic motion pathways arising from direction selective cells in layers 4B and 6 (Gur and Snodderly 2007). In addition to high direction selectivity, cells in L3 show high orientation selectivity and small RFs.

Although typically studied together, L2 is functionally distinct from L3. L2 has higher levels of ongoing activity, less spatially selective RFs, lower orientation selectivity and no direction selectivity (Gur and Snodderly 2008), thus, resembling more the input than output layers of V1.

In V2, the tuning properties of neuronal RFs in different layers show greater similarity than in V1 (Tootell and Hamilton 1989), but L3 has the largest proportion of neurons tuned for visual stimulus parameters (Shipp and Zeki 2002a). The layers receiving feedback (L1, L2, L5 and L6), show more often (27 vs 18%) combined tuning to chromatic and spatial features, suggesting higher-order feature binding in these layers

than in the layers receiving the feed-forward input (L4 and L3; Shipp et al. 2009).

Diversity of response properties in parallel pathways

As reviewed in Schiller et al. (1976), the input from the LGN is transformed into five main ways within V1. First, the concentric center-antagonistic surround RFs become a minority in V1, while orientation selectivity emerges. Second, many units become selective for motion direction. Third, many cells acquire “complex” RFs, i.e. they respond to both light increments and decrements in their RFs. Fourth, most cells become driven by both eyes and, fifth, become more selective for spatial frequency. In addition, some cells show double color opponency (Livingstone and Hubel 1984a), and most cells sum contrast non-linearly as a function of visual stimulus size (Sceniak et al. 1999; Angelucci, Levitt, Walton, et al. 2002; Cavanaugh et al. 2002).

The functional architecture of the macaque visual cortex and parallel processing strategies have been more extensively reviewed previously (Casagrande and Royal 2004; Roe 2004; Sincich and Horton 2005; Nassi and Callaway 2009). In brief, Figure 3 *top* depicts the parallel FF pathways from LGN to V1. Afferent geniculate connections from the two eyes remain segregated into OD columns in the input layers of V1 (Hubel and Wiesel 1968). CO blobs are prominent in layers 2/3, but to some extent visible also in layers 1, 4B, 5 and 6 in register with the L2/3 blobs (Horton 1984).

In V2, the CO stripes run orthogonally to the V1/V2 border (Tootell et al. 1983), and are visible, albeit weakly, in most layers and moderately in L4 (Balaram et al. 2014). Across V2, there are about 28 complete sets of CO stripes, a full stripe cycle encompassing on average 4 mm (Olavarria and Van Essen 1997). Table 5 presents a quantitative overview of early electrophysiological single unit recording studies showing the prevalence of various visual stimulus tuning properties in the different V2 stripes

(modified from Shipp and Zeki 2002a). Electrophysiological recordings have demonstrated that many visual response properties are present, albeit with differing prevalence, in all stripe types, and there has been much debate and controversy over the functional specificity, or lack thereof, of distinct stripes (Shipp and Zeki 2002a).

Intrinsic signal optical imaging (OI) is better suited than single unit recordings to reveal the predominant response within a neuronal population and, in addition, it allows investigations of the spatial layout of particular visual responses (Blasdel and Salama 1986; Grinvald et al. 1986; Ts'o et al. 1990). This technique has revealed that while neuronal responses to the various visual stimulus parameters are present in most CO compartments, only some of these parameters are systematically mapped within a given compartment.

Figure 3 *right* lists the functional feature selectivity and maps found in the various CO compartments of V1 and V2. Unfortunately, macaque V5 is buried within the superior temporal sulcus, and thus is not accessible to OI. In V1, OI has revealed multiple, and at least partially independent, spatial representations or maps of visual stimulus features, including ocular dominance (Blasdel and Salama 1986; Bartfeld and Grinvald 1992; Blasdel 1992), orientation (Bartfeld and Grinvald 1992; Blasdel 1992; Ramsden et al. 2014; Felleman et al. 2015), motion direction (Lu et al. 2010; Hu et al. 2018), binocular disparity (Ts'O et al. 2001; Chen et al. 2008), color (Ts'O et al. 2001; Landisman and Ts'o 2002; Xiao et al. 2003, 2007; Lu and Roe 2008) and brightness/luminance (Roe et al. 2005; Wang et al. 2007) maps.

Based on microelectrode recordings by Hubel and Wiesel (1974a) Braitenberg and Braitenberg (1979) suggested that iso-orientation domains are arranged around orientation singularities. This local “pinwheel-like” organization of orientations was later confirmed by optical imaging of intrinsic signal (Blasdel and Salama 1986; Ts'o et al. 1990; Malach

et al. 1993; Landisman and Ts'o 2002; Nauhaus et al. 2008) and two-photon imaging (Nauhaus et al. 2012); for a critical and quantitative analysis of data and models, see (Obermayer and Blasdel 1993; Erwin et al. 1995).

Many studies have examined the relative spatial relationships between these various feature maps in V1. CO blobs (Horton and Hubel 1981) and orientation pinwheel centers (Bartfeld and Grinvald 1992) lie close to the center of OD bands [(the latter 300-670 μm wide (LeVay et al. 1975; Horton and Hocking 1996)], but it has remained controversial whether CO blobs and pinwheel centers align with each other (Bartfeld and Grinvald 1992; Blasdel 1992; Obermayer and Blasdel 1993; Lu and Roe 2008). This controversy may have been aggravated by spatial low-pass filtering of neural responses by optical imaging method which may cause systematic shift of pinwheel centers (Polimeni et al. 2005). In our unpublished data (Merlin et al. 2012), we find a strong association between CO blobs and pinwheel centers, with 85-90% of blobs containing a pinwheel center. However, as pinwheel centers are more numerous than CO blobs in V1, only about 50% of pinwheel centers reside in blobs, therefore suggesting at least partially independent representations of orientation and CO blob maps. The CO blobs seem to coincide with color patches revealed by OI (Lu and Roe 2008), and each color patch contains an orderly and overlapping mapping of responses to distinct hues (Xiao et al. 2007). Despite this partially independent spatial arrangement between orientation pinwheels and color patches, many neurons in V1 are tuned both to color and orientation (Garg et al. 2019).

OI studies have shown that in V2 each CO stripe contains distinct feature maps. Each thick stripe contains one or more (200 μm wide x 1 mm long) topological representation of horizontal retinal disparities (Chen et al. 2008), and a pinwheel-like (about 1 mm wide) or linear representation of different motion directions (Lu et al. 2010). In addition, thick stripes contain ordered orientation maps which have diameter of 0.7-1.5 mm (Ts'O et al.

2001). Orientation domains are also found in the pale stripes, in response to both real and illusory contours (Ramsden et al. 2014). Thin stripes represent hue in a systematic fashion [0.07-0.32 wide x 1.3 mm long bands of varying shape (Xiao et al. 2003)], as well as brightness increments/decrements, the latter forming distinct domains about 0.7 mm apart (Wang et al. 2007).

Table 5. Functional selectivity of V2 stripes. Median % (range) of cells tuned to the specific visual stimulus parameter (single or multi-unit recordings) across seven electrophysiological studies published up to 2002. Modified from the summary of (Shipp and Zeki 2002a). The definitions of tuning and stripe type varied between studies. * Disparity or binocular interaction. Data originally from: 1. DeYoe and Van Essen 1985; 2. Peterhans and von der Heydt 1993; 3. Levitt, Kiper, et al. 1994; 4. Munk et al. 1995; 5. Roe and Ts'o 1995; 6. Gegenfurtner et al. 1996; 7. Shipp and Zeki 2002a.

	Thick	Thin	Pale	References
Orientation	85 (51-88)	41 (20-73)	80 (17-96)	1-7
Direction	29 (11-60)	6 (0-21)	13 (0-34)	1-4, 6-7
Color	16 (7-39)	63 (53-86)	27 (12-64)	1,3-7
Disparity*	68 (38-77)	21 (10-33)	15 (1-22)	1-2,5

Physiology

Conduction velocities and latencies

The hierarchy of anatomical connections suggests that areas higher in the hierarchy have increasingly longer response latencies to visual stimulation. Experimental evidence supports this claim to some extent for the areas in the occipitotemporal ventral stream, but

not for the areas in the parietal and frontal dorsal stream (Schmolesky et al. 1998). In the LGN, the Magno pathway has about a 20-ms lead in response onset relative to the Parvo pathway. In V1, magnorecipient L4C α has a corresponding 20-ms lead relative to parvorecipient L4C β (Nowak et al. 1995). This segregation of latencies continues in the distinct functional compartments of V2 (Bullier and Nowak 1995). Interestingly, the inhibitory responses are as early as the excitatory responses, and the shortest latencies in V2 are in the infragranular layers (Nowak et al. 1995). Thereafter, cortical latencies show a wide distribution (Nowak and Bullier 1997; Schmolesky et al. 1998).

Intracortical conduction velocity has been measured for connections between V1 and V2 (Girard et al. 2001). The following values are a lower bound for the true velocities, because they were estimated assuming direct connections in Cartesian 3D space. The median FF conduction velocity was 3.7 m/s (range 3 – 6 m/s), and the FB conduction velocity 3.4 m/s (range 1.5 – 9.5 m/s). This is very fast compared to the conduction velocity of upper layer local V1 axons (0.33 m/s) enabling a rapid FF-FB loop between V1 and V2, particularly faster for the Magno signals which are conveyed to V2 and back to V1 even before the Parvo signals (80% of optic nerve fibers) arrive to V1. Functionally, Magno signals may prime V1 with contextual/top-down information before Parvo signals arrive to V1, and the loop via extrastriate cortices would be necessary in particular for long-distance interactions (reviewed in Bullier, 2001; Bullier et al., 2001; Angelucci and Bressloff, 2006). It is noteworthy that Girard et al. (2001) briefly reported that intrinsic horizontal connections within the infragranular layers of V1 may conduct signals faster than upper layer axons (up to 1m/s), albeit still slower than interareal V1-V2 connections; however, layer differences were not thoroughly characterized in that study and will need further investigation.

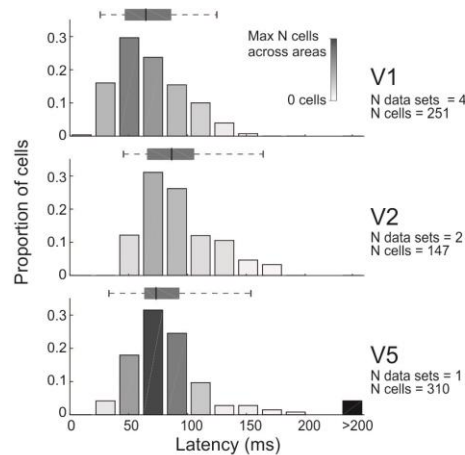


Figure 5. Onset latencies of spiking responses to visual stimulation. The proportions of cells are displayed as a function of latency. The number of distinct figures providing the source data, some in the same papers, are indicated on the right (N data sets), together with the total number of cells across the data sets. Bar darkness reflects the number of cells in each bin normalized to largest number of cells in any of the bins across the three cortical areas. The black bar on the right contains outlier values above the reported cutoff at the tick mark value. The whisker plots indicate the 2.5, 25, 50, 75 and 97.5 percentiles of the data, calculated from the histograms in the original data. Data for V1 are from (Maunsell and Gibson 1992; Nowak et al. 1995), for V2 from (Nowak et al. 1995), and for V5 from (Raiguel et al. 1989).

Figure 5 shows response onset latencies in areas V1, V2 and V5, and Supplementary Figure 1 shows the cumulative density functions and pairwise uncorrected Mann-Whitney U tests between the areas' median latency values. Response onset latencies overlap in the different areas, but median latency increases from V1 to V5 to V2 (65, 73 and 86 ms, respectively). Onset latencies are strongly dependent on various visual stimulus parameters, especially luminance, which affects integration time in the retina (Mansfield 1973). Moreover, there is significant variability between individual animals in onset latencies (Maunsell and Gibson 1992), which complicates comparison across studies. The study of Schmolesky et al. (1998) compared latencies in different cortical areas. Mean latencies were shortest in V1, 66 ms (SD 10.7, range 34-97), longest in V2 82 ms (SD 21.1, range 56-118) and intermediate in V5 72 ms (SD 10.3, range 49-98). These latencies

resemble our summary data from multiple studies.

The earliest responses at the top of L4C of V1 cause oscillations at 50-100 Hz (Maunsell and Gibson 1992). Within V2, the thick (median multi-unit onset latency 63 ms) and pale (70 ms) stripes show earlier response onset compared to the color-sensitive thin stripes (81 ms; Munk et al. 1995).

Firing rate statistics

The ability of a neural system to provide the same response with high temporal precision is highly dependent on the variance of the input, suggesting neural systems have low intracellular noise (Mainen and Sejnowski 1995). High temporal precision enables a system to transmit information using less resources. Because neuronal response statistics differs in alert vs. anesthetized monkeys, in the discussion below we specify the state of anesthesia.

In alert monkeys, individual V1 neurons show high temporal precision of spike latency in response to an optimal stimulus, with the median Fano factor (variance/mean) across layers ranging between 0.2 and 0.35, and the mean across V1 being 0.33 ± 0.17 (SD, range across cells $<0.1-1$). However, when stimulus contrast is reduced to near threshold, variability increases, and Fano Factors grow closer to 1 (Gur and Snodderly 2006).

The spontaneous spike rate in V1 has an exponential distribution across cells with very low average rates (simple cells 1.2 Hz, N=137, complex cells 4.9 Hz, N=245, anesthetized; Schiller et al. 1976).

Rasch et al. (2011) studied the statistics of V1 spiking during movie viewing in anesthetized monkeys. They found a mean firing rate of 5.1 ± 0.8 (SD) Hz, and an exponential distribution of firing rates, with the exponent being on average -0.8 ± 0.6 s

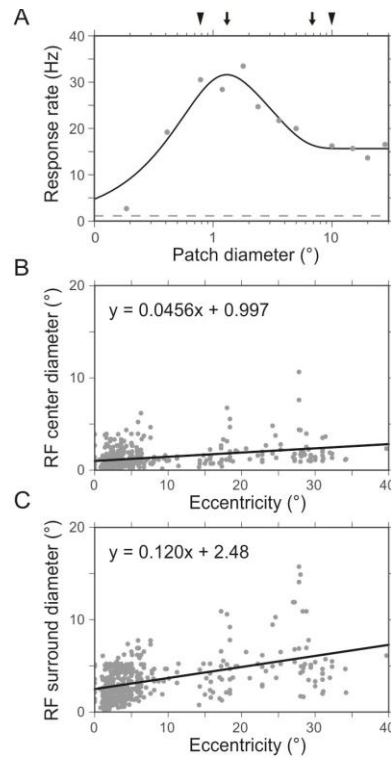
(range -2.4 s – -0.2 s). For individual neurons, the Fano factor across multiple presentations of the same stimulus was close to 1 for very short ≤ 10 ms epochs and increased for longer epochs. The population response was, as expected, more reliable for short epochs (smaller Fano factor than for individual neurons), but increased again with longer epochs, suggesting that the firing rates of individual neurons go up and down together. There are probably important differences in firing rate statistics due to anesthesia. First, the Fano factors are significantly lower in awake than anesthetized animals (Gur and Snodderly 2006); moreover, when fixational eye movements are carefully controlled in awake animals (Gur and Snodderly 2006; McFarland et al. 2016), Fano factors cease to increase at longer epochs. In summary, response variability might be significantly smaller in awake visual cortex than previously assumed and stay constant over time.

There are few studies on the firing rate statistics of extrastriate areas. Because Fano factor is affected by anesthesia, epoch length and, in awake animals, fixational eye movements, areas V1, V2 and V5 need to be compared under identical conditions. Yang et al (2009) compared anesthetized young and old adult monkeys and found that Fano factors in V1 and V5 during drifting grating stimulation are very similar, but increase with age in both areas. Mean Fano factors were (young/old) 1.4/2.4 in V1, and 1.5/2.5 in V5.

Visual field representation in cortex

The representation of the visual field in cortex can be characterized by three parameters, namely RF size, magnification factor (or it's 2D generalization log conformal mapping), and cortical point image. These representations are however not smooth, because local discontinuities arise from RF scatter and additional dimensions, such as

1334 ocular dominance (V1;(LeVay et al. 1975) and cytochrome oxidase (V2) bands (Roe and
 1335 Ts'o 1995; Shipp and Zeki 2002b).
 1336



1337 **Figure 6. Area summation function in V1.** A: Area summation function for an example V1 neuron. Solid
 line represents fit to the data (dots) using the difference of Gaussians (DoG) model. Dashed line indicates the
 mean spontaneous firing rate. Arrows indicate the center and surround diameters obtained using the DoG fit.
 Arrowheads indicate the center and surround diameters extracted from the empirically measured responses
 (without any fit). Data from (Shushruth et al. 2009). B: RF center diameter with respect to eccentricity. Solid
 line represents linear fit to the data (dots, N=425). C: RF surround diameter with respect to eccentricity. Solid
 line represents linear fit to the data (dots, N=425). B, C data from (Cavanaugh et al. 2002).

1338
 1339 Receptive field size

1340 In macaque V1, a typical single-cell response to an enlarging stimulus first shows an
 1341 increase, then a decrease, until an asymptote is reached (Fig. 6A). The RF size is defined
 1342 as the stimulus radius at peak response, and the region beyond peak response, where the

cells response is suppressed is termed the surround. This patch-size tuning curve, also called the area summation function (ASF), has been modeled as antagonistic excitatory and inhibitory Gaussian mechanisms, interacting either divisively (ratio of Gaussians, RoG, model; Cavanaugh et al., 2002) or subtractively (difference of Gaussians, DoG, model; Sceniak et al. 1999). In the DoG model, the area summation function is:

$$R(dia) = R_0 + K_c \int_{-dia/2}^{dia/2} e^{-(2x/w_c)^2} dx - K_s \int_{-dia/2}^{dia/2} e^{-(2x/w_s)^2} dx$$

Here, dia is the diameter of the stimulus, R_0 the spontaneous firing rate, K_c , K_s , the gain and w_c , w_s the extent of the receptive field center and surround, respectively. The center and surround mechanisms are thought to be generated by distinct connections: the excitatory center primarily by geniculocortical FF and intra-V1 horizontal connections, while the inhibitory surround primarily by both local intra-V1 and interareal FB connections (Angelucci, Levitt, Walton, et al. 2002; Schwabe et al. 2006). A recent review (Angelucci et al. 2017) discusses how the cortical microcircuit might give rise to the area summation function.

Neurons show significant variability in their ASFs and the center and surround extents vary with visual field eccentricity (Fig. 6B, C). In parafoveal V1 (at 3-7° eccentricity) using a high contrast grating patch increasing in size, the RF radius measured on average $0.36^\circ \pm 0.13^\circ$ (N=79; range $0.11^\circ - 0.82^\circ$, Shushruth et al. 2009), and in a different study 0.39° (N=148; eccentricity $< 5^\circ$, Cavanaugh et al. 2002). These same studies estimated the surround radius to be $1.62^\circ \pm 0.62^\circ$ (N=79; range $0.55^\circ - 2.66^\circ$) and 2.5° (N=148) respectively. The extents were determined using the DoG fits to the spatial summation data (Shushruth et al. 2009), or directly from the data (Cavanaugh et al. 2002), and defining RF extent as the smallest stimulus radius at the peak of the fitted function, or (for

cells that did not show surround suppression) that elicited 95% of the maximum response, and the surround extent as the smallest stimulus for which the response was reduced to 5% of its asymptotic value.

Similarly, in parafoveal V2 (up to 10° eccentricity), the RF radius has been reported to average $0.74^\circ \pm 0.50^\circ$ (N=91; range $0.16^\circ - 2.43^\circ$) and the surround radius $3.56^\circ \pm 1.94^\circ$ (N=83; range $1.06^\circ - 10.55^\circ$). Thus in V2, the RF sizes are on average double the sizes of V1 RFs (Shushruth et al. 2009).

For V5, similar nonlinear ASFs as in V1 and V2 have been reported (Pack et al. 2005; Hunter and Born 2011). The peak response appears to be larger than in V1 or V2, in many cases larger than the largest stimulus diameter used for the measurements (30°). The “classical RF” for V5 cells, which is measured using small stimuli rather than gratings of increasing size, was defined by the following equation: $\text{size (deg)} = 0.72E + 1.35$ (Desimone and Ungerleider 1986). The optimal RF size, corresponding summation field, is about 10 times larger in V5 than in V1 (Albright and Desimone 1987; Maunsell and van Essen 1987).

Mapping of visual field in cortex

The representation of foveal and parafoveal visual field in V1 can be characterized as (Schwartz 1980, 1994) :

$$w = k * \log(z + a) \quad \text{Eq 1}$$

where w is the position in cortex, and z is the position in visual field. The real part of z represents the eccentricity, and the imaginary part the polar angle (azimuth) in visual field. The parameters k and a scale the transformation, and a defines the foveal part of the

visual field, respectively. For the existing macaque data (Daniel and Whitteridge 1961), Schwartz (1980) used a value of $a=1$ (in his Figure 1), and k would scale for the individual V1 size.

Schwartz's log mapping has been generalized to cover full field V1, V2 and V3, and to account for shear that conformal (i.e. angle-preserving) mappings cannot model (Polimeni et al. 2006). For numerical simulations, the log mapping provides a straightforward way to map the visual field into cortical coordinates, and it has recently been applied to visual cortical prosthetics as well (Li 2015).

Several previous studies have provided quantitative data on the one-dimensional derivative of the log conformal map, i.e. the magnification factor. This is the distance in cortex that represents a given distance in visual field (Daniel and Whitteridge 1961). The parameters k and a of the log conformal mapping are related to the magnification factor (M), because the inverse of the magnification factor can be defined as a linear function of eccentricity (Schwartz 1994):

$$\frac{1}{M} = \frac{a}{k} + \frac{1}{k} * \text{eccentricity} \quad \text{Eq. 2}$$

Although none of the cortical areas show smooth mappings of the visual field, as they all have some sub-structure, V1 has in early studies been characterized with a single magnification value. Nevertheless, the relation of eccentricity to M^{-1} is not fully linear (Dow et al. 1981), and additionally shows significant horizontal-vertical anisotropy (Tootell, Switkes, et al. 1988). This anisotropy calls for the aforementioned more comprehensive 2D mapping of the visual cortex than what the M factor allows (Polimeni et al. 2006). However, since these parameters are nonexistent for V5, here we only report magnification factor.

1418 The area V1 magnification factor, M , as a function of eccentricity is $1/(0.077 + 0.082$
 1419 $\times E)$ mm/deg, as determined using the 2 deoxyglucose method (2DG) method within the
 1420 central 10° (Tootell et al. 1982), and $1/(0.0404 + 0.116 \times E)$ mm/deg, as determined using
 1421 electrophysiological recordings within the central 2.5° (Dow et al. 1981) or $1/(0.109 +$
 1422 $0.0637 \times E)$ mm/deg outside the foveal representation (Hubel and Wiesel 1974b; Hubel
 1423 and Freeman 1977). The slope of M^{-1} at the fovea is about half the slope outside the fovea.
 1424 The OD columns cause anisotropy by reducing the M factor to about half the value in the
 1425 direction orthogonal to the OD bands (LeVay et al. 1975).

1426 Early V2 studies reported that the three CO stripes have separate maps of the visual
 1427 field. The representations are, however, continuous within the same type of stripe (Roe
 1428 and Ts'o 1995; Shipp and Zeki 2002b). Each of the V2 CO compartments had similar
 1429 values of magnification factor (interstripes 1.44 mm/deg, thin stripes 1.4 mm/deg and
 1430 thick stripes 1.25 mm/deg; Roe and Ts'o 1995).

1431 The magnification factor for area V5 is $1.14 \times E^{-0.76}$ (Gattass and Gross 1981; Albright
 1432 and Desimone 1987). Because the sizes of cortical areas vary across individuals (as also
 1433 shown for humans in Amunts et al., 2000), the magnification factors show also individual
 1434 variability.

1435

1436 Cortical point image

1437 The literature on cortical point image, *i.e.* the cortical representation of one point in
 1438 visual field, is a function of the average cortical RF size and scatter. In V1, the cortical
 1439 point image shows discrepant values, depending on whether it was measured by
 1440 electrophysiological recordings or by optical imaging with voltage sensitive dyes (VSDI).
 1441 Electrophysiological recordings demonstrate an exponential reduction of the cortical
 1442 point image with increasing eccentricity. At the fovea the point image approaches 10 mm,

whereas in the periphery it is about 1 mm (Dow et al. 1981). In contrast, VSDI shows a constant point image, at least in the parafoveal representation (2°-5°, Palmer et al., 2012). The former method measures action potentials, i.e. the output of neurons, whereas the latter measures the subthreshold voltage variations. The discrepancy may, thus, be related to differences in neuronal tuning of synaptic vs. action potentials (Jia et al. 2010), and may partially reflect non-linear mapping from subthreshold to suprathreshold responses (Anderson et al. 2000; Miller and Troyer 2002).

Including LGN in a computational model requires mapping the visual field onto LGN cells, and then LGN cells onto visual cortex. The visual field forms retinotopic representation in each Parvo- and Magno layer. The LGN represents the visual field with a smaller number of cells than V1, and the ratio of LGN/V1 cell numbers changes as a function of eccentricity (Connolly and Van Essen 1984). The number of cells per square degree of visual field (M_c , cells/deg²) as a function of eccentricity (E) is given by:

$$M_c = k(a + E)^{-x}$$

where $k=83700$, $a=1.28$ and $x=1.96$, for Parvo layers, and $k=3520$, $a=3.12$ and $x=1.56$, for Magno layers. These results suggest that the Magno/Parvo cell ratio in LGN increases by a factor of up to 20 from the fovea to the periphery.

Livingstone and Hubel (1988b), instead, found an approximately equal M/P-ratio across eccentricities, and suggested that the Connolly and Van Essen (1984) analysis was flawed. The anatomical data of Livingstone and Hubel (1988b) were later challenged by Malpeli et al. (1996), who attributed the discrepancy to a number of potential factors, such as technical issues related to the retrograde transport of the tracers, the omission of the Koniocellular channel (which was discovered in 1994, after the Livingstone and

Hubel's study), or a plateau in the magnitude of the magnification factor of the Magno channel at the eccentricities where the tracer injections were placed. Malpeli et al. (1996) showed that the M/P cell ratio in LGN grows by a factor of at least 14 from the fovea to the periphery, thus confirming the original study by Connolly and Van Essen (1984).

Based on the results by Connolly and Van Essen (1984), Schein and de Monasterio (1987) estimated the point images from LGN cells onto V1. Point images are very different for the LGN Parvo and Magno cells' mapping onto the cortex, which results from the different type of scaling of N neurons/unit area as a function of eccentricity. Outside the fovea, the ratio of LGN Parvo cells to unit area of cortex is close to constant, being 550/mm² at 1° eccentricity, and increasing to 872/mm² at 80°. In contrast, the density of Magno cells increases steeply, from 13/mm² at 1° to 206/mm² at 80° eccentricity. The point image in V1 behaves exactly the opposite, namely for Parvo cells it decreases steeply with eccentricity, whereas it is almost constant for the Magno cells.

The cortical point image size grows along the ventral stream hierarchy, but stays constant along the dorsal stream, including V5 (Gattass et al. 2005).

Orientation selectivity

In V1 about 70% of cells are tuned to the orientation of edge stimuli, the rest having non-orientation-sensitive RFs (Bullier and Henry 1980). The distribution of orientation selectivity across V1 layers is discussed in the section "Diversity of response properties in V1 layers" under "Functional anatomy". Quantitatively, orientation selectivity can be defined by two parameters, circular variance (CV) and bandwidth (BW). The circular variance is a global measure, based on firing rate responses (r) to all orientations (Θ).

$$\text{Circular Variance} = 1 - \left| \frac{\sum r e^{i2\theta}}{\sum r} \right| \quad \text{Eq. 3}$$

A CV of zero indicates high orientation selectivity, and CV of 1 no selectivity. Figure 7 and Supplementary Figure 1 show that the CV in V1 is somewhat higher than in V2. All datasets in V1 and V2 were from (Goris et al. 2015), and were originally reported as orientation selectivity index (OSI), which we have converted into CV (1-OSI) for the data shown in Fig. 7. For V5, Albright (1984) reported that 83% (74/89) of units were tuned for orientation, but, because he quantified orientation tuning as the difference between the max and min responses, this data could not be converted to CV.

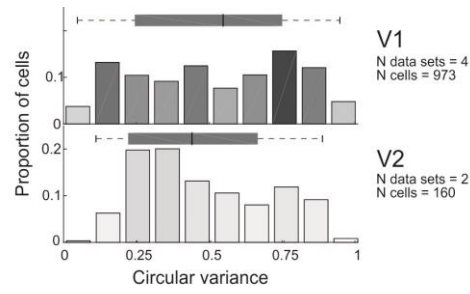


Figure 7. Circular variance. Conventions are as in Figure 5. Data for V1 are from (Ringach et al. 2002; Gur et al. 2005; Goris et al. 2015) and for V2 from (Goris et al. 2015).

Orientation bandwidth is a local measure, defined as the response distribution close to the orientation causing the peak response (Figure 8, Supplementary Fig 1).

$$BW_{\theta} = \theta_{r_{1/2}max} - \theta_{r_{1/2}min} \quad \text{Eq. 4}$$

where

$\theta_{r_{1/2}max}$ is the max (min) orientation producing half of the response strength. Studies reporting BW at $1/2^{1/2}$, or 70.7%, of the peak response (Ringach et al. 2002; Gur et al. 2005) instead of the half-height, were transformed to half-height values by assuming a Gaussian distribution of the tuning, and multiplying the BW values by the square root of

two. The full bandwidth was reported only by Albright et al. (1984), whereas we doubled the values from other studies which reported the half-bandwidth. The outlier cutoff was set at 160 deg. Fig. 8 and Supplementary Fig. 1 demonstrate that orientation bandwidth is slightly wider in V1 than V2, but bandwidth in V5 is not significantly different from V1 and V2.

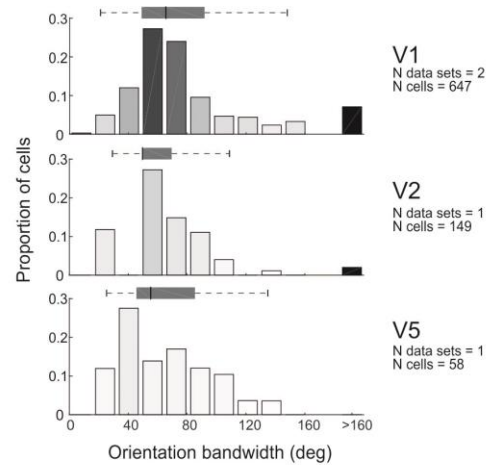


Figure 8. Orientation bandwidth. Conventions are as in Figure 5. Data for V1 are from (Ringach et al. 2002; Gur et al. 2005), for V2 from (Levitt, Kiper, et al. 1994), and for V5 from (Albright 1984).

Direction selectivity

The direction selectivity index (DSI) reported in Figure 9, is based on nine previous studies. The DSI is defined as follows:

$$DSI = 1 - \frac{r_{null\ direction}}{r_{preferred\ direction}} \quad \text{Eq. 5}$$

A DSI = 0 indicates a non-direction selective cell and a DSI =1 a highly directionally selective cell. Values >1 appear when the minimal response to stimuli moving in the non-preferred direction is below the spontaneous firing rate. One study (De Valois, Yund, et al.

1982) reported V1 DSI as null/preferred response; in this case were recalculated the DSI values according to Eq. 5. De Valois et al. did not report values when the null response was below baseline, leading to a max DSI value of 1. However, a similar secondary peak at 1 in V1 was observed in two other data sets. The distribution in Figure 9 did not change much with the De Valois et al. dataset removed (222 cells).

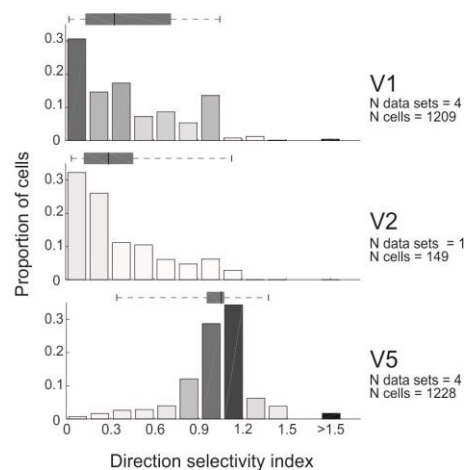


Figure 9. Direction selectivity index. Conventions are as in Figure 5. Data for V1 are from (De Valois, Yund, et al. 1982; Albright 1984; Movshon and Newsome 1996; Wang and Movshon 2016), for V2 from (Levitt, Kiper, et al. 1994), and for V5 from (Maunsell and Van Essen 1983c; Albright 1984; Movshon and Newsome 1996; Wang and Movshon 2016).

Direction selectivity clearly differs in different areas. Most cells in V1 and V2 are poorly or moderately directionally selective, and the two areas show overlapping distribution, whereas most cells in V5 are strongly directionally selective.

Spatial frequency selectivity

In contrast to the retinogeniculate pathway, where most cells show low-pass characteristics, in visual cortex the majority of cells are band-pass tuned (De Valois, Albrecht, et al. 1982). Spatial frequency (SF) has typically been described by two

parameters, the optimal response (peak) and the bandwidth.

Figure 10 shows the distribution of peak SFs in the three cortical areas. The eccentricities of the recorded neurons varied a little between studies, but the range was similar: 2-5° in V1, 0-5° in V2, and 0-8° in V5. The large variability in peak SF precluded setting the outlier threshold at the same cutoff value for all areas, because the low outlier cutoff in V1 (<0.5 , De Valois et al., 1982a) encompassed most data in V5. The number of outliers in the original data were low, 4 cells (1.5%) in V1, 22 (9.4%) in V2, and none in V5, thus they could only minimally skew the data in Figure 10.

The peak SF differed significantly between areas, with the highest values in V1, and progressively lower values in V2 and V5 (Suppl. Fig. 1). Functionally this suggests that the three areas co-operate to detect a wide range of SFs. Because the low SFs would be lost after band-pass filtering in V1, these data in addition suggest either that V2 and V5 have direct access to visual information from LGN (as, indeed, reported in the anatomy section above) or that the few units in V1 tuned to low SFs have high response gain.

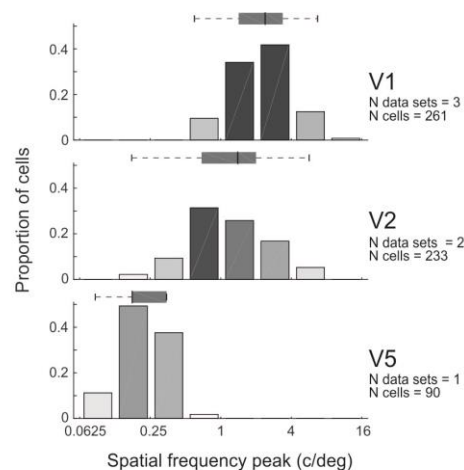


Figure 10. Spatial frequency peak. Conventions are as in Figure 5. Data for V1 are from (De Valois, Albrecht, et al. 1982; Foster et al. 1985), for V2 from (Levitt, Kiper, et al. 1994), and for V5 from (Yuan et al. 2014).

Datasets on the SF bandwidth are limited, due to different metrics used to report it in different studies (Fig. 11). The bandwidth in Fig. 11 is reported as full width at half-height, on a logarithmic scale (octaves, *i.e.* \log_2):

$$BW_{SF} = SF_{r_{1/2}max} - SF_{r_{1/2}min} \quad \text{Eq. 6}$$

V5 has significantly wider SF bandwidth compared to V1 and V2 (Suppl. Fig. 1). In addition, higher areas showed increasingly higher numbers of cells whose SF bandwidth could not be defined (black bars), as their response did not drop to half of the maximum response on either side of the peak. Cells with such wide-band tuning could be sensitive to sharp edges.

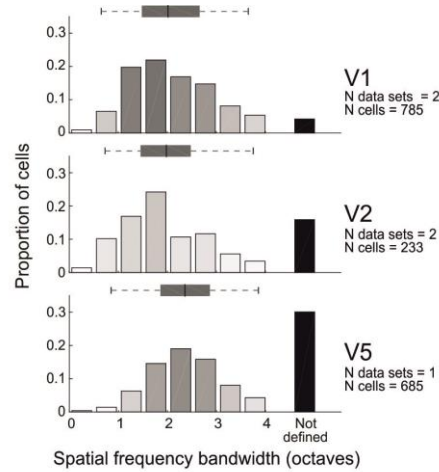
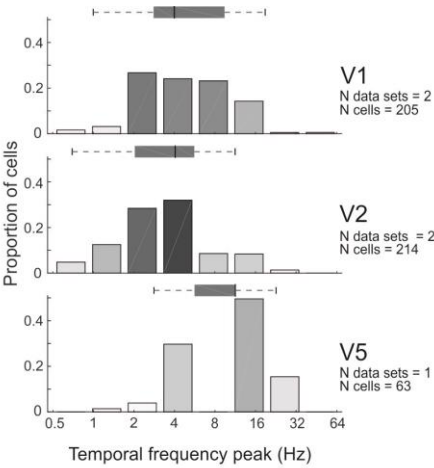


Figure 11. Spatial frequency bandwidth. Conventions are as in Figure 5. Data for V1 are from (Foster et al. 1985; Wang and Movshon 2016), for V2 from (Foster et al. 1985; Levitt, Kiper, et al. 1994), and for V5 from (Wang and Movshon 2016).

Temporal frequency selectivity

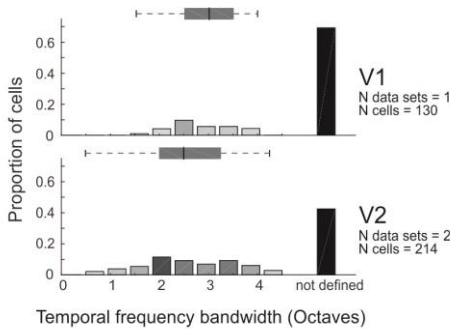
Peak temporal frequency (TF) was characterized in five studies (Fig. 12). The original

1580 data have sparse bins, and small numbers of cells, hampering comparison between areas.
1581 V5 significantly prefers higher optimal TFs compared to V1 and V2, whereas V2 shows a
1582 distribution with somewhat lower TF values than V1 (Suppl. Fig. 1).
1583



1584 **Figure 12. Temporal frequency peak.** Conventions are as in Figure 5. Data for V1 are from (Foster et al.
1585 1985; Hawken et al. 1996), for V2 from (Foster et al. 1985; Levitt, Kiper, et al. 1994), and for V5 from (Yuan
1586 et al. 2014).

1587 The TF bandwidth (Fig. 13) was characterized in the literature only for a minority of
1588 cells, most not reaching the threshold of 50% response strength, and most of them having
1589 low-pass temporal response function. The TF bandwidth was significantly wider in V1
than in V2 (Suppl. Fig. 1). We found no published data for V5.



1590 **Figure 13. Temporal frequency bandwidth.** Conventions are as in Figure 5. Data for V1 are from (Foster
1591 et al. 1985), and for V2 from (Foster et al. 1985; Levitt, Kiper, et al. 1994).

Contrast response function

The contrast response function is quantified using the following equation

$$R = b + \frac{c^\gamma}{c^\gamma + c_{50}^\gamma} \quad \text{Eq. 7}$$

where R is response, b baseline firing rate and C contrast (independent variable). The fitted variables are γ , the exponent, and C_{50} , the semisaturation contrast, i.e. the contrast value at which the response curve reaches 50% of its maximum value.

Figure 14 shows the distributions of semisaturation contrast and contrast exponent for areas V1, V2 and V5. For each study we reviewed both parameters. The only logarithmic semisaturation contrast plot (V2) in (Levitt, Kiper, et al. 1994) was turned into a linear scale, for comparison.

Figure 15 visualizes the normalized contrast response functions attainable with the median exponent and semisaturation contrast for each area. Figures 14 and 15 as well as Suppl. Fig 1 demonstrate that V5 has significantly higher contrast sensitivity than the two other areas, followed by V2 and V1. This is due to the varying semisaturation contrast, whereas the median exponents are similar in the three areas.

Figure 16 shows that there is a similar distribution of maximum firing rates across the cell population in V1 and V5. The original data were binned at 10 spikes/s and peaked between 10 and 20 Hz in both V1 and V5, with about 50% drop in the 0-10 Hz bin (Sclar et al. 1990).

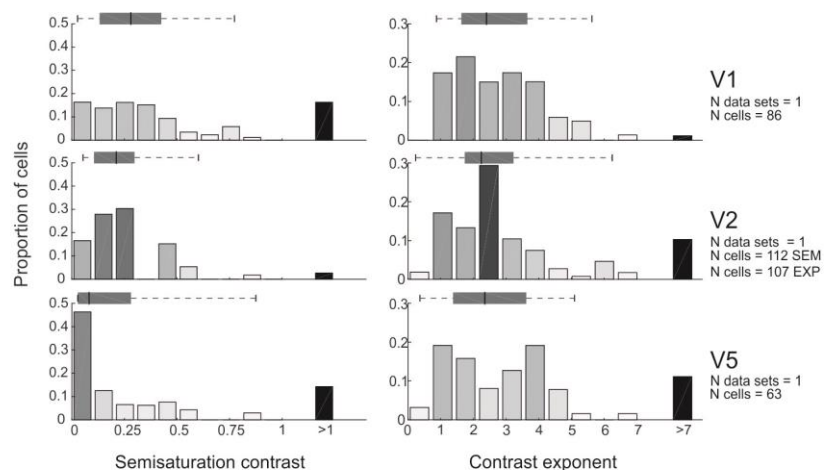


Figure 14. Semisaturation contrast and contrast exponent of the contrast response function.

Conventions are as in Figure 5. Data for V1 are from (Sclar et al. 1990), for V2 from (Levitt, Kiper, et al. 1994), and for V5 from (Sclar et al. 1990).

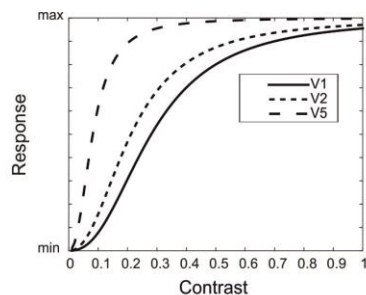


Figure15. Contrast response function. Based on the median parameters of the data reported in Figure 14.

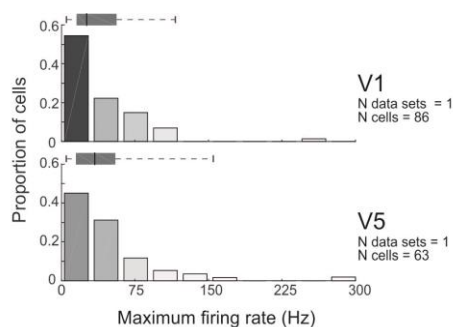


Figure 16. Maximum firing rate. Stimuli were sinusoidal gratings at 120 cd/m² luminance and saturating contrast; the grating orientation, spatial frequency, motion direction and speed were optimized for each cell. Conventions are as in Figure 5. Data for V1 and V5 are from (Sclar et al. 1990).

Higher-order feature selectivity in V2 and V5

In addition to the low-level feature selectivity, neurons in V2 and V5 become selective to more complex RF features. These higher-order features are related presumably to pattern, object, speed and depth computations in V2 and V5.

About one third of V2 cells are selective for complex gratings or forms (Hegdé and Van Essen 2000). These responses are dependent on anisotropic orientation sensitivity in the classical RF and its surroundings (Ito 2004; Anzai et al. 2007). Most V2 cells (63%) are sensitive to natural texture statistics, i.e. in the higher order correlation of image features across spatial frequencies, orientations and positions. This is in sharp contrast to V1, where only 15% show such selectivity (Freeman et al. 2013). Interestingly, this increased sensitivity in V2 derives from stronger surround suppression from non-natural (gratings, noise) than from natural texture stimuli (Ziemba et al. 2018).

Stereoscopic depth perception is dependent on relative disparity between the retinal images of the two eyes. While V1, V2 and V5 all have cells which are tuned for retinal disparity, only the cells in V2 and V5 contribute to depth perception (Maunsell and Van Essen 1983a; DeAngelis et al. 1998; Nienborg 2006). Another depth cue, motion parallax, arises from self-motion in stationary surroundings. Eighteen percent of V5 cells contribute significantly to behavioral judgments based on motion parallax (Kim et al. 2015).

The V2 cells assign contrast edges to particular object, or code “border ownership”, more often than V1 cells (59% in V2 vs 18% in V1; Zhou et al. 2000). This may be related to emergent segregation of objects from background in V2.

Many V5 cells become more sensitive to motion of a whole pattern than motion of the components of the pattern. Estimates for the proportion of cells which prefer pattern motion in macaque V5 range from 23-25%, whereas such cells are rare in V1 (Movshon

et al. 1985; Wang and Movshon 2016).

Neuronal membrane physiology

The neuronal membrane physiology has not been systemically studied in macaque visual cortex. Some parameters have been extracted from prefrontal cortex, but given the structural differences of neurons in different areas (Elston 2003; Luebke 2017) it is unclear whether such values are relevant for the visual areas considered in this review, therefore, those data were excluded. In visual cortices, some biophysical parameters are available for V1 L3 pyramidal neurons (Table 6, Amatrudo et al., 2012; Luebke et al., 2015; Gilman et al., 2017). While all neurons have tonic regular spiking patterns, many also show phasic activity. Amatrudo et al. (2012) tuned a model neuron to the structure of a single pyramidal cell providing an example table of biophysical model parameters (their Table 1).

Table 6. Biophysical parameters for area V1 L3 pyramidal neurons. Data from Amatrudo et al., 2012; Luebke et al., 2015; Gilman et al., 2017). sEPSC, sIPSC= spontaneous EPSP, IPSP. Mean (range) across studies.

Membrane time constant (ms)	23 (19– 28)
Input resistance (<u>Mohm</u>)	238 (205– 285)
Resting membrane potential (mV)	-66 (-66.4 – -65.8)
Action potential threshold (mV)	-42 (-42.8 – -41.8)
Rheobase (pA)	82 (79– 87)
<u>sEPSC freq</u> (Hz)	1.4 (1.2 – 1.5)
rise (ms)	1.1 (1.0 – 1.2)
decay (ms)	4.7 (4.2 – 5.4)
amplitude (pA)	6.7 (6.4 – 7.3)
<u>sIPSC_freq</u> (Hz)	0.33
rise (ms)	2.8
decay (ms)	7.6
amplitude (pA)	20

1660

1661

1662 In V1 L3 pyramidal cells, a depolarizing current step of 80 pA evokes on average (SD)
 1663 a 14.9 (1.8) Hz response, and a 180 pA current step evokes a 19.6 (2.4) Hz response,
 1664 clearly higher than in prefrontal cortex (Gilman et al. 2017). This is likely due to the
 1665 smaller cell size, and thus membrane capacitance, in visual than prefrontal cortex,
 1666 resulting in more responsive neurons to the same input current.

1667

The need for future quantitative studies

We have reviewed the literature and summarized quantitative data about the structure and function of, and interactions between macaque visual areas V1, V2 and V5. Although available data are insufficient to support a complete quantitative microcircuit diagram, it, however, allows to construct a binary diagram, including partial data on relative connection strength, which allows to identify dominant and sparse connections in a microcircuit, helping to constrain the parameter search spaces for numerical simulations.

This review omits several areas in the occipital lobe, such as V3, V3A, V6/PO and V4. These areas lack either a unique definition (Angelucci and Rosa 2015; Angelucci et al. 2015; Gamberini et al. 2015; Zhu and Vanduffel 2019), clear homologues between humans and macaques (Kaas 1992; Tootell et al. 1997; Hadjikhani et al. 1998), thus precluding prospective generalization of the model system to humans, or have not been sufficiently studied to justify their inclusion into a quantitative review. The exclusion of these visual areas naturally limits the type of visual analysis that can be expected from a model and may also lead to inaccuracies in the model receptive fields, if the latter are shaped by feedback in the real biological system.

In the early nineties, Felleman and Van Essen (1991) provided a binary diagram of connections between macaque visual cortical areas and studied their mutual hierarchy. The CoCoMac database (Stephan et al. 2001; Kötter 2004; Bakker et al. 2012) later provided online access to interareal anatomical tract tracing data. Later these connections were studied quantitatively, revealing the dense connectome between areas (Barone et al. 2000; Markov et al. 2011; Markov, Ercsey-Ravasz, et al. 2014). The macroscopic scale is however insufficient for model simulations aiming to replicate single neuron function. Instead, we need a model at the microcircuit level.

1693 Missing parts for a synthetic blueprint

1694 Much information is still missing in order to build a comprehensive model of the
1695 macaque visual cortex. First, we need information on which cell types contact which
1696 other cell types, making how many synapses, and the probability distribution of synapses
1697 along the dendritic tree. Unfortunately, the construction of such a detailed connectome
1698 directly from anatomical data is not technically possible, because no current method
1699 allows reading and visualizing massive anatomical volumes at synaptic resolution.

1700 Fortunately, partial data samples may allow us to extract statistical rules which could
1701 lead to the establishment of a representative connectome and synaptome of a neural
1702 system (DeFelipe 2010, 2015). Two studies, both in rat somatosensory cortex, have
1703 presented approaches to build a comprehensive model from sparse connectivity data. In
1704 the first study, Egger et al. (2014) combined experimental anatomical volumetric data,
1705 soma distributions, examples of neuron type specific morphologies (axonal and dendritic
1706 fields), relative frequency of neuron types, and subcellular structural connectivity data
1707 between cell types. This subcellular connectivity included neuron-type specific density of
1708 postsynaptic targets, separately for the soma and apical- and basal dendrites. Using these
1709 data, the software calculated dense instantiations of a microcircuit, which were available
1710 for numerical simulations (such as Landau et al., 2016). In the second study, Reimann et
1711 al. (2015) build microcircuit models based on five types of data. The first defines
1712 morphological neuron types, and their local density distributions. Then, they estimate the
1713 total length of axons, and the density of boutons on the axons for each type of neuron. For
1714 each connection between two neuron types, the approach requires connection probability
1715 and the mean and standard deviation of number of synapses per connection. This
1716 algorithm was later used to build a comprehensive microcircuit model of rat
1717 somatosensory cortex (Markram et al. 2015).

Table 7 lists some of the key data that are still missing for macaque. In the literature there are many anatomical tracing studies of interareal connections. Unfortunately, there are only partial data on the densities of distinct morphological neuron types in different layers for V1 and none for V2 or V5. Moreover, inhibitory cell types have not been quantified by layer, and quantitative data of dendritic length and bouton or synapse numbers on different cell types, and in different layers, are missing.

A recent cluster analysis of V1 L6 neurons provides a sense of the correlations between functional parameters (Hawken et al. 2019). The study reports six major clusters of RF properties, on the basis of simple/complex RFs (f0/f1 modulation;(Skottun et al. 1991), direction selectivity, and temporal frequency tuning. Such cluster analyses for other layers could reveal the inter-parameter correlations, which may significantly limit a model's parameter search space.

In addition, we are missing subcellular data on synaptic connection strengths, although it is likely that the latter are also dynamically adjusted by homeostasis (Turrigiano et al. 1998; van Rossum et al. 2000; Turrigiano 2008). For state-of-the-art Hodgkin-Huxley membrane voltage dynamics, we would, additionally, need information on the relative density of distinct ion channels. For a comprehensive multicompartmental model, the detailed dendritic morphology of distinct cell types would be required in digital format. Some data are available at <http://neuromorpho.org/index.jsp> mainly for V1 L6 pyramidal and spiny stellate neurons (Briggs et al. 2016) and L3 pyramidal cells (Luebke et al. 2015).

Table 7. Missing data for macaque V1, V2, V5 needed for microcircuit reconstruction.

PC: pyramidal cell

Parameter	Missing data
Total N neurons by layer	V2, V5
Excitatory cell type counts by layer	PC subtypes sparse for V1, missing for V2 and V5
Inhibitory cell type counts by layer	V1, V2, V5
Interlaminar cell type specific connectivity	Partial data for V1, sparse for V2, missing for V5
Horizontal distribution of local axons	Partial data for V1, V2 and V5
Axonal structure, incl. N boutons	Sparse data for V1, missing for V2 and V5
Dendritic structure	Partial data for V1, V2, missing for V5
Neural membrane electrophysiology	Sparse data for V1, missing for V2 and V5
Cell type specific neural structural model	V1, V2, V5

Fortunately, a complete microcircuit connectome is not necessary for simplified model simulations. Simplified models allow avoiding unnecessary complexity for some research questions and increase computational efficiency (Hokkanen et al. 2019). Figure 17 presents two levels of connection detail that can be implemented in a model. If the neural model is point-like, with fixed synaptic dynamics and firing patterns, the required level of description of the system is the identification of pre- and postsynaptic neuron types, the fraction of pre- and postsynaptic neurons contacting each other, the number of synapses per connection, and the amount of divergence and convergence in interareal connectivity (Fig. 17 *top*). However, more detailed and biologically realistic models require additional details on the morphology and firing rate statistics of the presynaptic neuron, as well as synapse location and dynamics of the postsynaptic neurons (Fig. 17 *bottom*).

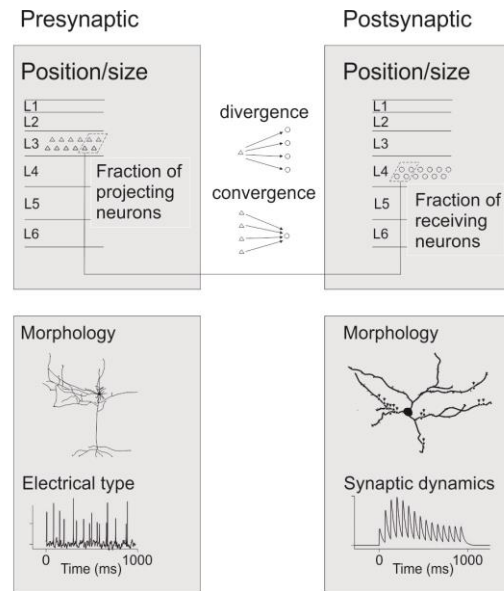


Figure 17. Describing connections between two neuron groups in silico. A) A simple point-like phenomenological neural model with fixed synaptic dynamics only needs to incorporate data on position and population size as well as data on the divergence and convergence of connections. B) A more comprehensive, biophysically meaningful, multicompartmental model requires, in addition, data on the cellular morphology, distribution of synapses, and electrical types of neurons and synaptic dynamics.

Studies on anatomical tracer injections targeted to specific CO compartments of V1 or V2, have typically reported the percentages of resulting labeled neurons in each compartment. To calibrate such measures, we need data on the density of projecting fibers/mm² of cortical surface area for each V2 compartment. For V1, where distinct layers have unique projection patterns, such data should also indicate the amount of projecting fibers/mm³ of cortex. Given the known layer thickness, one would thus be able to estimate the amount of projecting fibers.

Filling in missing macaque data for numerical simulations

For missing local connectivity data for macaque visual cortex, a theoretician is forced to use available data from other mammalian species, such as cat, rat and mouse, whose

local connections have been studied more extensively (Thomson and Lamy 2007; Markram et al. 2015). In addition, neural cell membrane electrophysiology has been studied more extensively in rodents (Markram et al. 1998; Thomson and Destexhe 1999; Gupta et al. 2000), and there is a clear underrepresentation of monkey data in the neuroinformatics databases, such as NeuroElectro at <http://neuroelectro.org/>.

Binzegger et al. (2004) collected local structural data for cat primary visual cortex, and suggested a canonical microcircuit diagram based on those data and remaining assumptions. For this diagram one needs essentially three quantities: the number of each neuron type in each layer, each neuron type's average dendritic length in each layer, and the number of synapses formed by each cell type in each layer. Moreover, one needs to assume that synapses form between cell types with equal probability (Peters' rule, Braitenberg and Schuz, 1998). However, many parameters remain uncertain in such a diagram. For example, how synapses are distributed onto the postsynaptic cells' dendritic trees, the short-term synaptic dynamics and potential for long-term plasticity in distinct neuron types, potential local anatomical anisotropies, such as those of patchy local horizontal connections.

Thomson et al (2002) provided local structural network data for rat and cat cortex, together with connection strength measured by dual or triple intracellular electrophysiological recordings in cortical slices. Most differences between species were just scale differences. Thomson et al (2002) reported apparent deviations from Peter's rule, particularly an asymmetry between interlaminar FF (e.g. L4 to 3 and L3 to 5) and FB projections (e.g. from L3 to L4, and from L5 to L3). The excitatory targets of FF connections were primarily the larger pyramidal neurons; the FB targets were horizontally more diffuse than the FF targets, and the FB-induced EPSPs were very small, below threshold. Moreover, FB connections were stronger onto inhibitory than onto excitatory

neurons, the latter being generally very sparse. The authors suggested that this asymmetry prevents reverberating excitation within the local circuit.

Interspecies differences may unfortunately hamper the ability to supplement a monkey model with rodent data (Luebke 2017). For example, the basket cells show lower input resistance and higher firing thresholds in rat compared to monkey, causing them to have lower excitability in rats than monkeys (Povysheva et al. 2008).

Schmidt et al. (2017) estimated the quantitative anatomical connectivity of macaque visual areas by combining CoCoMac databases (Stephan et al. 2001; Bakker et al. 2012) with the fraction of supragranular presynaptic neurons in a source area (Barone et al. 2000; Markov et al. 2011; Markov, Vezoli, et al. 2014) and an exponential distance rule (Ercsey-Ravasz et al. 2013). As local connectivity data from macaque were largely missing, the model of Schmidt et al. (2017) used Potjans and Diesmann's (2014) local microcircuit model, which was based on data from rats and cats. While Schmidt et al. (2017) provided a full graph of connections of macaque visual cortex, as well as explicit tables of the heuristics and assumptions included in their model, our reported anatomical data are different. We provide the details of published experimental data, including the rich substructure and layer-specific connectivity. Although we provide relative rather than absolute connection strengths, and there are uncertainties about the completeness of layer-specific connectivity graphs between two areas, our work goes one step forward compared to existing interareal connectivity graphs (Felleman and Van Essen 1991; Markov, Ercsey-Ravasz, et al. 2014).

In conclusion, here we have collated data from the literature with the goal of facilitating construction of biophysically meaningful models of macaque visual cortex and validation of such models by numerical simulation of neuronal RF properties. In the short run, it will be challenging to establish how the model structure gives rise to RF

1817 properties that resemble those measured in the real cortex, because multiple unknown
1818 factors affect RF responses. In the long run, however, a comprehensive model could
1819 nevertheless help elucidate the relation between macroscopic activation, local spiking and
1820 signal processing in a neural population.
1821

1822

1823 **Funding**

1824 This work was supported by Helsinki University Hospital research funds
1825 (TYH2016257, Y1249NEUR1) to S.V.; grants from the NIH (R01 EY026812, R01
1826 EY019743, BRAIN U01 NS099702), NSF (IOS 1355075 and 1755431, EAGER
1827 1649923), and University of Utah Neuroscience Initiative, to A.A.; grants from Research
1828 to Prevent Blindness, Inc. and a core grant from the NIH (EY014800) to the Department
1829 of Ophthalmology, University of Utah.

1830

1831 **Acknowledgments**

1832 We thank Vafa Andalibi for technical support and prof Patrizia Fattori and Dr Michela
1833 Gamberini for help with physiological data analysis.

1834

1835

References

- Adams MM, Hof PR, Gattass R, Webster MJ, Ungerleider LG. 2000. Visual cortical projections and chemoarchitecture of macaque monkey pulvinar. *J Comp Neurol.* 419:377–393.
- Ahmad A, Spear PD. 1993. Effects of aging on the size, density, and number of rhesus monkey lateral geniculate neurons. *J Comp Neurol.* 334:631–643.
- Ahmed B, Cordery PM, McLelland D, Bair W, Krug K. 2012. Long-range clustered connections within extrastriate visual area V5/MT of the rhesus macaque. *Cereb Cortex.* 22:60–73.
- Albright TD. 1984. Direction and orientation selectivity of neurons in visual area MT of the macaque. *J Neurophysiol.* 52:1106–1130.
- Albright TD, Desimone R. 1987. Local precision of visuotopic organization in the middle temporal area (MT) of the macaque. *Exp Brain Res.* 65:582–592.
- Amatrudo JM, Weaver CM, Crimins JL, Hof PR, Rosene DL, Luebke JI. 2012. Influence of Highly Distinctive Structural Properties on the Excitability of Pyramidal Neurons in Monkey Visual and Prefrontal Cortices. *J Neurosci.* 32:13644–13660.
- Amir Y, Harel M, Malach R. 1993. Cortical hierarchy reflected in the organization of intrinsic connections in macaque monkey visual cortex. *J Comp Neurol.* 334:19–46.
- Amunts K, Malikovic A, Mohlberg H, Schormann T, Zilles K. 2000. Brodmann’s areas 17 and 18 brought into stereotaxic space—where and how variable. *Neuroimage.* 11:66–84.
- Anderson JC, Binzegger T, Martin KAC, Rockland KS. 1998. The connection from cortical area V1 to V5: A light and electron microscopic study. *J Neurosci.* 18:10525–10540.
- Anderson JC, Martin KAC. 2002. Connection From Cortical Area V2 to MT in Macaque

- 1861 Monkey. *J Comp Neurol.* 443:56–70.
- 1862 Anderson JC, Martin KAC. 2009. The Synaptic Connections between Cortical Areas V1
- 1863 and V2 in Macaque Monkey. *J Neurosci.* 29:11283–11293.
- 1864 Anderson JS, Lampl I, Gillespie DC, Ferster D. 2000. The Contribution of Noise to
- 1865 Contrast Invariance of Orientation Tuning in Cat Visual Cortex. *Science.* 290:1968–
- 1866 1972.
- 1867 Angelucci A, Bijanzadeh M, Nurminen L, Federer F, Merlin S, Bressloff PC. 2017.
- 1868 Circuits and Mechanisms for Surround Modulation in Visual Cortex. *Annu Rev*
- 1869 *Neurosci.* 40:425–451.
- 1870 Angelucci A, Bressloff PC. 2006. Contribution of feedforward, lateral and feedback
- 1871 connections to the classical receptive field center and extra-classical receptive field
- 1872 surround of primate V1 neurons. *Prog Brain Res.* 154:93–120.
- 1873 Angelucci A, Levitt JB, Lund JS. 2002. Anatomical origins of the classical receptive field
- 1874 and modulatory surround field of single neurons in macaque visual cortical area V1.
- 1875 *Prog Brain Res.* 136:373–388.
- 1876 Angelucci A, Levitt JB, Walton EJ, Hupe JM, Bullier J, Lund JS. 2002. Circuits for local
- 1877 and global signal integration in primary visual cortex. *J Neurosci.* 22:8633–8646.
- 1878 Angelucci A, Roe AW, Sereno MI. 2015. Controversial issues in visual cortex mapping:
- 1879 Extrastriate cortex between areas V2 and MT in human and nonhuman primates. *Vis*
- 1880 *Neurosci.* 32:e025.
- 1881 Angelucci A, Rosa MGP. 2015. Resolving the organization of the third tier visual cortex
- 1882 in primates: A hypothesis-based approach. *Vis Neurosci.* 32:e010.
- 1883 Anzai A, Peng X, Van Essen DC. 2007. Neurons in monkey visual area V2 encode
- 1884 combinations of orientations. *Nat Neurosci.* 10:1313–1321.
- 1885 Ascoli GA, Alonso-Nanclares L, Anderson SA, Barrionuevo G, Benavides-Piccione R,

- 1886 Burkhalter A, Buzsáki G, Cauli B, DeFelipe J, Fairén A, Feldmeyer D, Fishell G,
1887 Fregnac Y, Freund TF, Gardner D, Gardner EP, Goldberg JH, Helmstaedter M,
1888 Hestrin S, Karube F, Kisvárdy ZF, Lambolez B, Lewis DA, Marin O, Markram H,
1889 Muñoz A, Packer A, Petersen CCH, Rockland KS, Rossier J, Rudy B, Somogyi P,
1890 Staiger JF, Tamas G, Thomson AM, Toledo-Rodriguez M, Wang Y, West DC, Yuste
1891 R. 2008. Petilla terminology: nomenclature of features of GABAergic interneurons
1892 of the cerebral cortex. *Nat Rev Neurosci.* 9:557–568.
- 1893 Bakker R, Wachtler T, Diesmann M. 2012. CoCoMac 2.0 and the future of tract-tracing
1894 databases. *Front Neuroinform.* 6:Article 30.
- 1895 Balaram P, Kaas JH. 2014. Towards a unified scheme of cortical lamination for primary
1896 visual cortex across primates: Insights from NeuN and VGLUT2 immunoreactivity.
1897 *Front Neuroanat.* 8:Article 81.
- 1898 Balaram P, Young N a, Kaas JH. 2014. Histological features of layers and sublayers in
1899 cortical visual areas V1 and V2 of chimpanzees, macaque monkeys, and humans.
1900 *Eye Brain.* 6:5–18.
- 1901 Baldwin MKL, Kaskan PM, Zhang B, Chino YM, Kaas JH. 2012. Cortical and
1902 subcortical connections of V1 and V2 in early postnatal macaque monkeys. *J Comp*
1903 *Neurol.* 520:544–569.
- 1904 Barone P, Batardiere A, Knoblauch K, Kennedy H. 2000. Laminar distribution of neurons
1905 in extrastriate areas projecting to visual areas V1 and V4 correlates with the
1906 hierarchical rank and indicates the operation of a distance rule. *J Neurosci.* 20:3263–
1907 3281.
- 1908 Bartfeld E, Grinvald A. 1992. Relationships between orientation-preference pinwheels,
1909 cytochrome oxidase blobs, and ocular-dominance columns in primate striate cortex.
1910 *Proc Natl Acad Sci.* 89:11905–11909.

- 1911 Beaulieu C, Kisvarday Z, Somogyi P, Cynader M, Cowey A. 1992. Quantitative
1912 distribution of gaba-immunopositive and -immunonegative neurons and synapses in
1913 the monkey striate cortex (area 17). *Cereb Cortex*. 2:295–309.
- 1914 Benevento LA, Rezak M. 1976. The cortical projections of the inferior pulvinar and
1915 adjacent lateral pulvinar in the rhesus monkey (*macaca mulatta*): An
1916 autoradiographic study. *Brain Res*. 108:1–24.
- 1917 Betizeau M, Dehay C, Kennedy H. 2013. Conformity and Specificity of Primate
1918 Corticogenesis. In: Werner JS,, Chalupa LM, editors. *The New Visual*
1919 *Neurosciences*. Cambridge, Massachusetts: The MIT Press. p. 1407–1422.
- 1920 Bijanzadeh M, Nurminen L, Merlin S, Angelucci A. 2018. Distinct Laminar Processing of
1921 Local and Global Context in Primate Primary Visual Cortex. *Neuron*. 100:259–274.
- 1922 Binzegger T, Douglas RJ, Martin KA. 2004. A quantitative map of the circuit of cat
1923 primary visual cortex. *J Neurosci*. 24:8441–8453.
- 1924 Blasdel GG. 1992. Differential Imaging of Ocular Dominance and Orientation Selectivity
1925 in Monkey Striate Cortex. *J Neurosci*. 12:3115–3138.
- 1926 Blasdel GG, Campbell D. 2001. Functional retinotopy of monkey visual cortex. *J*
1927 *Neurosci*. 21:8286–8301.
- 1928 Blasdel GG, Fitzpatrick D. 1984. Physiological organization of layer 4 in macaque striate
1929 cortex. *J Neurosci*. 4:880–895.
- 1930 Blasdel GG, Lund JS. 1983. Termination of afferent axons in macaque striate cortex. *J*
1931 *Neurosci*. 3:1389–1413.
- 1932 Blasdel GG, Salama G. 1986. Voltage-sensitive dyes reveal a modular organization in
1933 monkey striate cortex. *Nature*. 321:579–585.
- 1934 Born RT, Bradley DC. 2005. Structure and function of visual area MT. *Annu Rev*
1935 *Neurosci*. 28:157–189.

- 1936 Braitenberg V, Braitenberg C. 1979. Geometry of orientation columns in the visual cortex.
1937 Biol Cybern. 33:179–186.
- 1938 Braitenberg V, Schuz A. 1998. Cortex: Statistics and geometry of Neuronal connectivity.
1939 2nd ed. Berlin: Springer.
- 1940 Briggs F, Callaway EM. 2001. Layer-specific input to distinct cell types in layer 6 of
1941 monkey primary visual cortex. J Neurosci. 21:3600–3608.
- 1942 Briggs F, Callaway EM. 2005. Laminar patterns of local excitatory input to layer 5
1943 neurons in Macaque primary visual cortex. Cereb Cortex. 15:479–488.
- 1944 Briggs F, Kiley CW, Callaway EM, Usrey WM. 2016. Morphological Substrates for
1945 Parallel Streams of Corticogeniculate Feedback Originating in Both V1 and V2 of
1946 the Macaque Monkey. Neuron. 90:388–399.
- 1947 Briggs F, Usrey WM. 2009. Parallel Processing in the Corticogeniculate Pathway of the
1948 Macaque Monkey. Neuron. 62:135–146.
- 1949 Brodmann K, Garey LJ. 2006. Brodmann’s Localisation in the Cerebral Cortex, Springer.
- 1950 Bullier J. 2001. Integrated model of visual processing. Brain Res Brain Res Rev. 36:96-
1951 107.
- 1952 Bullier J, Girard P, Salin P-A. 1994. The role of area 17 in the transfer of visual
1953 information to extrastriate visual cortex. In: Peters A,, Rockland KS, editors.
1954 Cerebral Cortex. New York: Plenum Press. p. 301–330.
- 1955 Bullier J, Henry GH. 1980. Ordinal position and afferent input of neurons in monkey
1956 striate cortex. J Comp Neurol. 193:913–935.
- 1957 Bullier J, Hupe JM, James AC, Girard P. 2001. The role of feedback connections in
1958 shaping the responses of visual cortical neurons. Prog Brain Res. 134:193–204.
- 1959 Bullier J, Kennedy H. 1983. Projection of the Lateral Geniculate Nucleus onto Cortical
1960 Area V2 in the Macaque Monkey. Exp Brain Res. 53:168–172.

- 1961 Bullier J, Nowak G. 1995. Parallel versus serial processing: new vistas on the distributed
1962 organization of the visual system. *Curr Biol.* 5:497–503.
- 1963 Callaway EM. 1998a. Local circuits in primary visual cortex of the macaque monkey.
1964 *Annu Rev Neurosci.* 21:47–74.
- 1965 Callaway EM. 1998b. Prenatal development of layer-specific local circuits in primary
1966 visual cortex of the macaque monkey. *J Neurosci.* 18:1505–1527.
- 1967 Callaway EM, Wiser AK. 1996. Contributions of individual layer 2-5 spiny neurons to
1968 local circuits in macaque primary visual cortex. *Vis Neurosci.* 13:907–922.
- 1969 Caputi A, Melzer S, Michael M, Monyer H. 2013. The long and short of GABAergic
1970 neurons. *Curr Opin Neurobiol.* 23:179–186.
- 1971 Carlos L, Silveira L. 2003. Comparative study of primate retina. In: Kaas JH,, Collins CE,
1972 editors. *The primate visual system*. London: CRC Press. p. 29–51.
- 1973 Casagrande VA, Kaas JH. 1994. The afferent, intrinsic and efferent connections of
1974 primary visual cortex in primates. In: Peters A,, Rockland KS, editors. *Cerebral*
1975 *Cortex, Volume 10, Primary visual cortex in primates*. New York: Plenum Press. p.
1976 201–259.
- 1977 Casagrande VA, Royal DW. 2004. Parallel visual pathways in a dynamic system. In: Kaas
1978 JH,, Collins CE, editors. *The primate visual system*. London: CRC Press. p. 1–27.
- 1979 Casagrande VA, Yazar F, Jones KD, Ding Y. 2007. The morphology of the koniocellular
1980 axon pathway in the macaque monkey. *Cereb Cortex.* 17:2334–2345.
- 1981 Cavanaugh JR, Bair W, Movshon JA. 2002. Nature and interaction of signals from the
1982 receptive field center and surround in macaque V1 neurons. *J Neurophysiol.*
1983 88:2530–2546.
- 1984 Chariker XL, Shapley R, Young L. 2016. Orientation Selectivity from Very Sparse LGN
1985 Inputs in a Comprehensive Model of Macaque V1 Cortex. *J Neurosci.* 36:12368–

- 1986 12384.
- 1987 Chen G, Lu HD, Roe AW. 2008. A Map for Horizontal Disparity in Monkey V2. *Neuron*.
- 1988 58:442–450.
- 1989 Chung K, Wallace J, Kim SY, Kalyanasundaram S, Andalman AS, Davidson TJ,
- 1990 Mirzabekov JJ, Zalocusky KA, Mattis J, Denisin AK, Pak S, Bernstein H,
- 1991 Ramakrishnan C, Grosenick L, Gradinaru V, Deisseroth K. 2013. Structural and
- 1992 molecular interrogation of intact biological systems. *Nature*. 497:332–337.
- 1993 Collins CE. 2011. Variability in neuron densities across the cortical sheet in primates. In:
- 1994 *Brain, Behavior and Evolution*. p. 37–50.
- 1995 Connolly M, Van Essen D. 1984. The representation of the visual field in parvocellular
- 1996 and magnocellular layers of the lateral geniculate nucleus in the macaque monkey. *J*
- 1997 *Comp Neurol*. 226:544–564.
- 1998 Daniel PM, Whitteridge D. 1961. The representation of the visual field on the cerebral
- 1999 cortex in monkeys. *J Physiol*. 159:203–221.
- 2000 De Valois RL, Albrecht DG, Thorell LG. 1982. Spatial frequency selectivity of cells in
- 2001 macaque visual cortex. *Vis Res*. 22:545–559.
- 2002 De Valois RL, Yund EW, Hepler N. 1982. The orientation and direction selectivity of cells
- 2003 in macaque visual cortex. *Vis Res*. 22:531–544.
- 2004 DeAngelis GC, Cumming BG, Newsome WT. 1998. Cortical area MT and the perception
- 2005 of stereoscopic depth. *Nature*. 394:677–680.
- 2006 DeFelipe J. 2010. From the Connectome to the synaptome: An epic love story. *Science*.
- 2007 330:1198–1201.
- 2008 DeFelipe J. 2011. The Evolution of the Brain, the Human Nature of Cortical Circuits, and
- 2009 Intellectual Creativity. *Front Neuroanat*. 5:Article 29.
- 2010 DeFelipe J. 2015. The anatomical problem posed by brain complexity and size: a

- 2011 potential solution. *Front Neuroanat.* 9:Article 104.
- 2012 DeFelipe J, González-Albo MC, Del Río MR, Elston GN. 1999. Distribution and patterns
- 2013 of connectivity of interneurons containing calbindin, calretinin, and parvalbumin in
- 2014 visual areas of the occipital and temporal lobes of the macaque monkey. *J Comp*
- 2015 *Neurol.* 412:515–526.
- 2016 DeFelipe J, López-Cruz PL, Benavides-Piccione R, Bielza C, Larrañaga P, Anderson S,
- 2017 Burkhalter A, Cauli B, Fairén A, Feldmeyer D, Fishell G, Fitzpatrick D, Freund TF,
- 2018 González-Burgos G, Hestrin S, Hill S, Hof PR, Huang J, Jones EG, Kawaguchi Y,
- 2019 Kisvárdy Z, Kubota Y, Lewis DA, Marín O, Markram H, McBain CJ, Meyer HS,
- 2020 Monyer H, Nelson SB, Rockland K, Rossier J, Rubenstein JLR, Rudy B, Scanziani
- 2021 M, Shepherd GM, Sherwood CC, Staiger JF, Tamás G, Thomson A, Wang Y, Yuste
- 2022 R, Ascoli GA. 2013. New insights into the classification and nomenclature of
- 2023 cortical GABAergic interneurons. *Nat Rev Neurosci.* 14:202–216.
- 2024 Denk W, Horstmann H. 2004. Serial block-face scanning electron microscopy to
- 2025 reconstruct three-dimensional tissue nanostructure. *PLoS Biol.* 2:e329.
- 2026 Denk W, Strickler JH, Webb WW. 1990. Two-photon laser scanning fluorescence
- 2027 microscopy. *Science.* 248:73–76.
- 2028 Derrington AM, Krauskopf J, Lennie P. 1984. Chromatic mechanisms in lateral geniculate
- 2029 nucleus of macaque. *J Physiol.* 357:241–265.
- 2030 Desimone R, Ungerleider LG. 1986. Multiple visual areas in the caudal superior temporal
- 2031 sulcus of the macaque. *J Comp Neurol.* 248:164–189.
- 2032 Douglas RJ, Martin KAC. 2004. Neuronal Circuits of the Neocortex. *Annu Rev Neurosci.*
- 2033 27:419–451.
- 2034 Dow BM, Snyder AZ, Vautin RG, Bauer R. 1981. Magnification Factor and Receptive
- 2035 Field Size in Foveal Striate Cortex of the Monkey. *Exp Brain Res.* 44:213–228.

- 2036 Egger R, Dercksen VJ, Udvary D, Hege H-C, Oberlaender M. 2014. Generation of dense
2037 statistical connectomes from sparse morphological data. *Front Neuroanat.* 8:Article
2038 129.
- 2039 Elston GN. 2003. Cortex, cognition and the cell: new insights into the pyramidal neuron
2040 and prefrontal function. *Cereb Cortex.* 13:1124–1138.
- 2041 Elston GN, Fujita I. 2014. Pyramidal cell development: postnatal spinogenesis, dendritic
2042 growth, axon growth, and electrophysiology. *Front Neuroanat.* 8.
- 2043 Elston GN, Rosa MGP. 1997. The occipitoparietal pathway of the macaque monkey:
2044 Comparison of pyramidal cell morphology in layer III of functionally related
2045 cortical visual areas. *Cereb Cortex.* 7:432–452.
- 2046 Elston GN, Rosa MGP. 1998. Morphological variation of layer III pyramidal neurones in
2047 the occipitotemporal pathway of the macaque monkey visual cortex. *Cereb Cortex.*
2048 8:278–294.
- 2049 Ercsey-Ravasz M, Markov NT, Lamy C, Van Essen DC, Knoblauch K, Toroczkai Z,
2050 Kennedy H. 2013. A predictive network model of cerebral cortical connectivity
2051 based on a distance rule. *Neuron.* 80:184–197.
- 2052 Erwin E, Obermayer K, Schulten K. 1995. Models of orientation and ocular dominance
2053 columns in the visual cortex: A Critical Comparison. *Neural Comput.* 7:425–468.
- 2054 Falchier A, Clavagnier S, Barone P, Kennedy H. 2002. Anatomical evidence of
2055 multimodal integration in primate striate cortex. *J Neurosci.* 22:5749–5759.
- 2056 Federer F, Merlin S, Angelucci A. 2015. Anatomical and functional specificity of V2-to-
2057 V1 feedback circuits in the primate visual cortex. In: *Soc. Neurosci. Abstr.* p.
2058 Online: 699.602.
- 2059 Federer F, Williams D, Ichida JM, Merlin S, Angelucci A. 2013. Two Projection Streams
2060 from Macaque V1 to the Pale Cytochrome Oxidase Stripes of V2. *J Neurosci.*

2061 33:11530–11539.

2062 Felleman DJ, Lim H, Xiao Y, Wang Y, Eriksson A, Parajuli A. 2015. The Representation
 2063 of Orientation in Macaque V2: Four Stripes Not Three. *Cereb Cortex*. 25:2354–
 2064 2369.

2065 Felleman DJ, Van Essen DC. 1991. Distributed hierarchical processing in the primate
 2066 cerebral cortex. *Cereb Cortex*. 1:1–47.

2067 Fisker RA, Garey LJ, Powell TP. 1975. The intrinsic, association and commissural
 2068 connections of area 17 on the visual cortex. *Philos Trans R Soc L B Biol Sci*.
 2069 272:487–536.

2070 Fitzpatrick D, Lund JS, Schmechel DE, Towles AC. 1987. Distribution of GABAergic
 2071 neurons and axon terminals in the macaque striate cortex. *J Comp Neurol*. 264:73–
 2072 91.

2073 Franklin MS, Kraemer GW, Shelton SE, Baker E, Kalin NH, Uno H. 2000. Gender
 2074 differences in brain volume and size of corpus callosum and amygdala of rhesus
 2075 monkey measured from MRI images. *Brain Res*. 852:263–267.

2076 Freeman J, Ziemba CM, Heeger DJ, Simoncelli EP, Movshon JA. 2013. A functional and
 2077 perceptual signature of the second visual area in primates. *Nat Neurosci*. 16:974–
 2078 981.

2079 Freund TF, Martin KAC, Soltesz I, Somogyi P, Whitteridge D. 1989. Arborisation pattern
 2080 and postsynaptic targets of physiologically identified thalamocortical afferents in
 2081 striate cortex of the macaque monkey. *J Comp Neurol*. 289:315–336.

2082 Gamberini M, Fattori P, Galletti C. 2015. The medial parietal occipital areas in the
 2083 macaque monkey. *Vis Neurosci*. 32:e013.

2084 Garcia-Marin V, Kelly J, Hawken M. 2017. Major Feedforward Thalamic Input Into
 2085 Layer 4C of Primary Visual Cortex in Primate. *Cereb Cortex*. 29:134–149.

- 2086 Garg AK, Li P, Rashid MS, Callaway EM. 2019. Color and orientation are jointly coded
2087 and spatially organized in primate primary visual cortex. *Science*. 364:1275–1279.
- 2088 Gattas R, Sousa APB, Mishkin M, Ungerleider LG. 1997. Cortical projections of area V2
2089 in the macaque. *Cereb Cortex*. 7:110–129.
- 2090 Gattass R, Gross CG. 1981. Visual topography of striate projection zone (MT) in
2091 posterior superior temporal sulcus of the macaque. *J Neurophysiol*. 46:621–638.
- 2092 Gattass R, Nascimento-Silva S, Soares JGM, Lima B, Jansen AK, Diogo ACM, Farias
2093 MF, Botelho MM, EP, Mariani OS, Azzi J, Fiorani M. 2005. Cortical visual areas in
2094 monkeys: location, topography, connections, columns, plasticity and cortical
2095 dynamics. *Philos Trans R Soc B Biol Sci*. 360:709–731.
- 2096 Gattass R, Soares JGM, Desimone R, Ungerleider LG. 2014. Connectional subdivision of
2097 the claustrum: two visuotopic subdivisions in the macaque. *Front Syst Neurosci*.
2098 8:Article 63.
- 2099 Gegenfurtner KR. 2003. Cortical mechanisms of colour vision. *Nat Rev Neurosci*. 4:563–
2100 572.
- 2101 Giannaris EL, Rosene DL. 2012. A stereological study of the numbers of neurons and glia
2102 in the primary visual cortex across the lifespan of male and female rhesus monkeys.
2103 *J Comp Neurol*. 520:3492–3508.
- 2104 Gilbert CD. 1983. Microcircuitry of the Visual Cortex. *Annu Rev Neurosci*. 6:217–247.
- 2105 Gilman JP, Medalla M, Luebke JI. 2017. Area-Specific Features of Pyramidal Neurons-a
2106 Comparative Study in Mouse and Rhesus Monkey. *Cereb Cortex*. 27:2078–2094.
- 2107 Girard P, Hupe JM, Bullier J. 2001. Feedforward and feedback connections between areas
2108 V1 and V2 of the monkey have similar rapid conduction velocities. *J Neurophysiol*.
2109 85:1328–31.
- 2110 Goris RLT, Simoncelli EP, Movshon JA. 2015. Origin and Function of Tuning Diversity

2111 in Macaque Visual Cortex. *Neuron*. 88:819–831.

2112 Grinvald A, Lieke E, Frostig RD, Gilbert CD, Wiesel TN. 1986. Functional architecture
2113 of cortex revealed by optical imaging of intrinsic signals. *Nature*. 324:361–364.

2114 Gupta A, Wang Y, Markram H. 2000. Organizing Principles for a Diversity of GABAergic
2115 Interneurons and Synapses in the Neocortex. *Science*. 287:273–278.

2116 Gur M, Kagan I, Snodderly DM. 2005. Orientation and direction selectivity of neurons in
2117 V1 of alert monkeys: Functional relationships and laminar distributions. *Cereb*
2118 *Cortex*. 15:1207–1221.

2119 Gur M, Snodderly DM. 2006. High response reliability of neurons in primary visual
2120 cortex (V1) of alert, trained monkeys. *Cereb Cortex*. 16:888–895.

2121 Gur M, Snodderly DM. 2007. Direction selectivity in V1 of alert monkeys: Evidence for
2122 parallel pathways for motion processing. *J Physiol*. 585:383–400.

2123 Gur M, Snodderly DM. 2008. Physiological differences between neurons in layer 2 and
2124 layer 3 of primary visual cortex (V1) of alert macaque monkeys. *J Physiol*.
2125 586:2293–2306.

2126 Hadjikhani N, Liu a K, Dale a M, Cavanagh P, Tootell RB. 1998. Retinotopy and color
2127 sensitivity in human visual cortical area V8. *Nat Neurosci*. 1:235–241.

2128 Harris KD, Shepherd GMG. 2015. The neocortical circuit: themes and variations. *Nat*
2129 *Neurosci*. 18:170–181.

2130 Hassler R. 1966. Comparative anatomy of the central visual system in day and night-
2131 active primates. In: Hassler R., Stephan H, editors. *Evolution of the forebrain*.
2132 Stuttgart: Thieme. p. 419–434.

2133 Hawken MJ, Shapley RM, Disney AA, Garcia-Marin V, Henrie JA, Henry CA, Johnson
2134 EM, Joshi S, Kelly JG, Ringach DL, Xing D. 2019. Functional clusters of neurons
2135 in layer 6 of macaque V1. *bioRxiv*. doi: <https://doi.org/10.1101/685990>.

- 2136 Hegdé J, Van Essen DC. 2000. Selectivity for complex shapes in primate visual area V2. J
2137 Neurosci. 20:RC61.
- 2138 Hegdé J, Van Essen DC. 2003. Strategies of shape representation in macaque visual area
2139 V2. Vis Neurosci. 20:313–328.
- 2140 Hendrickson AE, Wilson JR, Ogren MP. 1978. The neuroanatomical organization of
2141 pathways between the dorsal lateral geniculate nucleus and visual cortex in Old
2142 World and New World primates. J Comp Neurol. 182:123–136.
- 2143 Hendry SH, Reid RC. 2000. The koniocellular pathway in primate vision. Annu Rev
2144 Neurosci. 23:127–153.
- 2145 Hendry SH, Schwark HD, Jones EG, Yan J. 1987. Numbers and proportions of GABA-
2146 immunoreactive neurons in different areas of monkey cerebral cortex. J Neurosci.
2147 7:1503–1519.
- 2148 Hendry SHC, Yoshioka T. 1994. A neurochemically distinct third channel in the macaque
2149 dorsal lateral geniculate nucleus. Science. 264:575–577.
- 2150 Hofman MA. 1989. On the evolution and geometry of the brain in mammals. Prog
2151 Neurobiol. 32:137–158.
- 2152 Hokkanen H, Andalibi V, Vanni S. 2019. Controlling Complexity of Cerebral Cortex
2153 Simulations-II: Streamlined microcircuits. Neural Comput. 31:1066–1084.
- 2154 Horton JC. 1984. Cytochrome oxidase patches: a new cytoarchitectonic feature of
2155 monkey visual cortex. Philos Trans R Soc Lond B Biol Sci. 304:199–253.
- 2156 Horton JC, Hocking DR. 1996. Intrinsic variability of ocular dominance column
2157 periodicity in normal macaque monkeys. J Neurosci. 16:7228–7339.
- 2158 Horton JC, Hubel DH. 1981. Regular patchy distribution of cytochrome oxidase staining
2159 in primary visual cortex of macaque monkey. Nature. 292:762–764.
- 2160 Hu J, Ma H, Zhu S, Li P, Xu H, Fang Y, Chen M, Han C, Fang C, Cai X, Yan K, Lu HD.

2161 2018. Visual Motion Processing in Macaque V2. *Cell Rep.* 25:157-167.e5.

2162 Hubel D, Wiesel T. 1968. Receptive fields and functional architecture of monkey striate
2163 cortex. *J Physiol.* 215–243.

2164 Hubel DH, Freeman DC. 1977. Projection into the visual field of ocular dominance
2165 columns in macaque monkey. *Brain Res.* 122:336–343.

2166 Hubel DH, Wiesel TN. 1972. Laminar and columnar distribution of geniculo-cortical
2167 fibers in the macaque monkey. *J Comp Neurol.* 146:421–450.

2168 Hubel DH, Wiesel TN. 1974a. Sequence regularity and geometry of orientation columns
2169 in the monkey striate cortex. *J Comp Neurol.* 158:267–294.

2170 Hubel DH, Wiesel TN. 1974b. Uniformity of monkey striate cortex: A parallel
2171 relationship between field size, scatter, and magnification factor. *J Comp Neurol.*
2172 158:295–305.

2173 Hubel DH, Wiesel TN. 1977. Ferrier lecture. Functional architecture of macaque monkey
2174 visual cortex. *Proc R Soc London Ser B, Biol Sci.* 198:1–59.

2175 Hubener M, Bolz J. 1992. Relationships between Dendritic Morphology and
2176 Cytochrome-Oxidase Compartments in Monkey Striate Cortex. *J Comp Neurol.*
2177 324:67–80.

2178 Hunter JN, Born RT. 2011. Stimulus-Dependent Modulation of Suppressive Influences in
2179 MT. *J Neurosci.* 31:678–686.

2180 Hupé J-MM, James AC, Girard P, Bullier J. 2001. Response modulations by static texture
2181 surround in area V1 of the macaque monkey do not depend on feedback connections
2182 from V2. *J Neurophysiol.* 85:146-63.

2183 Hupé JM, James AC, Payne BR, Lomber SG, Girard P, Bullier J. 1998. Cortical feedback
2184 improves discrimination between figure and background by V1, V2 and V3 neurons.
2185 *Nature.* 394:784–787.

- 2186 Ito M. 2004. Representation of Angles Embedded within Contour Stimuli in Area V2 of
2187 Macaque Monkeys. *J Neurosci.* 24:3313–3324.
- 2188 Jerison HJ. 1955. Brain to body ratios and the evolution of intelligence. *Science.*
2189 121:447–449.
- 2190 Jia H, Rochefort NL, Chen X, Konnerth A. 2010. Dendritic organization of sensory input
2191 to cortical neurons in vivo. *Nature.* 464:1307–1312.
- 2192 Jones EG. 1993. Gabaergic neurons and their role in cortical plasticity in primates. *Cereb*
2193 *Cortex.* 3:361–372.
- 2194 Jones EG, Dell’Anna ME, Molinari M, Rausell E, Hashikawa T. 1995. Subdivisions of
2195 macaque monkey auditory cortex revealed by calcium-binding protein
2196 immunoreactivity. *J Comp Neurol.* 362:153–170.
- 2197 Kaas JH. 1992. Do humans see what monkeys see? *Trends Neurosci.* 15:1–3.
- 2198 Kaas JH. 1995. The evolution of isocortex. *Brain Behav Evol.* 46:187–196.
- 2199 Kaas JH. 2003. Early visual areas: V1, V2, V3, DM, DL, and MT. In: Kaas JH., Collins
2200 CE, editors. *The primate visual system.* London: CRC Press. p. 139–159.
- 2201 Kaas JH. 2005. The evolution of visual cortex in primates. In: Kremers J, editor. *The*
2202 *primate visual system.* John Wiley & Sons Ltd. p. 267–284.
- 2203 Katz LC, Gilbert CD, Wiesel TN. 1989. Local circuits and ocular dominance columns in
2204 monkey striate cortex. *J Neurosci.* 9:1389–1399.
- 2205 Kelly JG, Hawken MJ. 2017. Quantification of neuronal density across cortical depth
2206 using automated 3D analysis of confocal image stacks. *Brain Struct Funct.*
2207 222:3333–3353.
- 2208 Kennedy H, Bullier J. 1985. A double-labeling investigation of the afferent connectivity
2209 to cortical areas V1 and V2 of the macaque monkey. *J Neurosci.* 5:2815–2830.
- 2210 Kim HR, Angelaki DE, DeAngelis GC. 2015. A Functional Link between MT Neurons

- 2211 and Depth Perception Based on Motion Parallax. *J Neurosci.* 35:2766–2777.
- 2212 Kisvarday ZF, Cowey A, Smith a D, Somogyi P. 1989. Interlaminar and lateral excitatory
2213 amino acid connections in the striate cortex of monkey. *J Neurosci.* 9:667–682.
- 2214 Kötter R. 2004. Online Retrieval, Processing, and Visualization of Primate Connectivity
2215 Data From the CoCoMac Database. *Neuroinformatics.* 2:127–144.
- 2216 Kravitz DJ, Saleem KS, Baker CI, Mishkin M. 2011. A new neural framework for
2217 visuospatial processing. *Nat Rev Neurosci.* 12:217–230.
- 2218 Kravitz DJ, Saleem KS, Baker CI, Ungerleider LG, Mishkin M. 2013. The ventral visual
2219 pathway: An expanded neural framework for the processing of object quality. *Trends*
2220 *Cogn Sci.* 17:26–49.
- 2221 Kritzer MF, Cowey a, Somogyi P. 1992. Patterns of inter- and intralaminar GABAergic
2222 connections distinguish striate (V1) and extrastriate (V2, V4) visual cortices and
2223 their functionally specialized subdivisions in the rhesus monkey. *J Neurosci.*
2224 12:4545–4564.
- 2225 Landau ID, Egger R, Dercksen VJ, Oberlaender M, Sompolinsky H. 2016. The Impact of
2226 Structural Heterogeneity on Excitation-Inhibition Balance in Cortical Networks.
2227 *Neuron.* 92:1106–1121.
- 2228 Landisman CEC, Ts'o DY. 2002. Color processing in macaque striate cortex:
2229 relationships to ocular dominance, cytochrome oxidase, and orientation. *J*
2230 *Neurophysiol.* 87:3126–3137.
- 2231 Large I, Bridge H, Ahmed B, Clare S, Kolasinski J, Lam WW, Miller KL, Dyrby TB,
2232 Parker AJ, Smith JET, Daubney G, Sallet J, Bell AH, Krug K. 2016. Individual
2233 Differences in the Alignment of Structural and Functional Markers of the V5/MT
2234 Complex in Primates. *Cereb Cortex.* 26:3928–3944.
- 2235 Larkman AU. 1991. Dendritic morphology of pyramidal neurones of the visual cortex of

- 2236 the rat: I. Branching patterns. *J Comp Neurol.* 306:307–319.
- 2237 Larkum M. 2013. A cellular mechanism for cortical associations: An organizing principle
2238 for the cerebral cortex. *Trends Neurosci.* 36:141–151.
- 2239 Larkum ME, Senn W, Lüscher HR. 2004. Top-down dendritic input increases the gain of
2240 layer 5 pyramidal neurons. *Cereb Cortex.* 14:1059–1070.
- 2241 le Gros Clark WE. 1941. The laminar organization and cell content of the lateral
2242 geniculate body in the monkey. *J Anat.* 75:419–433.
- 2243 Lee SH, Hjerling-Leffler J, Zagha E, Fishell G, Rudy B. 2010. The largest group of
2244 superficial neocortical GABAergic interneurons expresses ionotropic serotonin
2245 receptors. *J Neurosci.* 30:16796–16808.
- 2246 Lee WCA, Bonin V, Reed M, Graham BJ, Hood G, Glattfelder K, Reid RC. 2016.
2247 Anatomy and function of an excitatory network in the visual cortex. *Nature.*
2248 532:370–374.
- 2249 Lennie P, Movshon JA. 2005. Coding of color and form in the geniculostriate visual
2250 pathway (invited review). *J Opt Soc Am A Opt Image Sci Vis.* 22:2013–2033.
- 2251 LeVay S, Hubel D, Wiesel T. 1975. The Pattern of Ocular Dominance Columns in
2252 Macaque Visual Cortex Revealed by a Reduced Silver Stain. *J Comp Neurol.*
2253 159:559–576.
- 2254 Levitt JB, Kiper DC, Movshon JA. 1994. Receptive-Fields and Functional Architecture of
2255 Macaque V2. *J Neurophysiol.* 71:2517–2542.
- 2256 Levitt JB, Lund JS, Yoshioka T. 1996. Anatomical substrates for early stages in cortical
2257 processing of visual information in the macaque monkey. *Behav Brain Res.* 76:5–
2258 19.
- 2259 Levitt JB, Yoshioka T, Lund JS. 1994. Intrinsic cortical connections in macaque visual
2260 area V2: evidence for interaction between different functional streams. *J Comp*

- 2261 Neurol. 342:551–570.
- 2262 Li H, Fukuda M, Tanifuji M, Rockland KS. 2003. Intrinsic collaterals of layer 6 Meynert
2263 cells and functional columns in primate V1. *Neuroscience*. 120:1061–1069.
- 2264 Li WH. 2015. A fast and flexible computer vision system for implanted visual prostheses.
2265 In: *Lecture Notes in Computer Science*. p. 686–701.
- 2266 Livingstone M, Hubel D. 1988a. Segregation of form, color, movement and depth:
2267 anatomy, physiology and perception. *Science*. 240:740–749.
- 2268 Livingstone MS, Hubel DH. 1984a. Anatomy and physiology of a color system in the
2269 primate visual cortex. *J Neurosci*. 4:309–356.
- 2270 Livingstone MS, Hubel DH. 1984b. Specificity of intrinsic connections in primate
2271 primary visual cortex. *J Neurosci*. 4:2830–2835.
- 2272 Livingstone MS, Hubel DH. 1988b. Do the relative mapping densities of the magno- and
2273 parvocellular systems vary with eccentricity? *J Neurosci*. 8:4334–4339.
- 2274 Lu HD, Chen G, Tanigawa H, Roe AW. 2010. A Motion Direction Map in Macaque V2.
2275 *Neuron*. 68:1002–1013.
- 2276 Lu HD, Roe AW. 2008. Functional organization of color domains in V1 and V2 of
2277 Macaque monkey revealed by optical imaging. *Cereb Cortex*. 18:516–533.
- 2278 Luebke JI. 2017. Pyramidal Neurons Are Not Generalizable Building Blocks of Cortical
2279 Networks. *Front Neuroanat*. 11:Article 11.
- 2280 Luebke JI, Medalla M, Amatrudo JM, Weaver CM, Crimins JL, Hunt B, Hof PR, Peters
2281 A. 2015. Age-related changes to layer 3 pyramidal cells in the rhesus monkey visual
2282 cortex. *Cereb Cortex*. 25:1454–1468.
- 2283 Lund JS. 1973. Organization of neurons in the visual cortex, area 17, of the monkey
2284 (Macaca mulatta). *J Comp Neurol*. 147:455–495.
- 2285 Lund JS. 1987. Local circuit neurons of macaque monkey striate cortex: I. Neurons of

- 2286 laminae 4C and 5A. *J Comp Neurol.* 257:60–92.
- 2287 Lund JS. 1988. Anatomical Organization of Macaque Monkey Striate Visual Cortex.
- 2288 *Annu Rev Neurosci.* 11:253–288.
- 2289 Lund JS, Angelucci A, Bressloff PC. 2003. Anatomical substrates for functional columns
- 2290 in macaque monkey primary visual cortex. *Cereb Cortex.* 13:15–24.
- 2291 Lund JS, Boothe RG. 1975. Interlaminar Connections and Pyramidal Neuron
- 2292 Organisation in the Visual Cortex, Area 17, of the Macaque Monkey. *J Comp*
- 2293 *Neurol.* 159:305–334.
- 2294 Lund JS, Griffiths S, Rumberger A, Levitt JB. 2001. Inhibitory Synapse Cover on the
- 2295 Somata of Excitatory Neurons in Macaque Monkey Visual Cortex. *Cereb Cortex.*
- 2296 11:783–795.
- 2297 Lund JS, Hawken MJ, Parker AJ. 1988. Local circuit neurons of macaque monkey striate
- 2298 cortex: II. Neurons of laminae 5B and 6. *J Comp Neurol.* 276:1–29.
- 2299 Lund JS, Hendrickson AE, Ogren MP, Tobin EA. 1981. Anatomical organization of
- 2300 primate visual cortex area VII. *J Comp Neurol.* 202:19–45.
- 2301 Lund JS, Lund RD, Hendrickson AE, Bunt AH, Fuchs AF. 1975. The origin of efferent
- 2302 pathways from the primary visual cortex, area 17, of the macaque monkey as shown
- 2303 by retrograde transport of horseradish peroxidase. *J Comp Neurol.* 164:287–303.
- 2304 Lund JS, Wu CQ. 1997. Local circuit neurons of macaque monkey striate cortex: IV.
- 2305 Neurons of laminae 1-3a. *J Comp Neurol.* 384:109–126.
- 2306 Lund JS, Yoshioka T. 1991. Local circuit neurons of macaque monkey striate cortex: III.
- 2307 Neurons of laminae 4B, 4A, and 3B. *J Comp Neurol.* 311:234–258.
- 2308 Lund JS, Yoshioka T, Levitt JB. 1993. Comparison of intrinsic connectivity in different
- 2309 areas of macaque monkey cerebral cortex. *Cereb Cortex.* 3:148–162.
- 2310 Lund JS, Yoshioka T, Levitt JB. 1994. Substrates for interlaminar connections in area V1

- 2311 of macaque monkey cerebral cortex. In: Peters A., Rockland KS, editors. Cerebral
2312 Cortex, Volume 10, Primary visual cortex in primates. New York: Plenum Press. p.
2313 37–60.
- 2314 Luo L, Callaway EM, Svoboda K. 2008. Genetic Dissection of Neural Circuits. *Neuron*.
2315 57:634–660.
- 2316 Mainen Z, Sejnowski T. 1995. Reliability of spike timing in neocortical neurons. *Science*.
2317 268:1503–1506.
- 2318 Malach R, Amir Y, Harel M, Grinvald A. 1993. Relationship between intrinsic
2319 connections and functional architecture revealed by optical imaging and in vivo
2320 targeted biocytin injections in primate striate cortex. *Proc Natl Acad Sci*. 90:10469–
2321 10473.
- 2322 Malpeli JG, Lee D, Baker FH. 1996. Laminar and retinotopic organization of the macaque
2323 lateral geniculate nucleus: Magnocellular and parvocellular magnification functions.
2324 *J Comp Neurol*. 375:363–377.
- 2325 Mansfield RJW. 1973. Latency functions in human vision. *Vision Res*. 13:2219–2234.
- 2326 Marino L. 1998. A comparison of encephalization between odontocete cetaceans and
2327 anthropoid primates. *Brain Behav Evol*. 51:230–238.
- 2328 Markov NT, Ercsey-Ravasz M, Ribeiro Gomes AR, Lamy C, Magrou L, Vezoli J, Misery
2329 P, Falchier A, Quilodran R, Gariel MA, Sallet J, Gamanut R, Huissoud C,
2330 Clavagnier S, Giroud P, Sappey-Marini D, Barone P, Dehay C, Toroczkai Z,
2331 Knoblauch K, Van Essen DC, Kennedy H. 2014. A weighted and directed interareal
2332 connectivity matrix for macaque cerebral cortex. *Cereb Cortex*. 24:17–36.
- 2333 Markov NT, Ercsey-Ravasz M, Van Essen DC, Knoblauch K, Toroczkai Z, Kennedy H.
2334 2013. Cortical high-density counterstream architectures. *Science*. 342:1238406.
- 2335 Markov NT, Misery P, Falchier A, Lamy C, Vezoli J, Quilodran R, Gariel MA, Giroud P,

2336 Ercsey-Ravasz M, Pilaz LJ, Huissoud C, Barone P, Dehay C, Toroczkai Z, Van
2337 Essen DC, Kennedy H, Knoblauch K. 2011. Weight consistency specifies
2338 regularities of macaque cortical networks. *Cereb Cortex*. 21:1254–1272.

2339 Markov NT, Vezoli J, Chameau P, Falchier A, Quilodran R, Huissoud C, Lamy C, Misery
2340 P, Giroud P, Ullman S, Barone P, Dehay C, Knoblauch K, Kennedy H. 2014.
2341 Anatomy of hierarchy: feedforward and feedback pathways in macaque visual
2342 cortex. *J Comp Neurol*. 522:225–259.

2343 Markram H, Muller E, Ramaswamy S, Reimann MW, Abdellah M, Sanchez CA,
2344 Ailamaki A, Alonso-Nanclares L, Antille N, Arsever S, Kahou GA, Berger TK,
2345 Bilgili A, Buncic N, Chalimourda A, Chindemi G, Courcol JD, Delalondre F,
2346 Delattre V, Druckmann S, Dumusc R, Dynes J, Eilemann S, Gal E, Gevaert ME,
2347 Ghobril JP, Gidon A, Graham JW, Gupta A, Haenel V, Hay E, Heinis T, Hernando
2348 JB, Hines M, Kanari L, Keller D, Kenyon J, Khazen G, Kim Y, King JG, Kisvarday
2349 Z, Kumbhar P, Lasserre S, Le Be J V, Magalhaes BR, Merchan-Perez A, Meystre J,
2350 Morrice BR, Muller J, Munoz-Cespedes A, Muralidhar S, Muthurasa K, Nachbaur
2351 D, Newton TH, Nolte M, Ovcharenko A, Palacios J, Pastor L, Perin R, Ranjan R,
2352 Riachi I, Rodriguez JR, Riquelme JL, Rossert C, Sfyarakis K, Shi Y, Shillcock JC,
2353 Silberberg G, Silva R, Tauheed F, Telefont M, Toledo-Rodriguez M, Trankler T, Van
2354 Geit W, Diaz J V, Walker R, Wang Y, Zaninetta SM, DeFelipe J, Hill SL, Segev I,
2355 Schurmann F. 2015. Reconstruction and Simulation of Neocortical Microcircuitry.
2356 *Cell*. 163:456–492.

2357 Markram H, Toledo-Rodriguez M, Wang Y, Gupta A, Silberberg G, Wu C. 2004.
2358 Interneurons of the neocortical inhibitory system. *Nat Rev Neurosci*. 5:793–807.

2359 Markram H, Wang Y, Tsodyks M. 1998. Differential signaling via the same axon of
2360 neocortical pyramidal neurons. *Proc Natl Acad Sci U S A*. 95:5323-8.

- 2361 Mates SL, Lund JS. 1983. Neuronal composition and development in lamina 4C of
2362 monkey striate cortex. *J Comp Neurol.* 221:60–90.
- 2363 Maunsell JH, Gibson JR. 1992. Visual response latencies in striate cortex of the macaque
2364 monkey. *J Neurophysiol.* 68:1332–1344.
- 2365 Maunsell JH, Van Essen DC. 1983a. Functional properties of neurons in middle temporal
2366 visual area of the macaque monkey. II. Binocular interactions and sensitivity to
2367 binocular disparity. *J Neurophysiol.* 49:1148–1167.
- 2368 Maunsell JHR, van Essen DC. 1987. Topographic organization of the middle temporal
2369 visual area in the macaque monkey: Representational biases and the relationship to
2370 callosal connections and myeloarchitectonic boundaries. *J Comp Neurol.* 266:535–
2371 555.
- 2372 Maunsell JHR, Van Essen DC. 1983b. The connections of the middle temporal visual area
2373 (MT) and their relationship to a cortical hierarchy in the macaque monkey. *J*
2374 *Neurosci.* 3:2563–2586.
- 2375 Maunsell JHR, Van Essen DC. 1987. The topographic organization of the middle
2376 temporal visual area in the macaque monkey and its relationship to callosal
2377 connections. *J Comp Neurol.* 266:535–555.
- 2378 McFarland JM, Cumming BG, Butts DA. 2016. Variability and Correlations in Primary
2379 Visual Cortical Neurons Driven by Fixational Eye Movements. *J Neurosci.*
2380 36:6225–6241.
- 2381 McGuire BA, Gilbert CD, Rivlin PK, Wiesel TN. 1991. Targets of horizontal connections
2382 in macaque primary visual cortex. *J Comp Neurol.* 305:370–392.
- 2383 Medalla M, Luebke JI. 2015. Diversity of Glutamatergic Synaptic Strength in Lateral
2384 Prefrontal versus Primary Visual Cortices in the Rhesus Monkey. *J Neurosci.*
2385 35:112–127.

- 2386 Mejias JF, Murray JD, Kennedy H, Wang X-J. 2016. Feedforward and feedback
2387 frequency-dependent interactions in a large-scale laminar network of the primate
2388 cortex. *Sci Adv.* 2:e1601335.
- 2389 Merigan WH, Maunsell JHR. 1993. How Parallel are the Primate Visual Pathways? *Annu*
2390 *Rev Neurosci.* 16:369–402.
- 2391 Merlin S, Ichida J, Federer F, Schiessl I, Angelucci A. 2012. Systematic relationship
2392 between cytochrome oxidase (CO) blobs, orientation singularities and dendritic
2393 spines in macaque V1. In: *Soc. Neurosci. Abstr. Online.* p. 568.02.
- 2394 Miller KD, Troyer TW. 2002. Neural noise can explain expansive, power-law
2395 nonlinearities in neural response functions. *J Neurophysiol.* 87:653–659.
- 2396 Montero VM, Zempel J. 1986. The proportion and size of GABA-immunoreactive
2397 neurons in the magnocellular and parvocellular layers of the lateral geniculate
2398 nucleus of the rhesus monkey. *Exp Brain Res.* 62:215–223.
- 2399 Mortazavi F, Stankiewicz A, Zhdanova I. 2019. Looking through Brains with Fast Passive
2400 CLARITY: Zebrafish, Rodents, Non-human Primates and Humans. *BIO-*
2401 *PROTOCOL.* 9:e3321.
- 2402 Movshon JA, Adelson EH, Gizzi MS, Newsome WT. 1985. The Analysis of Moving
2403 Visual Patterns. In: Chagas C., Gattas R., Gross CG, editors. *Pattern Recognition*
2404 *Mechanisms.* Rome: Vatican Press. p. 119–151.
- 2405 Munk MH, Nowak LG, Girard P, Chounlamountri N, Bullier J. 1995. Visual latencies in
2406 cytochrome oxidase bands of macaque area V2. *Proc Natl Acad Sci.* 92:988–992.
- 2407 Nassi JJ, Callaway EM. 2006. Multiple Circuits Relaying Primate Parallel Visual
2408 Pathways to the Middle Temporal Area. *J Neurosci.* 26:12789–12798.
- 2409 Nassi JJ, Callaway EM. 2007. Specialized Circuits from Primary Visual Cortex to V2 and
2410 Area MT. *Neuron.* 55:799–808.

- 2411 Nassi JJ, Callaway EM. 2009. Parallel processing strategies of the primate visual system.
2412 Nat Rev Neurosci. 10:360–372.
- 2413 Nassi JJ, Lomber SG, Born RT. 2013. Corticocortical Feedback Contributes to Surround
2414 Suppression in V1 of the Alert Primate. J Neurosci. 33:8504–8517.
- 2415 Nauhaus I, Benucci A, Carandini M, Ringach DL. 2008. Neuronal Selectivity and Local
2416 Map Structure in Visual Cortex. Neuron. 57:673–679.
- 2417 Nauhaus I, Nielsen KJ, Disney AA, Callaway EM. 2012. Orthogonal micro-organization
2418 of orientation and spatial frequency in primate primary visual cortex. Nat Neurosci.
2419 15:1683–1690.
- 2420 Nealey TA, Maunsell JH. 1994. Magnocellular and parvocellular contributions to the
2421 responses of neurons in macaque striate cortex. J Neurosci. 14:2069–79.
- 2422 Nhan HL, Callaway EM. 2012. Morphology of superior colliculus- and middle temporal
2423 area-projecting neurons in primate primary visual cortex. J Comp Neurol. 520:52–
2424 80.
- 2425 Nienborg H. 2006. Macaque V2 Neurons, But Not V1 Neurons, Show Choice-Related
2426 Activity. J Neurosci. 26:9567–9578.
- 2427 Nieuwenhuys R. 1994. The neocortex. An overview of its evolutionary development,
2428 structural organization and synaptology. Anat Embryol. 190:307–337.
- 2429 Nowak LG, Bullier J. 1997. The timing of information transfer in the visual system. In:
2430 Rockland KS,, Kaas JH,, Peters A, editors. Cerebral Cortex. London: Plenum Press.
2431 p. 205–241.
- 2432 Nowak LG, Munk MH, Girard P, Bullier J. 1995. Visual latencies in areas V1 and V2 of
2433 the macaque monkey. Vis Neurosci. 12:371–384.
- 2434 Nurminen L, Merlin S, Bijanzadeh M, Federer F, Angelucci A. 2018. Top-down feedback
2435 controls spatial summation and response amplitude in primate visual cortex. Nat

- 2436 Commun. 9:Article number 2281.
- 2437 O’Kusky J, Colonnier M. 1982a. Postnatal changes in the number of neurons and
 2438 synapses in the visual cortex (area 17) of the macaque monkey: A stereological
 2439 analysis in normal and monocularly deprived animals. *J Comp Neurol.* 210:291–
 2440 306.
- 2441 O’Kusky J, Colonnier M. 1982b. A laminar analysis of the number of neurons, glia, and
 2442 synapses in the visual cortex (area 17) of adult Macaque monkeys. *J Comp Neurol.*
 2443 210:278–290.
- 2444 Obermayer K, Blasdel GG. 1993. Geometry of orientation and ocular dominance columns
 2445 in monkey striate cortex. *J Neurosci.* 13:4114–4129.
- 2446 Oga T, Elston GN, Fujita I. 2017. Postnatal dendritic growth and spinogenesis of layer-V
 2447 pyramidal cells differ between visual, inferotemporal, and prefrontal cortex of the
 2448 macaque monkey. *Front Neurosci.* 11:Article 118.
- 2449 Oga T, Okamoto T, Fujita I. 2016. Basal Dendrites of Layer-III Pyramidal Neurons do not
 2450 Scale with Changes in Cortical Magnification Factor in Macaque Primary Visual
 2451 Cortex. *Front Neural Circuits.* 10:Article 74.
- 2452 Olavarria JF, Van Essen DC. 1997. The global pattern of cytochrome oxidase stripes in
 2453 visual area V2 of the macaque monkey. *Cereb Cortex.* 7:395–404.
- 2454 Pack CC, Hunter NJ, Born RT. 2005. Contrast Dependence of Suppressive Influences in
 2455 Cortical Area MT of Alert Macaque. *J Neurophysiol.* 93:1809–1815.
- 2456 Palmer CR, Chen Y, Seidemann E. 2012. Uniform spatial spread of population activity in
 2457 primate parafoveal V1. *J Neurophysiol.* 107:1857–1867.
- 2458 Perkel DJ, Bullier J, Kennedy H. 1986. Topography of the afferent connectivity of area 17
 2459 in the macaque monkey: A double-labelling study. *J Comp Neurol.* 253:374–402.
- 2460 Peters A, Payne BR, Budd J. 1994. A numerical analysis of the geniculocortical input to

- 2461 striate cortex in the monkey. *Cereb Cortex*. 4:215–229.
- 2462 Peters A, Sethares C. 1991a. Layer IVA of rhesus monkey primary visual cortex. *Cereb*
2463 *Cortex*. 1:445–462.
- 2464 Peters A, Sethares C. 1991b. Organization of pyramidal neurons in area 17 of monkey
2465 visual cortex. *J Comp Neurol*. 306:1–23.
- 2466 Petruzza S, Venkat A, Gyulassy A, Scorzelli G, Federer F, Angelucci A, Pascucci V,
2467 Bremer PT. 2017. ISAVS: Interactive scalable analysis and visualization system. In:
2468 SIGGRAPH ASIA 2017.
- 2469 Petruzza S, Venkat A, Gyulassy A, Scorzelli G, Federer F, Angelucci A, Pascucci V,
2470 Bremer PT. 2018. Scaling big data neuroscience: From interactive analytics to HPC
2471 platforms. *Adv Parallel Comput*. 33:53–68.
- 2472 Polimeni JR, Balasubramanian M, Schwartz EL. 2006. Multi-area visuotopic map
2473 complexes in macaque striate and extra-striate cortex. *Vision Res*. 46:3336–3359.
- 2474 Polimeni JR, Granquist-Fraser D, Wood RJ, Schwartz EL. 2005. Physical limits to spatial
2475 resolution of optical recording: Clarifying the spatial structure of cortical
2476 hypercolumns. *Proc Natl Acad Sci U S A*. 102:4158–4163.
- 2477 Potjans TC, Diesmann M. 2014. The cell-type specific cortical microcircuit: Relating
2478 structure and activity in a full-scale spiking network model. *Cereb Cortex*. 24:785–
2479 806.
- 2480 Povysheva N V, Zaitsev A V, Rotaru DC, Gonzalez-Burgos G, Lewis DA, Krimer LS.
2481 2008. Parvalbumin-positive basket interneurons in monkey and rat prefrontal cortex.
2482 *J Neurophysiol*. 100:2348–2360.
- 2483 Preuss TM. 2004. Specializations of the human visual system: The monkey model meets
2484 the human reality. In: Kaas JH,, Collins CE, editors. *The primate visual system*.
2485 London: CRC Press. p. 231–259.

- 2486 Rall W. 1962. Theory of physiological properties of dendrites. *Ann N Y Acad Sci.*
2487 96:1071–1092.
- 2488 Ramsden BM, Hung CP, Roe AW. 2014. Orientation domain diversity in macaque area
2489 V2. *Eye Brain.* 6:97–112.
- 2490 Rasch MJ, Schuch K, Logothetis NK, Maass W. 2011. Statistical Comparison of Spike
2491 Responses to Natural Stimuli in Monkey Area V1 With Simulated Responses of a
2492 Detailed Laminar Network Model for a Patch of V1. *J Neurophysiol.* 105:757–778.
- 2493 Reimann MW, King JG, Muller EB, Ramaswamy S, Markram H. 2015. An algorithm to
2494 predict the connectome of neural microcircuits. *Front Comput Neurosci.* 9:Article
2495 120.
- 2496 Ringach DL, Shapley RM, Hawken MJ. 2002. Orientation selectivity in macaque V1:
2497 diversity and laminar dependence. *J Neurosci.* 22:5639–5651.
- 2498 Rockland KS. 1985. A reticular pattern of intrinsic connections in primate area V2 (area
2499 18). *J Comp Neurol.* 235:467–478.
- 2500 Rockland KS. 1989. Bistratified Distribution Of Terminal Arbors Of Individual Axons
2501 Projecting From Area V1 To Middle Temporal Area (MT) In The Macaque Monkey.
2502 *Vis Neurosci.* 3:155–170.
- 2503 Rockland KS. 1994. The organization of feedback connections from area V2 (18) to V1
2504 (17). In: Peters A., Rockland KS, editors. *Cerebral Cortex, Volume 10, Primary*
2505 *visual cortex in primates.* New York: Plenum Press. p. 261–299.
- 2506 Rockland KS. 1995. Morphology of individual axons projecting from area V2 to MT in
2507 the macaque. *J Comp Neurol.* 355:15–26.
- 2508 Rockland KS. 1997. Elements of cortical architecture: Hierarchy revisited. In: Rockland
2509 KS., Kaas JH., Peters A, editors. *Cerebral Cortex Volume 12: Extrastriate cortex in*
2510 *primates.* London: Plenum Press. p. 243–293.

- 2511 Rockland KS, Lund JS. 1983. Intrinsic laminar lattice connections in primate visual
2512 cortex. *J Comp Neurol.* 216:303–318.
- 2513 Rockland KS, Ojima H. 2003. Multisensory convergence in calcarine visual areas in
2514 macaque monkey. *Int J Psychophysiol.* 50:19–26.
- 2515 Rockland KS, Pandya DN. 1979. Laminar origins and terminations of cortical
2516 connections of the occipital lobe in the rhesus monkey. *Brain Res.* 179:3–20.
- 2517 Rockland KS, Virga A. 1989. Terminal arbors of individual “Feedback” axons projecting
2518 from area V2 to V1 in the macaque monkey: A study using immunohistochemistry
2519 of anterogradely transported Phaseolus vulgaris-leucoagglutinin. *J Comp Neurol.*
2520 285:54–72.
- 2521 Rockland KS, Virga A. 1990. Organization of Individual Cortical Axons Projecting From
2522 Area VI (area 17) to V2 (area 18) In The Macaque Monkey. *Vis Neurosci.* 4:11–28.
- 2523 Roe AW. 2004. Modular complexity of area V2 in the macaque monkey. In: Kaas JH.,
2524 Collins CE, editors. *The primate visual system.* London: CRC Press. p. 109–138.
- 2525 Roe AW, Lu HD, Hung CP. 2005. Cortical processing of a brightness illusion. *Proc Natl*
2526 *Acad Sci.* 102:3869–3874.
- 2527 Roe W, Ts'o DY. 1995. Visual Topography in Primate V2: Multiple Representation across
2528 Functional Stripes. *J Neurosci.* 15:3689–3715.
- 2529 Rosa MGP, Tweedale R. 2005. Brain maps, great and small: Lessons from comparative
2530 studies of primate visual cortical organization. *Philos Trans R Soc B Biol Sci.*
2531 360:665–691.
- 2532 Rudy B, Fishell G, Lee S, Hjerling-Leffler J. 2011. Three groups of interneurons account
2533 for nearly 100% of neocortical GABAergic neurons. *Dev Neurobiol.* 71:45–61.
- 2534 Saleem KS, Price JL, Hashikawa T. 2007. Cytoarchitectonic and chemoarchitectonic
2535 subdivisions of the perirhinal and parahippocampal cortices in macaque monkeys. *J*

- 2536 Comp Neurol. 500:973–1006.
- 2537 Sawatari A, Callaway EM. 2000. Diversity and cell type specificity of local excitatory
2538 connections to neurons in layer 3B of monkey primary visual cortex. *Neuron*.
2539 25:459–471.
- 2540 Sceniak MP, Ringach DL, Hawken MJ, Shapley R. 1999. Contrast's effect on spatial
2541 summation by macaque V1 neurons. *Nat Neurosci*. 2:733–739.
- 2542 Schein SJ, de Monasterio FM. 1987. Mapping of retinal and geniculate neurons onto
2543 striate cortex of macaque. *J Neurosci*. 7:996–1009.
- 2544 Schiller PH, Finlay BL, Volman SF. 1976. Quantitative studies of single-cell properties in
2545 monkey striate cortex. I. Spatiotemporal organization of receptive fields. *J*
2546 *Neurophysiol*. 39:1288–1319.
- 2547 Schmidt M, Bakker R, Hilgetag CC, Diesmann M, van Albada SJ. 2018. Multi-scale
2548 account of the network structure of macaque visual cortex. *Brain Struct Funct*.
2549 223:1409–1435.
- 2550 Schmolesky MT, Wang Y, Hanes D, Thompson KG, Leutgeb S, Schall JD, Leventhal AG.
2551 1998. Signal timing across macaque visual system. *J Neurophysiol*. 79:3272–3278.
- 2552 Schwabe L, Obermayer K, Angelucci A, Bressloff PC. 2006. The role of feedback in
2553 shaping the extra-classical receptive field of cortical neurons: a recurrent network
2554 model. *J Neurosci*. 26:9117–9129.
- 2555 Schwartz EL. 1980. Computational anatomy and functional architecture of striate cortex:
2556 A spatial mapping approach to perceptual coding. *Vision Res*. 20:645–669.
- 2557 Schwartz EL. 1994. Computational studies of the spatial architecture of primate visual
2558 cortex. In: Peters A., Rockland KS, editors. *Cerebral Cortex*, Volume 10, Primary
2559 visual cortex in primates. New York: Plenum Press. p. 359–411.
- 2560 Sclar G, Maunsell JHR, Lennie P. 1990. Coding of image contrast in central visual

- 2561 pathways of the macaque monkey. *Vision Res.* 30:1–10.
- 2562 Self MW, van Kerkoerle T, Supèr H, Roelfsema PR. 2013. Distinct roles of the cortical
- 2563 layers of area V1 in figure-ground segregation. *Curr Biol.* 23:2121–2129.
- 2564 Shepherd GMG. 2013. Corticostriatal connectivity and its role in disease. *Nat Rev*
- 2565 *Neurosci.* 14:278–291.
- 2566 Shipp S. 2007. Structure and function of the cerebral cortex. *Curr Biol.* 17:R443–R449.
- 2567 Shipp S, Adams DL, Moutoussis K, Zeki S. 2009. Feature binding in the feedback layers
- 2568 of area V2. *Cereb Cortex.* 19:2230–2239.
- 2569 Shipp S, Zeki S. 2002a. The functional organization of area V2, I: specialization across
- 2570 stripes and layers. *Vis Neurosci.* 19:187–210.
- 2571 Shipp S, Zeki S. 2002b. The functional organization of area V2, II: The impact of stripes
- 2572 on visual topography. *Vis Neurosci.* 19:211–231.
- 2573 Shipp S, Zeki S, Shipp S. 1989. The organization of connections between areas V5 and
- 2574 V2 in macaque monkey visual cortex. *Eur J Neurosci.* 1:309–332.
- 2575 Shushruth S, Ichida JM, Levitt JB, Angelucci A. 2009. Comparison of spatial summation
- 2576 properties of neurons in macaque V1 and V2. *J Neurophysiol.* 102:2069–2083.
- 2577 Sincich LC, Adams DL, Horton JC. 2003. Complete flatmounting of the macaque
- 2578 cerebral cortex. *Vis Neurosci.* 20:663–686.
- 2579 Sincich LC, Horton JC. 2002. Divided by cytochrome oxidase: A map of the projections
- 2580 from V1 to V2 in macaques. *Science.* 295:1734–1737.
- 2581 Sincich LC, Horton JC. 2003. Independent projection streams from macaque striate
- 2582 cortex to the second visual area and middle temporal area. *J Neurosci.* 23:5684–
- 2583 5692.
- 2584 Sincich LC, Horton JC. 2005. The Circuitry of V1 and V2: Integration of Color, Form,
- 2585 and Motion. *Annu Rev Neurosci.* 28:303–326.

- 2586 Sincich LC, Park KF, Wohlgenuth MJ, Horton JC. 2004. Bypassing V1: a direct
2587 geniculate input to area MT. *Nat Neurosci.* 7:1123–1128.
- 2588 Skottun BC, De Valois RL, Grosof DH, Movshon JA, Albrecht DG, Bonds AB. 1991.
2589 Classifying simple and complex cells on the basis of response modulation. *Vision*
2590 *Res.* 31:1079–1086.
- 2591 Snodderly DM, Gur M. 1995. Organization of striate cortex of alert, trained monkeys
2592 (*Macaca fascicularis*): ongoing activity, stimulus selectivity, and widths of receptive
2593 field activating regions. *J Neurophysiol.* 74:2100–2125.
- 2594 Spear PD, Moore RJ, Kim CB, Xue JT, Tumosa N. 1994. Effects of aging on the primate
2595 visual system: spatial and temporal processing by lateral geniculate neurons in
2596 young adult and old rhesus monkeys. *J Neurophysiol.* 72:402–420.
- 2597 Stelzer EHK. 2015. Light-sheet fluorescence microscopy for quantitative biology. *Nat*
2598 *Methods.* 12:23–26.
- 2599 Stephan KE, Kamper L, Bozkurt A, Burns GAPC, Young MP, Kotter R. 2001. Advanced
2600 database methodology for the Collation of Connectivity data on the Macaque brain
2601 (CoCoMac). *Philos Trans R Soc B Biol Sci.* 356:1159–1186.
- 2602 Ta’afua SF, Federer F, Merlin S, Angelucci A. 2018. Parallel feedback pathways between
2603 macaque visual areas V2 and V1. In: *Soc. Neurosci. Abstr. Online.* p. 219.20.
- 2604 Tamamaki N, Tomioka R. 2010. Long-range GABAergic connections distributed
2605 throughout the neocortex and their possible function. *Front Neurosci.* 4:Article 202.
- 2606 Tanigawa H, Wang Q, Fujita I. 2005. Organization of horizontal axons in the inferior
2607 temporal cortex and primary visual cortex of the macaque monkey. *Cereb Cortex.*
2608 15:1887–1899.
- 2609 Tasic B, Yao Z, Graybiuck LT, Smith KA, Nguyen TN, Bertagnolli D, Goldy J, Garren E,
2610 Economo MN, Viswanathan S, Penn O, Bakken T, Menon V, Miller J, Fong O,

2611 Hirokawa KE, Lathia K, Rimorin C, Tieu M, Larsen R, Casper T, Barkan E, Kroll
2612 M, Parry S, Shapovalova N V., Hirschstein D, Pendergraft J, Sullivan HA, Kim TK,
2613 Szafer A, Dee N, Groblewski P, Wickersham I, Cetin A, Harris JA, Levi BP, Sunkin
2614 SM, Madisen L, Daigle TL, Looger L, Bernard A, Phillips J, Lein E, Hawrylycz M,
2615 Svoboda K, Jones AR, Koch C, Zeng H. 2018. Shared and distinct transcriptomic
2616 cell types across neocortical areas. *Nature*. 563:72–78.

2617 Teichert T, Wachtler T, Michler F, Gail A, Eckhorn R. 2007. Scale-invariance of receptive
2618 field properties in primary visual cortex. *BMC Neurosci*. 8:Article 38.

2619 Thomson AM. 2002. Synaptic Connections and Small Circuits Involving Excitatory and
2620 Inhibitory Neurons in Layers 2-5 of Adult Rat and Cat Neocortex: Triple
2621 Intracellular Recordings and Biocytin Labelling In Vitro. *Cereb Cortex*. 12:936–953.

2622 Thomson AM, Destexhe A. 1999. Dual intracellular recordings and computational models
2623 of slow inhibitory postsynaptic potentials in rat neocortical and hippocampal slices.
2624 *Neuroscience*. 92:1193–1215.

2625 Thomson AM, Lamy C. 2007. Functional maps of neocortical local circuitry. *Front*
2626 *Neurosci*. 1:19–42.

2627 Tomioka R, Rockland KS. 2007. Long-distance corticocortical GABAergic neurons in the
2628 adult monkey white and gray matter. *J Comp Neurol*. 505:526–538.

2629 Tootell R, Silverman M, Switkes E, De Valois R. 1982. Deoxyglucose analysis of
2630 retinotopic organization in primate striate cortex. *Science*. 218:902–904.

2631 Tootell RB, Hamilton SL. 1989. Functional anatomy of the second visual area (V2) in the
2632 macaque. *J Neurosci*. 9:2620–2644.

2633 Tootell RB, Mendola JD, Hadjikhani NK, Ledden PJ, Liu AK, Reppas JB, Sereno MI,
2634 Dale AM. 1997. Functional analysis of V3A and related areas in human visual
2635 cortex. *J Neurosci*. 17:7060–7078.

- 2636 Tootell RBH, Silverman MS, De Valois RL, Jacobs GH. 1983. Functional organization of
2637 the second cortical visual area in primates. *Science*. 220:737–739.
- 2638 Tootell RBH, Silverman MS, Hamilton SL, Switkes E, De Valois RL. 1988. Functional
2639 anatomy of macaque striate cortex. V. Spatial frequency. *J Neurosci*. 8:1610–1624.
- 2640 Tootell RBH, Switkes E, Silverman MS, Hamilton SL. 1988. Functional anatomy of
2641 macaque striate cortex. II. Retinotopic organization. *J Neurosci*. 8:1531–1568.
- 2642 Trojanowski JQ, Jacobson S. 1976. Areal and laminar distribution of some pulvinar
2643 cortical efferents in rhesus monkey. *J Comp Neurol*. 169:371–392.
- 2644 Ts'o DY, Frostig RD, Lieke EE, Grinvald A. 1990. Functional organization of primate
2645 visual cortex revealed by high resolution optical imaging. *Science*. 249:417–420.
- 2646 Ts'O DY, Roe AW, Gilbert CD. 2001. A hierarchy of the functional organization for color,
2647 form and disparity in primate visual area V2. *Vision Res*. 41:1333–1349.
- 2648 Turrigiano GG. 2008. The self-tuning neuron: synaptic scaling of excitatory synapses.
2649 *Cell*. 135:422–435.
- 2650 Turrigiano GG, Leslie KR, Desai NS, Rutherford LC, Nelson SB. 1998. Activity-
2651 dependent scaling of quantal amplitude in neocortical neurons. *Nature*. 391:892–
2652 896.
- 2653 Ungerleider LG, Desimone R. 1986. Cortical connections of visual area MT in the
2654 macaque. *J Comp Neurol*. 248:190–222.
- 2655 Ungerleider LG, Mishkin M. 1979. The striate projection zone in the superior temporal
2656 sulcus of *Macaca mulatta*: Location and topographic organization. *J Comp Neurol*.
2657 188:347–366.
- 2658 Valverde F. 1978. The organization of area 18 in the monkey - A Golgi study. *Anat*
2659 *Embryol (Berl)*. 154:305–334.
- 2660 Van Essen DC. 2003. Organization of visual areas in macaque and human cerebral cortex.

- 2661 In: Chalupa L., Werner J, editors. Visual Neurosciences. MIT Press. p. 507–521.
- 2662 Van Essen DC, Glasser MF, Dierker DL, Harwell J. 2012. Cortical parcellations of the
2663 macaque monkey analyzed on surface-based atlases. *Cereb Cortex*. 22:2227–2240.
- 2664 Van Essen DC, Newsome WT. 1984. The visual field representation in the striate cortex
2665 of the macaque monkey: Asymmetries, anisotropies, and individual variability.
2666 *Vision Res*. 24:429–448.
- 2667 van Rossum MC, Bi GQ, Turrigiano GG. 2000. Stable Hebbian learning from spike
2668 timing-dependent plasticity. *J Neurosci*. 20:8812–8821.
- 2669 Venkat A, Christensen C, Gyulassy A, Summa B, Federer F, Angelucci A, Pascucci V.
2670 2016. A scalable cyberinfrastructure for interactive visualization of terascale
2671 microscopy data. In: 2016 New York Scientific Data Summit, NYSDS 2016 -
2672 Proceedings. p. doi: 10.1109/NYSDS.2016.7747805.
- 2673 Vidyasagar TR, Eysel UT. 2015. Origins of feature selectivities and maps in the
2674 mammalian primary visual cortex. *Trends Neurosci*. 38:475–485.
- 2675 Wandell BA, Dumoulin SO, Brewer AA. 2007. Visual field maps in human cortex.
2676 *Neuron*. 56:366–383.
- 2677 Wang HX, Movshon JA. 2016. Properties of pattern and component direction-selective
2678 cells in area MT of the macaque. *J Neurophysiol*. 115:2705–2720.
- 2679 Wang Y, Xiao Y, Felleman DJ. 2007. V2 thin stripes contain spatially organized
2680 representations of achromatic luminance change. *Cereb Cortex*. 17:116–129.
- 2681 Weller RE, Kaas JH. 1983. Retinotopic patterns of connections of area 17 with visual
2682 areas V-II and MT in macaque monkeys. *J Comp Neurol*. 220:253–279.
- 2683 Williams SR, Stuart GJ. 2002. Dependence of EPSP efficacy on synapse location in
2684 neocortical pyramidal neurons. *Science*. 295:1907–1910.
- 2685 Wiser A, Callaway E. 1996. Contributions of individual layer 6 pyramidal neurons to

- 2686 local circuitry in macaque primary visual cortex. *J Neurosci.* 16:2724–2739.
- 2687 Wiser AK, Callaway EM. 1997. Ocular dominance columns and local projections of layer
- 2688 6 pyramidal neurons in macaque primary visual cortex. *Vis Neurosci.* 14:241–251.
- 2689 Xiao Y, Casti A, Xiao J, Kaplan E. 2007. Hue maps in primate striate cortex. *Neuroimage.*
- 2690 35:771–786.
- 2691 Xiao Y, Wang Y, Felleman DJ. 2003. A spatially organized representation of colour in
- 2692 macaque cortical area V2. *Nature.* 421:535–539.
- 2693 Yabuta NH, Sawatari A, Callaway EM. 2001. Two functional channels from primary
- 2694 visual cortex to dorsal visual cortical areas. *Science.* 292:297–300.
- 2695 Yang Y, Liang Z, Li G, Wang Y, Zhou Y. 2009. Aging affects response variability of V1
- 2696 and MT neurons in rhesus monkeys. *Brain Res.* 1274:21–27.
- 2697 Yarch J, Federer F, Angelucci A. 2017. Local Circuits of V1 Layer 4B Neurons Projecting
- 2698 to V2 Thick Stripes Define Distinct Cell Classes and Avoid Cytochrome Oxidase
- 2699 Blobs. *J Neurosci.* 37:422–436.
- 2700 Yarch J, Larsen H, Chen M, Angelucci A. 2019. Morphological cell types projecting from
- 2701 V1 layer 2B to V2 thick and thin stripes. *J Neurosci.* epub ahead of print.
- 2702 Yoshioka T, Blasdel GG, Levitt JB, Lund JS. 1996. Relation between patterns of intrinsic
- 2703 lateral connectivity, ocular dominance, and cytochrome oxidase-reactive regions in
- 2704 macaque monkey striate cortex. *Cereb Cortex.* 6:297–310.
- 2705 Zeki S. 2015. Area V5—a microcosm of the visual brain. *Front Integr Neurosci.* 9:Article
- 2706 21.
- 2707 Zeki S, Shipp S. 1988. The functional logic of cortical connections. *Nature.* 335:311–317.
- 2708 Zhou H, Friedman HS, von der Heydt R. 2000. Coding of Border Ownership in Monkey
- 2709 Visual Cortex. *J Neurosci.* 20:6594–6611.
- 2710 Zhu Q, Vanduffel W. 2019. Submillimeter fMRI reveals a layout of dorsal visual cortex in

2711 macaques, remarkably similar to New World monkeys. Proc Natl Acad Sci U S A.
2712 116:2306–2311.
2713 Ziemba CM, Freeman J, Simoncelli EP, Movshon JA. 2018. Contextual modulation of
2714 sensitivity to naturalistic image structure in macaque V2. J Neurophysiol. 120:409–
2715 420.
2716